NASA-CR-165188
PWA-5635-43

NASA

IMPROVED METHODS FOR FAN SOUND FIELD DETERMINATION

by

D.E. Cicon, T.G. Sofrin and D.C. Mathews

January 1981

Pratt & Whitney Aircraft Group
Commercial Products Division

Prepared For

National Aeronautics and Space Administration
NASA-Lewis Research Center
Contract NAS3-21391

1 Report No	2 Government Accession No	3 Recipient's Catalog No
NASA-CR-165188		

4 Title and Subtitle	5 Report Date
IMPROVED METHODS FOR FAN SOUND FIELD DETERMINATION	January 1981
	6 Performing Organization Code

7 Author(s)	8 Performing Organization Report No
D. E. Cicon, T. G. Sofrin and D. C. Mathews	PWA-5635-43
	10 Work Unit No

9 Performing Organization Name and Address	11 Contract or Grant No
United Technologies Corporation Pratt & Whitney Aircraft Group Commercial Products Division East Hartford, Connecticut 06108	NAS3-21391
	13 Type of Report and Period Covered

12 Sponsoring Agency Name and Address	14 Sponsoring Agency Code
National Aeronautics and Space Administration Washington, D.C. 20546	

15 Supplementary Notes

NASA Project Manager, Dr. E. J. Rice

NASA - Lewis Research Center, 21000 Brookpark Rd., Cleveland, Ohio 44135

16 Abstract

Several new methods for determining acoustic mode structure in aircraft turbofan engines using wall microphone data were studied. A method for reducing data was devised and implemented which makes the definition of discrete coherent sound fields measured in the presence of engine speed fluctuation more accurate.

For the new analytical methods, algorithms were developed to define the dominant circumferential modes from full and partial circumferential arrays of microphones. Axial arrays were explored to define mode structure as a function of cutoff ratio, and the use of data taken at several constant speeds was also evaluated in an attempt to reduce instrumentation requirements. Sensitivities of the various methods to microphone density, array size and measurement error were evaluated and results of these studies showed these new methods to be impractical.

The data reduction method used to reduce the effects of engine speed variation consisted of an electronic circuit which windowed the data so that signal enhancement could occur only when the speed was within a narrow range. The method was verified by measuring the coherent mode structure produced by a 10-inch fan rig at 5 steady speeds and comparing results with results obtained from a variable speed record.

17 Key Words (Suggested by Author(s))	18 Distribution Statement
Fan sound mode structures Amplitude Phase Coherent sound modes	

19 Security Classif (of this report)	20 Security Classif (of this page)	21 No of Pages	22 Price*
		174	

*For sale by the National Technical Information Service, Springfield, Virginia 22161

NASA C-168 Rev. 10-75

TABLE OF CONTENTS

TABLE OF CONTENTS (Cont'd)

LIST OF ILLUSTRATIONS

LIST OF ILLUSTRATIONS (Cont'd)

LIST OF ILLUSTRATIONS (Cont'd)

LIST OF ILLUSTRATIONS (Cont'd)

LIST OF TABLES

LIST OF TABLES (Cont'd)

LIST OF TABLES (Cont'd)

IMPROVED METHODS FOR FAN SOUND FIELD DETERMINATION

FINAL REPORT

by

D. E. Cicon, T. G. Sofrin, D. C. Mathews

1.0 SUMMARY

An analytical and experimental program was conducted to examine certain procedures for determining fan sound mode structure from in-duct pressure measurements using fixed, flush-mounted microphones in the inlet duct.

Three basic topics were explored:

Topic A

In many specific practical cases the principal source of coherent fan interaction noise is unknown or speculative, so that there is no reliable information in advance of testing about which circumferential modes dominate the fan noise field. The problem is to determine by tests which of all the possible propagating modes are dominant. For this purpose, an array of circumferentially distributed wall microphones was established as a device for extracting, during fan rig or engine tests, sufficient information for determination of these dominant circumferential modes.

A comprehensive analytical investigation was made, leading to establishment of the significant properties of circumferential arrays when used to measure circumferential mode structure. Array types included full and partial circumferential extent and symmetrical and unsymmetrical arrangements. Various methods of processing the array signals were explored, and test procedures were examined that included data acquisition at several fan speeds.

Basic results of this study are: 1.) When the fan blade noise frequencies are relatively low, so that comparatively few modes can propagate, circumferential flush-mounted wall arrays provide a convenient system for data acquisition and processing, and avoid the contamination by extraneous noise that is present with microphones protruding into the inlet duct airflow. 2.) However, when the blade passage noise is of higher frequency, as is the case in most engines and fan rigs, many more circumferential modes propagate. This condition requires that a large number of microphone locations be used in the array and places an excessive burden upon instrumentation and/or test time requirements.

Topic B

There are fan noise reduction applications, such as the design of optimum sound-absorbing inlet liners, where it is important to know how the blade frequency noise is distributed with respect to cutoff ratio of the modes carrying the sound energy. In this phase of the study an investigation was made of the use of flush-mounted inlet duct arrays to measure this energy distribution directly, without the need to obtain individual circumferential-radial mode strengths.

It was found that the basic array geometry required is a linear array of flush-mounted microphones extending axially along the inlet duct wall. Detailed operating characteristics of such arrays in defining acoustic energy distribution were determined. In the case of coherent (phase-locked) blade frequency modes, a complication was found to arise from coupling of the array signals from modes having an essentially common cutoff ratio. This effect could be eliminated by replicating the array in a plurality of locations, a step that would lead to an undesirably large number of microphones. However, it was found that in the case of incoherent or random noise the intermodal coupling was absent, suggesting that a single axial array would suffice to obtain cutoff ratio distributions for random fan noise components.

Topic C

In all types of engine and fan rig noise tests where local pressure amplitude and phase must be measured accurately, inadvertent fan speed variations during the run introduce one or more types of error. This problem was addressed by designing a circuit that would pass the microphone signals only when rig speed fell within a preselected narrow range or window.

This speed window procedure was evaluated experimentally using a 10-inch fan rig that could be run either at a number of very constant speeds or under a condition of controlled cyclic speed variation. It was demonstrated that the window procedure applied during transient operation produced data in satisfactory agreement with results of steady speed runs. Use of the speed window procedure thus should be of value in test programs where fan speed cannot be controlled as closely as required for accurate acoustic amplitude and phase measurements.

2.0 INTRODUCTION

2.1 Background

The study of means for reducing levels of fan noise emission has been a continuing effort for more than two decades. In this work, a definition of the nature of the noise from a configuration which is to be reduced by development programs or suppressed by acoustic liner design, is clearly essential. Such definition is provided by the function called a modal spectrum, which characterizes the sound field in the fan duct in terms, not only of frequency, but also of circumferential and radial wavenumbers.

This investigation is concerned with coherent, discrete-frequency fan noise at blade passage frequency and its harmonics. If the mode structure at blade frequency is known in terms of the dominant circumferential modes, the sources of noise can be reliably inferred from blade-vane interaction theory, pointing a way to corrective measures. Another parameter over which the distribution of modes is useful is cutoff ratio. This parameter involves both circumferential and radial wavenumbers. If, however, a direct measure of modal distribution may be found experimentally in terms of cutoff ratio, this distribution may be used to estimate far field directivity, for example, or in selection of design parameters for efficient acoustical duct liners.

A great many methods, including variations and refinements, for measuring fan noise mode structure in ducts, have been used in previous investigations. A small sample of these methods may be found in References 1 through 9. Most of the available methods suffer from two basic problems: the use of fixed position microphones generally leads to an impractically large number of microphones, and if some microphones are deployed radially inward from the wall, the interaction of the rotor with their wakes generates a contaminating noise field. To overcome the requirement for large numbers of microphones, traversing systems have been used to sweep one or a few microphones to a large number of locations. For extensive laboratory tests, involving small, constant speed model fan rigs, such procedures have been successful. In full scale powerplants, both in flight and on ground tests, the time involved in such data acquisition is excessive, and also, because of the higher axial flow velocity, the probe wake/rotor interaction contaminating noise is a problem.

A further difficulty encountered in fan noise mode measurements is the effect of inadvertent engine or rig speed variations during the run. These deviations affect each mode differently, in general, and result in unreliable measurements of local sound pressure amplitudes and phases, which seriously distort the calculated modes.

The objective of this investigation was to explore means for overcoming these problems. To prevent the generation of microphone wake/rotor interaction noise contamination, only flush-mounted microphones installed in the duct wall were to be considered. Fixed microphones rather than traversing systems were to be used to reduce data acquisition time. The essential problem then reduced to finding the trade off between number of microphones required and performance

of the system in addressing some specific tasks. There is, of course, no well-defined meaning for what is an acceptable, or reasonably small number of microphones. But a number of examples of mode structure determination were examined here that provide a clear indication of the limits of mode structure information that can be obtained as a function of the number of microphones employed.

Basically, two systems of wall-mounted microphones, called arrays, were explored. In the first system, an array of microphones extending circumferentially over a fraction of the duct perimeter was examined for its ability to detect circumferential mode structure. In the second basic investigation, the objective was to obtain the modal distribution with respect to the cutoff ratio by employing an axially extended flush mounted array. In both cases the basic array principle is to enhance the target mode, or set of modes, by use of progressive time delays that cause the array to track on the basis of phase velocity in the array direction.

In neither of these systems is the prime objective to measure accurately the amplitude of all the propagating modes, but rather to determine which of the circumferential modes are dominant, and for the cutoff ratio array, to find a smooth distribution function that broadly characterizes the sound field distribution with respect to cutoff ratio. In the practical cases where very many modes are propagating, the task of accurately measuring amplitudes of all the possible modes leads to a requirement for a correspondingly excessive number of microphones, which would violate one of the guidelines of the present study.

The problem of speed variations during a modal measurement run was also studied in this investigation. An experimental program was conducted on a 10-inch fan rig to allow comparison of results taken under steady-state conditions and with controlled speed variations. An improved data acquisition and reduction procedure was developed and evaluated to minimize effects of inadvertent speed fluctuations.

2.2 Program Description and Documentation

The work reported in this investigation has been described briefly in the Summary and will be detailed in various sections of the text, for which the Table of Contents provides a guide. This work, performed under Contract NAS3-21391, was segregated by "Tasks" having designations and sequences that may not always be immediately identifiable in terms of report section headings.

Therefore, to provide a bridge between the contract task designations and the location in this report where the corresponding work is described, the following cross-reference listing is provided:

Contract Task Designation	Contract Description (abbreviated)	Section Location in Report
Task I Part 1	Development of partial circumferential array method for measuring dominant circumferential modes	3.1

Contract Task Designation	Contract Description (abbreviated)	Section Location in Report
Part 2	Evaluate procedure for using data from arrays at a plurality of fan speeds to allow detection of more modes per microphone.	3.2
Part 3	Develop an experimental procedure to allow data acquisition at selected intervals during a test where fan speed varies inadvertently.	4.1
Part 4	Evaluate the procedure of Part 3 by tests on the 10-inch fan rig using deliberate speed variations and steady-state comparison runs.	4.2
Task II	Study and evaluate arrays that could measure acoustic power of a set of modes in a band propagating at essentially common cutoff ratio.	3.3

3.0 ANALYTICAL STUDIES

3.1 PARTIAL CIRCUMFERENTIAL ARRAY METHOD

3.1.1 Background

At each harmonic of fan blade passage frequency the sound field in a fan duct consists of a superposition of circumferential-radial (m, μ) modes, each of which is a "natural" or characteristic distribution of sound pressure over the duct cross section. A knowledge of the modal coefficients or strengths may be put to various uses. The application that motivates the current investigation is the identification of the most significant or dominant modes, so that the specific noise source(s) may be identified and corrective action (source modification and/or optimum acoustic liner design) can be taken.

Of the pair of wave numbers, m for circumferential and μ denoting radial, the circumferential wave number is the more important generally, for it points most clearly to the identity of the source (stator vanes, inlet distortion, etc.) that is responsible for the noise. If it subsequently is decided to explore the strength of the radial modes associated with a dominant circumferential mode, the microphone location program (MLP) and modal calculation program (MCP), reported in Ref. 1, may then be employed.

Various methods have been used to measure modal structure in fan ducts (e.g., Refs. 2 through 9). In this investigation two important constraints have been imposed on the method: 1) the microphones shall be flush-mounted on the duct wall surface and 2) the number of microphones shall be "reasonably" small. The reason for the first restriction is to avoid the generation of extraneous noise caused by rotor interaction with the wakes of radial microphone rakes or circumferential traversing mechanisms. The second constraint is imposed by the practical considerations of microphone and recording channel availability.

At approach power in the JT9D engine, for example, there are about 150 possible propagating m-modes at twice the blade passage frequency. Providing anything like 150 microphone readings -- even if they were not recorded simultaneously -- would be impractical. Especially if measurements were needed in flight, the procedure of running a long sequence of flight tests with a limited number of microphones repositioned to different locations would be unacceptable.

The use of a limited number of microphones to determine the dominant circumferential modes is also justified on the following basis. Suppose that somehow the very large number of microphones needed to determine all the propagating m-modes (150 in the above JT9D example) could be provided and used in a circular array. The data would give all the modal coefficients evaluated at the wall in the plane of the array. But each such modal coefficient is the resultant of all the radial modes associated with each m-mode. Since these radial modes have different wave numbers, they propagate at different rates and their relative phase and sum at any fixed radius is a function of axial distance from the source. Thus, for example, two strong radial modes could combine to give either a large wall reading or a small reading depending on their relative phase.

Consequently, even with a complete circumferential array containing enough microphones to determine all the propagating circumferential modes, there is no certainty that significant or dominant modes will be detected. To avoid missing a dominant circumferential mode thus requires replicating the circumferential array at a number of axial locations so that the radial mode resultants will not give a false impression of low level due to cancellation effects.

Therefore, the identification of dominant modes without an excessive number of microphones would involve two or more circumferential arrays at different axial locations, and each array must employ a practical, limited number of microphones. These microphones need not all be deployed and recorded simultaneously, for periodic sampling techniques allow amplitude and phase to be determined with respect to a common rotor reference position. However, the number of microphone locations required must not be excessive to stay within reasonable testing and setup time limits.

Therefore, the objective of this investigation is to evaluate the feasibility of these array systems for identifying dominant circumferential modes using a limited number of microphone locations.

3.1.2 Characteristics of PCA Method

3.1.2.1 Full Circumferential Array Properties

A circular array employing N equally spaced microphones around the duct circumference is a basic reference array system for circumferential mode detection and will be described first. The physical basis for its operation provides a convenient way of formulating its properties. This basis is as follows:

At any harmonic of blade passage frequency $nB\Omega$, a circumferential mode having m cycles of pressure variation around the duct spins at a rate, $\Omega_m = nB\Omega/m$. This follows simply from the requirement that all such modes generate the same harmonic of blade passage frequency, $\omega = nB\Omega$. If in the array, signals from successive microphones are progressively delayed and then added, the resulting array signal will enhance the particular mode having a spin rate corresponding to the selected array delay rate. (For a coherent field the inter-microphone delay corresponds to a phase shift, but it is convenient to formulate the analysis in terms of time delays.)

An expression is needed for the instantaneous pressure sensed by a microphone in the array. This will be obtained from the following general expression for the pressure in the duct at a single frequency $\omega = nB\Omega$, corresponding to a specific harmonic, n, of blade passage frequency:

$$p(r,\theta,x,t) = \mathrm{Re} \sum_{m} \sum_{\mu} C_{m\mu} E_{m\mu}(k_{m\mu} r) \exp i (k_{xm\mu} x + m\theta - \omega t). \qquad (1)$$

(See Appendix B for notation)

Evaluating the pressure at the wall, r = b, and defining x = 0 at the plane of the array, Eq. (1) can be put in the form:

$$p(\theta, t) = \mathrm{Re} \sum_m C_m \, \mathrm{expi}\ (m\theta - \omega t), \tag{2}$$

where C_m is the resultant of the associated radial (μ) modes at the wall for the m-th circumferential mode:

$$C_m = \sum_{\mu} C_{m\mu}\ E_{m\mu}(k_{m\mu} b) \tag{3}$$

Eq. (2) is relevant to the circumferential array.

From (2) the pressure for the n-th microphone at θ_n is just

$$p_n(t) = p(\theta_n, t) = \mathrm{Re} \sum_m C_m \, \mathrm{expi}\ (m\theta_n - \omega t) \tag{4}$$

Let this signal be delayed by a time Δt_n proportional to the distance of the n-th microphone from the initial microphone at θ_o. If the separation between microphones is $\Delta\theta = 2\pi/N$, and θ_o is taken as zero, the n-th microphone is at $n\Delta\theta$ and the time delay will be $\eta\, n\Delta\theta$, where η is the delay rate, $\Delta t/\Delta\theta$, secs./radian.

The delayed signal is

$$p'_n(t) = p(n\Delta\theta,\ t + \eta\, n\Delta\theta) = \mathrm{Re} \sum_m C_m \, \mathrm{expi}\left[m\, n\Delta\theta - \omega(t + \eta\, n\Delta\theta)\right] \tag{5}$$

$$= \mathrm{Re}\ e^{-i\omega t} \sum_m C_m \, \mathrm{expi}\ (m - \omega\eta)\, n\Delta\theta$$

Summing and averaging over the N microphones gives the array signal

$$f_\eta(t) = \mathrm{Re}\ e^{-i\omega t} \sum_m C_m \frac{1}{N} \sum_{n=0}^{N-1} \mathrm{expi}\ (m - \omega\eta)\, n\Delta\theta \tag{6}$$

It will be convenient to work with the complex array signal, F_η, defined by:

$$f_\eta(t) = \mathrm{Re}\ F_\eta\ e^{-i\omega t} \tag{7}$$

From (6) the following can be formulated:

$$F_h = \sum_m C_m Z(\beta), \tag{8}$$

Where $Z(\beta)$ is called the array factor,

$$Z(\beta) = \frac{1}{N} \sum_{n=0}^{N-1} \exp i \beta \frac{2\pi}{N} n, \tag{9}$$

and

$$\beta = (m - \omega h) \tag{10}$$

The expression (9) for $Z(\beta)$ involves the sum of N unit complex numbers spaced $\beta\, 2\pi/N$ apart and can be evaluated in closed form. Since this sum and other closely related forms appear frequently in this study, the following brief derivation is presented here for convenience.

If eq. (9) is written as

$$Z(\beta) = \frac{1}{N} \sum_{n=0}^{N-1} \left[\exp i \beta \frac{2\pi}{N}\right]^n$$

it will be recognized as a geometric series of N terms, with the first term as unity and ratio $\exp i \beta\, 2\pi/N$. Therefore

$$Z(\beta) = \frac{1}{N} \frac{e^{i\beta 2\pi} - 1}{e^{i\beta 2\pi/N} - 1}$$

$$= \frac{1}{N} \frac{(e^{i\beta\pi} - e^{-i\beta\pi})\, e^{i\beta\pi}}{(e^{i\beta\pi/N} - e^{-i\beta\pi/N})\, e^{i\beta\pi/N}}$$

$$Z(\beta) = \frac{\sin \beta\pi}{N \sin \beta\pi/N} \exp i \frac{N-1}{N} \beta\pi \qquad (11)$$

From Eq. (11) the following important properties of the array factor, $Z(\beta)$ may be obtained:

$Z(\beta)$ is periodic with period N	(12a)
$Z(0) = 1$ is its greatest value	(12b)
$Z(\beta) = 0$ for all integer β not multiples of N	(12c)
$Z(\beta)$ has minor maxima between its zeros	(12d)
$Z(-\beta) = Z^*(\beta)$	(12e)
The "phase" of $Z(\beta)$ is a linear function of β	(12f)

In operation, the array is targeted to a specific $m = M$ by selecting the delay rate τ such that $\beta = (M - \omega\tau) = 0$. The array reading is then $F_\tau = C_M$. By property (12c), the contributions of all other modes having $m \neq M$ are zero, except for such modes as have $m = M \pm N$, $M \pm 2N$, etc. If such modes exist in the plane of the array, the array signal will be:

$$F_\tau = \ldots \; C_{M-N} + C_M + C_{M+N} + C_{M+2N} \ldots \qquad (13)$$

The condition represented by Eq. (13) is called aliasing. The array is unable to distinguish between members of the set of modes spaced N wave numbers apart. This characteristic renders the array useless and must be avoided. To prevent aliasing, it is necessary to determine how many propagating modes (or weakly decaying modes) can be present in the plane of the array at the highest frequency of interest and to then select the number of microphones, N, to be large enough so that the period of the array exceeds the range of the target mode set.

This requirement is simply:

$$N > 2m^* \qquad (14)$$

where m^* is the largest wave number in the set of propagating or weakly decaying modes.

The corresponding spacing between microphones, $\Delta\theta$, will be

$$\Delta\theta = \frac{2\pi}{2m^*} = \frac{1}{2}\left[\frac{2\pi}{m^*}\right] = \frac{1}{2}\lambda_{m^*} \qquad (15)$$

or one half the smallest circumferential wavelength of the propagating modes.

In Figure 1, some of the properties and uses of the array are illustrated. The assumed target mode set is shown in Figure 1a. Nine modes ranging from $m^* = -4$ to $m^* = 4$ are assumed to be propagating for illustration. All other modes have decayed to trivial levels in the array plane.

Figure 1b illustrates the use of a 5-microphone array. The delay rate is set to target the $m = 3$ mode. The array factor amplitude, $|Z(\beta)|$, is illustrated with the major lobe peak response targeting C_3. Note that the responses to C_4, C_2, C_1, C_0, and C_{-1} are zero, but at C_{-2} the array factor again becomes unity, giving the undesired or aliased reading C_{-2}. The array signal is thus $F_h = C_3 + C_{-2}$. This condition results from the period of the array factor, 5, being too small with respect to the range of the target mode set.

The aliasing is corrected by increasing N. Figure 1c shows a 10-microphone array giving the correct signal when targeted to C_3. Any number N greater than $2m^* = 8$ of microphones will also give alias-free operation for this target mode set.

This anti-aliasing requirement leads to an impractically large number of microphones in most fan rig and engine applications. For example, to measure twice blade frequency in the JT9D at approach power would require using more than 150 microphones. An array geometry that would involve significantly fewer microphones is examined next.

3.1.2.2 Partial Circumferential Arrays

The configuration to be examined involves N microphones equally spaced in a fraction, 1/F, of the duct circumference. With the resulting spacing $\Delta\theta = (2\pi/F)/N$ replacing the previous $2\pi/N$ spacing for a full array in Eq. (9), the array factor becomes:

$$Z(\beta) = \frac{1}{N} \sum_{n=0}^{N-1} \exp i\, \beta \frac{2\pi}{NF}\, n \qquad (16)$$

If β/F replaces β in Eq. (11) the corresponding closed form of Eq. (16) is obtained:

$$Z(\beta) = \frac{\sin \beta\pi/F}{N \sin \beta\pi/NF} \exp i \frac{N-1}{NF}\, \beta\pi \qquad (17)$$

where, as before, $\beta = (m - \omega h)$

The properties of the partial circumferential array factor differ in just two respects from those of the full array given by Equations (12):

$Z(\beta)$ is periodic with period NP (18a)

$Z(\beta) = 0$ for β = integer multiples of F, (excluding NF) (18b)

Property 18a is highly desirable. The period of the array factor has been extended by the multiple, F, relative to that of a full array with N microphones. This means that the anti-aliasing requirement can be met with a reduced number of microphones. The minimum microphone spacing, $\Delta\theta = (2\pi/F)/N$ is the same $\lambda_m^*/2$ as is necessary in a full array, but the array length and total number of microphones are significantly reduced. This reduction was the objective of the array configuration design.

Property (18b), however, introduces a complication. In the full array $Z(\beta) = 0$ for all β except for the target mode, $\beta = 0$. Now, the partial array responds (partially) to all but a few modes. The major lobe of the array factor (and the minor lobes as well) are broadened by a factor of F. The array signal contains, in addition to the target mode, contamination from off-target modes. This comparison between the full and partial circumferential arrays is illustrated in Figure 2.

Figure 2a shows the array factor amplitude for a reference, full circumferential array of N = 12 microphones. The null response to off-target modes may be noted. The same period (and thus the same anti-aliasing properties) is provided by the partial array illustrated in Figure 2b. This array with N = 4, F = 3, contains 4 microphones deployed in 1/3 the circumference. The plurality of off-target mode responses contaminating the array signal is clearly shown.

The presence in the array signal, F_n, of contributions from several modes other than the target means that a set of linear equations must be solved. If the array is successively targeted to all members of the target mode set, the following equations result:

$$\begin{bmatrix} F_1 \\ F_2 \\ F_3 \\ \cdot \\ \cdot \\ \cdot \\ F_P \end{bmatrix} = \begin{bmatrix} Z(0) & Z(1) & Z(2) & \cdots & Z(P-1) \\ Z(-1) & Z(0) & Z(1) & \cdots & Z(P-2) \\ Z(-2) & Z(-1) & Z(0) & \cdots & Z(P-3) \\ \cdot & \cdot & \cdot & & \cdot \\ \cdot & \cdot & \cdot & & \cdot \\ \cdot & \cdot & \cdot & & \cdot \\ Z(-P+1) & Z(-P+2) & Z(-P+3) & \cdots & Z(0) \end{bmatrix} \cdot \begin{bmatrix} C_{m1} \\ C_{m2} \\ C_{m3} \\ \cdot \\ \cdot \\ \cdot \\ C_{mP} \end{bmatrix} \quad (19)$$

F_1, F_2, ... F_p are the array signals when the array is successively targeted to members of the target mode set. C_{m1}, C_{m2} ... C_{mp} are the successive modal coefficients. There are assumed to be P modes to be found in the set, requiring P array signals.

The matrix, $[Z(\beta)]$, having array factors $Z(\beta)$, is called the array matrix. Elements along and parallel to the principal diagonal are common; this property characterizes what is called a Toeplitz matrix. Because the array factor is such that $Z(-\beta) = Z^*(\beta)$, the array matrix is also Hermitian.

It is interesting to examine the array matrix, $Z(\beta)$, when the number of target modes, P, equals, then exceeds NF (the period of the array factor). From the periodic and conjugate properties of $Z(\beta)$ we can write:

For $P = NF$, $[Z(\beta)] =$

$$\begin{bmatrix} Z(0) & Z(1) & Z(2) & .... & Z^*(3) & Z^*(2) & Z^*(1) \\ Z^*(1) & Z(0) & Z(1) & .... & Z^*(4) & Z^*(3) & Z^*(2) \\ Z^*(2) & Z^*(1) & Z(0) & .... & Z^*(5) & Z^*(4) & Z^*(3) \\ .. & .. & .. & .... & .. & .. & .. \\ .. & .. & .. & .... & .. & .. & .. \\ Z(1) & Z(2) & Z(3) & .... & Z^*(2) & Z^*(1) & Z(0) \end{bmatrix} \qquad (20)$$

To emphasize the symmetry, $Z(\beta)$ for successive values of β will be denoted by 1, a, b, c ... Then $Z(\beta)$ for P = NF becomes

$$[Z(\beta)]_{(P=NF)} = \begin{bmatrix} 1 & a & b & . . . & c^* & b^* & a^* \\ a^* & 1 & a & . . . & d^* & c^* & b^* \\ b^* & a^* & 1 & . . . & e^* & d^* & c^* \\ . & . & . & . . . & . & . & . \\ . & . & . & . . . & . & . & . \\ a & b & c & . . . & b^* & a^* & 1 \end{bmatrix} \qquad (21)$$

When the size of the target mode set, P, becomes one greater than the array period, NF, the array matrix becomes:

$$[Z(\beta)]_{(P=NF+1)} = \left[\begin{array}{ccccccc|c} 1 & a & b & . . . & c^* & b^* & a^* & 1 \\ a^* & 1 & a & . . . & d^* & c^* & b^* & a^* \\ b^* & a^* & 1 & . . . & e^* & d^* & c^* & b^* \\ . & . & . & . . . & . & . & . & . \\ . & . & . & . . . & . & . & . & . \\ \underline{a} & \underline{b} & \underline{c} & & \underline{b^*} & \underline{a^*} & \underline{1} & \underline{a} \\ 1 & a & b & & c^* & b^* & a^* & 1 \end{array}\right] \qquad (22)$$

Note that now the last row is identical to the first and the first and last columns are also identical. The array matrix is singular, reflecting the condition of aliasing when the target set size exceeds the period (NF) of the array factor.

Consequently, it is necessary that $P \leq NF$ in order to determine the coefficients by inversion of the array equations (19). This condition, however, is not sufficient to assure success of the method, and it is necessary next to examine the sensitivity of this system of equations (19).

3.1.3 Sensitivity of Partial Circumferential Array System

3.1.3.1 Basis of the Analysis

The accuracy of the solution of the array equations, (19) for the modal coefficients depends primarily on three things:

1. Computation accuracy in the inversion of the array matrix or any equivalent algorithm for solving Eqs. (19). This accuracy is basically a function of the number of significant figures carried in the computer system. Use of efficient algorithms and multiple precision programs in high speed computers, can reduce round-off errors to an insignificant level compared to other sources of error.

2. Errors in the elements, $Z(\beta)$, of the array matrix. The array factors $Z(\beta)$ are subject to error because the actual spacings between microphones $\Delta\theta_n$ may not be exactly identical and equal to $2\pi/NF$. In the Modal Calculation Program of Ref. 1, it was found that the microphone location errors were significantly less important than the following third source.

3. In the Reference 1 study, errors in measuring pressure amplitudes and phases were found to be the dominant error source. When the microphone data are processed to form the array signals, additional error may be introduced in executing the time delays or phase shifts. Thus the major error in the system will be in the array signals and the effects of such errors were examined exclusively here.

Two complementary methods were used in determining the sensitivity of the Partial Circumferential Array to array signal errors. In the first method, the condition number of the array matrix was computed. The second method involved computer simulation of input pressure errors. These methods are described briefly next.

Matrix Condition Number

In a single, linear, scalar equation, $ax = y$, errors in x and y (with "a" subject to zero error) are related by $a\delta x = \delta y$, so that $\delta x/x = \delta y/y$, and the relative errors in input and output are equal. This is also true if x and y are vectors and "a" is a diagonal matrix, as is the case for a full circumferential array without aliasing. Apart from this exceptional case, there is no comparable, useful equality for the matrix equation $Ax = y$. Instead there is a frequently-used inequality Refs (10, 11):

$$\frac{\|\delta x\|}{\|x\|} \leq K \frac{\|\delta y\|}{\|y\|} \tag{23}$$

Here $\|\delta x\|$ and $\|x\|$ are the so-called norms of the vectors δx and x, corresponding symbols apply to the other vector and its error vector, and K is called the condition number of the matrix. There are several types of vector norms, a common one being $\sqrt{\Sigma x_i^2}$ which gives a generalized length of a vector. Thus the ratio $\|\delta x\|/\|x\|$ in Eq. (23) provides a measure of relative error in x analogous to the scalar case.

There are also several types of condition number, K. The definition used here is the ratio of the extreme eigenvalues of the matrix A. As seen from Eq. (23), condition number provides a measure of the magnification of relative errors in solving the system $Ax = y$. Unity is the least possible condition number; large values of K imply correspondingly high sensitivity of the system to small input errors.

Condition numbers were found for several array matrices that are described presently. They provide one measure of the sensitivity of the array equation, (19) to errors in the array signals, F.

Simulation of Array Signal Errors

A second way of assessing sensitivity was used which provides a somewhat more direct and familiar result than the condition number. Essentially, values of the modal coefficients, C_m, were assumed, and the array signals, F, that would result were obtained. Then small errors were imposed on the array signals. These perturbed signals were used as input to the system (19) and the resulting modal coefficients were found. Comparison of these calculated coefficients with the original assumed values gives a direct measure of the error for the particular sample of input modes and signal errors used.

Generally, the array signal errors were obtained either by rounding or by truncating the individual microphone signals, or in some cases, by simply rounding or truncating the final array signal. The assumed modal coefficient sets took a variety of forms. The primary property under study was the effect of size of the mode set upon sensitivity. The specific m-modes selected for targeting are of little consequence since the array matrix is the same for any set of consecutive modes of a given size.

One of the most revealing procedures was to take one or a few modes at a common "significant" level, with all the other modes null. Depending on the size of the target set, errors were revealed by deviations in levels of the computed significant modes from their input values and, most noticably, by the appearance of non-trivial levels of the initially null modes.

There is, of course, no universal criterion for what constitutes an acceptable solution. As stated previously, the main objective of the PCA method is to identify, for further study, the "dominant" modes. If modes that are 20 dB below the dominant modes are considered trivial, then the computed levels of null input modes could approach -20 dB of the dominant levels and still be considered acceptable. Anything like 0 to -10 dB from the dominant would constitute a false signal. For the computed values of the dominant modes, certainly $\pm$3 dB of the correct value would be good, and even $\pm$6 dB might be considered acceptable for this application.

3.1.3.2 Numerical Results of Sensitivity Study

A specific Partial Circumferential Array configuration was selected on the basis of its possible application to continuing studies on the 10-inch fan rig. For twice blade passage frequency at 6000 rpm, there are about 26 propagating circumferential modes. Making a very conservative provision for decaying modes, the maximum possible number of modes involved is on the order of 40 (20 forward and 20 reverse). Anti-aliasing requires the array period to be NF > 2 x 20 or 40. A value of NF = 40 was provided with an N = 10 microphone array extending over 1/F = 1/4 of the circumference.

The calculation procedure was as follows:

1. Postulate a small number of known, dominant mode coefficients, C_m.

2. Compute resulting pressures at the 10 microphones from

$$P_n = \sum_m C_m \exp i\, m\, \theta_n \qquad (24)$$

3. Apply errors by rounding or truncating these pressures.

4. Compute the array signals from

$$F_M = \frac{1}{N} \sum_{n=0}^{N-1} P_n \exp - M\, \theta_n \qquad (25)$$

5. Solve eqs. (19) for the coefficients, C_m, and compare with the postulated initial values.

6. Compute condition number.

These steps are repeated as the size of the target mode set increases.

The essential features of the sensitivity of the array method are illustrated here with a small sample of the number of calculations that were made.

In each of Figures 3, 4, 5, and 6, three consecutive m-modes are input at the 100 dB level. Successive target mode set sizes are 3, 5, 7, etc.

In Figure 3 the 100 dB input modes are m = -1, 0, 1. To simulate measurement errors, the microphone signals resulting from these modes were truncated to 0.1 dB before forming the array signals. The input modes are shown, together with results of the calculations of the modal coefficients for these modes and for bordering consecutive null modes, as the size of the target set is increased. When the target set includes 7 modes, the calculated coefficients become grossly unsatisfactory - the input modes are in error by as much as 25 dB and some of the bordering null modes exceed 100 dB in level. Larger target set sizes display even worse performance.

Figure 4 represents similar calculation results based on 100 dB input modes of m = 10, 11, 12. Comparable performance is indicated - the system generates useless results for target set sizes greater than 5.

To study this behavior further, these calculations were repeated with no deliberate truncation errors applied to microphone signals. Results are shown in Figure 5 for the m = -1, 0, 1 input and in Figure 6 for 100 dB input modes m = 10, 11, 12.

These results are somewhat different from those where deliberate errors were introduced. Now, the extraneous or null mode levels are at least 100 dB below the input mode levels for target set sizes up through 9. However, when 11 modes are contained in the target set, the performance suffers an abrupt degradation -- the input modes develop substantial error and the null mode levels escalate to values comparable with the three input modes.

Study of these results suggests that two effects may be involved:

1. When deliberate signal errors are introduced, there is a noticeable degradation of performance, starting with very moderate target set size, and becoming worse with increasing target set size. This trend is also indicated by the growth of the array matrix condition numbers which are displayed on the figures.

2. In the absence of deliberate microphone error the abrupt change in the quality of the results between target set sizes of 9 and 11 suggests that the array matrix, $[Z(\theta)]$, may become singular when the target set size exceeds 10, the number of microphones in the array.

A discussion of these characteristics follows, starting with the question of singularity.

3.1.3.3 Singularity of the Array Matrix

It was shown earlier (Eq. 22) that when the size of the target mode set (number of equations and modes) exceeds the array period, NF, the array matrix becomes singular. This is evidenced by the last row replicating the first when NF+1 rows and columns are employed. There is no way of discerning from the elements of $[Z(\beta)]$ that a singularity appears much sooner, namely when the size exceeds N, the number of microphones. To reveal this early singularity it is necessary to examine the array signal rather than the array matrix.

The case of N + 1 modes and array signals will be considered. Each array signal is found from the time-delayed or phase shifted set of N microphone pressures:

$$F_M = \frac{1}{N} \sum_{n=0}^{N-1} P_n \exp i - M\theta_n \tag{25}$$

or, symbolically,

$$F_M = L_M \ (P_0, P_1 \ . \ . \ . \ P_{N-1}) \tag{26}$$

where L_M denotes a linear combination.

The set of array signals can then be simply written as

$$\begin{aligned} F_1 &= L_1 \ (P_0, P_1 \ . \ . \ . \ P_{N-1}) \\ F_2 &= L_2 \ (\qquad\qquad\qquad\qquad) \\ &\cdot \\ &\cdot \\ &\cdot \\ F_N &= L_N \ (\qquad\qquad\qquad\qquad) \\ F_{N+1} &= L_{N+1} \ (P_0, P_1 \ . \ . \ . \ P_{N-1}) \end{aligned} \tag{27}$$

Now, from the first N of these equations, the N microphone pressures, P_0, P_1, ... P_{N-1} can be expressed in terms of the N array signals F_1, F_2 ...F_N, as, for example:

$$\begin{aligned} P_0 &= \ell_1 (F_1, F_2 \ldots F_N) \\ P_1 &= \ell_2 (\quad\quad\quad\quad) \\ &\cdot \\ &\cdot \\ &\cdot \\ P_{N-1} &= \ell_N (F_1, F_2 \ldots F_N) \end{aligned} \qquad (28)$$

Therefore, the (N+1)-st array signal, F_{N+1}, can be expressed as a linear function of the first N signals:

$$F_{N+1} = L_{N+1}[\ell_1(F_1,F_2\ldots F_N),\ \ell_2(F_1,F_2\ldots F_N),\ \ldots \ell_N(F_1,F_2\ldots F_N)] \qquad (29)$$

Since the last signal is a linear function of the first N, the N+1 row of the array matrix, $[\Sigma(s)]$ must also be a linear function of the first N rows, and the system is singular.

(The specific linear relation cannot be found by simple inspection of either the array matrix or the array signal generating equations (25). In specific cases it can be obtained numerically by inverting the first N eqs. (27) for the P_0, P_1, etc. and substituting in the last eq. 27 to obtain F_{N+1}.)

There is, in parallel, a simpler, more direct explanation of the singularity; it is not possible to obtain more than N unknowns from N independent observations, and it is the microphone readings rather than the array signals that are the independent observations.

3.1.3.4 Effect of Adding Microphones to Remove Singularity

As has been seen from Figures 3 and 4 the performance of the system, incorporating small microphone errors, becomes unsatisfactory well before the singularity of the array matrix at size 11 is reached. It is not yet clear whether this is due to a target mode set size that is not small enough with respect to the number of microphones, or whether other factors are involved.

Accordingly, the effect of removing the singularity by greatly increasing the number of microphones in the array spanning 1/4 the circumference was examined.

The array factor for an array of 1/F of the circumference, when the number of microphones increases without bound, becomes, from eq. (17):

$$Z_{\infty}(\beta) = \lim_{N \to \infty} Z_N(\beta) = \frac{\sin \beta\pi/F}{\beta\pi/F} \exp i \beta\pi/F \qquad (30)$$

Values of the magnitude of the array factor are listed below for two arrays spanning 1/4 the circumference - an N = 10 array and an $N \to \infty$ configuration. The ratios $|Z_{10}(\beta)| / |Z_{\infty}(\beta)|$ are also given.

TABLE I

ARRAY FACTORS FOR N = 10 AND $N \to \infty$

	β	N = 10 $\lvert Z_{10}(\beta)\rvert$	$N \to \infty$ $\lvert Z_{\infty}(\beta)\rvert$	$\lvert Z_{10}(\beta)\rvert / \lvert Z_{\infty}(\beta)\rvert$
	0	1	1	1
Major	1	0.901243	0.900316	1.001
lobe	2	0.639245	0.636620	1.004
	3	0.302900	0.300105	1.009
	4	0	0	-
	5	0.184776	0.180063	1.026
First	6	0.220269	0.212206	1.038
minor	7	0.135332	0.128617	1.052
lobe	8	0	0	-

The arbitrarily large increase in microphone number has produced less than 1 percent change in response in the major lobe and at most about 5 percent change in the first minor lobe. Despite removal of any possible singularity with a finite target mode set, the minimal changes in $Z(\beta)$ suggest that the system sensitivity has remained essentially unchanged.

This matter was explored by comparing the performance of an N = 10 and an $N \to \infty$ array in 1/4 the circumference as the size of the target set increased. Input modes of m = -1, 0, and 1 were taken as 100 dB, the array signals were computed and then rounded to the nearest integer dB, to use in solving the array equations for the modal coefficients. Results are shown in Figure 7. It is seen that even when the target set size is as small as 5, the solutions are totally unacceptable for both arrays. (Previous results for 0.1 dB truncation applied to the individual microphones were satisfactory for this target set size.)

Consequently, increasing the number of microphones in an array spanning 1/F of the circumference is insufficient to reduce system sensitivity to input errors, even though the previous singularity has been eliminated.

3.1.3.5 Effect of Increasing Array Length

The effect of increasing array length ($F \rightarrow 1$) on sensitivity of the system remains to be examined. For this purpose, a set of arrays of increasing length, each having a continuous microphone distribution ($N \rightarrow \infty$), was evaluated for the same conditions as in the immediately preceding microphone number evaluation.

For each target mode set size, Figure 8 clearly shows that increasing array length improves performance. However, the required length is essentially a full circumference to assure satisfactory results. For example, with a size of 13 modes, an array spanning 3/4 the circumference is clearly unsatisfactory - a full circumferential array must be used.

With a full 360 degree array, only the requirement that $N > 2m^*$ must be met; further microphones are not needed. For such an array the matrix is the unit diagonal and the system is perfectly conditioned. There seems to be no significant middle ground where a partial array, used to reduce microphone requirements, can be assured of giving satisfactory results. Some additional concepts were explored to see if other means of reducing microphone requirements could be developed - these are described in the following subsections.

3.1.4 Supplementary Methods for Mode Detection

Some additional concepts for overcoming the limitations of the initial partial circumferential array configuration were explored. The basic limitation to be circumvented is the excessive number of microphones required to prevent array matrix singularity and the large array length needed for acceptable sensitivity to input errors. A description of these supplementary concepts follows.

3.1.4.1 Array Signal Power

This concept is addressed to the possibility of reducing the number of microphones needed to prevent singularity of the array matrix. It has been seen that no more than N complex modal coefficients, C_m, can be determined from N complex microphone readings, P_n. Now there are actually 2N independent input measurements - N microphone signal amplitudes and the corresponding N measurements of signal phase. Instead of using these 2N inputs to compute N modal amplitudes and N modal phases, the possibility of computing 2N modal amplitudes, neglecting phase, was examined. (Modal phase is of no interest in any of these circumferential array methods.)

An approach to eliminating phase from consideration is based on the following basic concept:

Let there be a harmonic time signal,

$$e(t) = \text{Re } E(t) = \text{Re } E_o\, e^{-i\omega t} \tag{31}$$

The "power", W, of the signal is defined as the mean-square value

$$W = \lim_{T\to\infty} \frac{1}{T} \int_o^T e^2(t)dt = \frac{1}{2} E_o E_o^* \tag{32}$$

Thus, in the expression for power, the phase of e(t), defined by the angle of the complex quantity E_o, has been eliminated since the real quantity, $E_o E_o^*$, is just the square of the signal amplitude.

This concept will be examined in the context of an arbitrary circumferential array by formulating the array signal power.

When targeted to the mode m = M, the complex array signal is

$$F_M = \sum_m C_m\, Z(m-M)$$

By eq (32), the corresponding signal power is

$$W_M = \frac{1}{2} F_M F_M^* = \frac{1}{2}\left[\sum_m C_m\, Z(m-M)\right]\left[\sum_m C_m\, Z\,(m-M)\right]^*$$

changing indices, and letting $\beta = m - M$ as before gives:

$$W_M = \frac{1}{2}\left[\sum_j C_j\, Z(\beta_j)\right]\left[\sum_k C_k\, Z(\beta_k)\right]^*$$

Separating terms with common and different modal indices,

$$W_M = \frac{1}{2} \sum_{j} C_j C_j^* \, Z(\beta_j) \, Z^*(\beta_j) + \frac{1}{2} \sum_{j \neq k} C_j C_k^* \, Z(\beta_j) \, Z^*(\beta_k) \qquad (33)$$

$$= S_1 + S_2 \qquad (33a)$$

Eq. (33) shows clearly that the array signal power includes in the sum S_1 the desired sum of the modal powers, $C_jC_j^*$ (weighted by the square of the array factor amplitudes). But also present, in the sum S_2, are terms which are cross-powers between pairs of modes. The terms in S_2 thus contaminate the array signal power, W_M. These cross power terms, $C_jC_k^*$ do involve phase angle between modal coefficients and thus prevent attainment of the objective of eliminating the necessity for computing modal phase.

Consequently, the concept of seeking only modal amplitudes, $[C_jC_j^*]^{1/2}$, to reduce the number of unknown quantities, is not feasible for discrete coherent modes.

3.1.4.2 Array with Irregular Spacing and Interpolated Microphone Signals

This array concept was directed to overcoming simultaneously the two limitations imposed by microphone number and array length. The need for array length to reduce sensitivity to input error was satisfied by utilizing the entire circumference, rather than a fraction, 1/F. However, the use of a reasonable number of equally spaced microphones would give an array period too small to prevent aliasing - the first requirement of array design.

If the spacing between microphones is chosen in some irregular pattern, the period of the array factor may be greatly extended. This property may be seen from the expression for $Z(\beta)$ for an array with microphones at arbitrary angles.

Instead of the expression, Eq. (9) for equal spacing,

$$Z(\beta) = \frac{1}{N} \sum_{n=0}^{N-1} \exp i \beta \frac{2\pi}{N} n \qquad (9)$$

the corresponding general form for microphones at arbitrary angles θ_n is

$$Z(\beta) = \frac{1}{N} \sum_{n=0}^{N-1} \exp i \beta \theta_n \qquad (34)$$

Unless the angles θ_n are multiples of some common factor, the value of β required to restore each of the complex numbers, $\exp i \beta \theta_n$, to the same (real, unity) value that exists when $\beta = 0$ will be quite large, and actually may not exist. Depending on details of the distribution of the set $\{\theta_o, \theta_1 \ldots \theta_n\}$, the period of the array factor may extend far beyond the size of the target propagating mode set, thus eliminating aliasing.

In this investigation, little effort was devoted to selecting the set of microphone angles, θ_n, by any systematic algorithm or process, or by any standard random number generation process. Instead, a few sequences of (N=10) angles were selected arbitrarily and used to compute the array factor by Eq. (34). (It will be noted that despite the non-existence of periodicity, $Z(-\beta) = Z^*(\beta)$ still holds.)

The following tabulation gives a set of microphone angles that was used for numerical investigation.

TABLE II

IRREGULARLY SPACED ARRAY ANGLES

Microphone No.	Angle, θ_n	Spacing $(\theta_n - \theta_{n-1})$
0	19.2°	41.2° (#9 to #0)
1	70.1	50.3
2	118	47.9
3	132	14
4	151	19
5	194.3	43.3
6	261	66.7
7	276	15
8	315	39
9	338	23

The amplitude of the resulting array factor is shown in Figure 9. The highly irregular variation of Z with β contrasts with the structured patterns of equi-spaced arrays seen previously. Minor lobe responses peak at irregular values of β and the highest of these are on the order of 5 dB less than the main lobe at $\beta = 0$, compared to about -13 dB for an equi-spaced array. Despite these properties the irregularly spaced array was found to give better performance in some applications.

At this stage, it is not possible to predict in closed form the sensitivity of systems incorporating this array factor. However an evaluation was done, as previously, by the numerical simulation of errors in target mode sets of increasing size. Furthermore, it is now recognized that it is necessary to provide at least as many microphone signal inputs as there are modes in the target set to avoid singularity of the array matrix.

If only 10 microphone signals are available, the array equation system must become singular for target set sizes exceeding 10. To circumvent this limitation, a concept was examined that would supply additional, simulated microphone readings. This simulation was accomplished by using values interpolated between pairs of actual microphones. In this way a total of 20 (or more) values of P_n could be generated for use in forming the array signals F_M.

Depending on details of the interpolation process, it was conjectured that significantly more than 10 linearly independent array signals, F_M, could be formed, thus avoiding the previous singularity.

The following is a summary of the features of this array system:

1. Use of the full circumference - to maximize array length and improve sensitivity to input error.

2. Use of irregular microphone spacing - to prevent aliasing.

3. Use of hypothetical, interpolated signals - to increase the "effective' number of microphones and thus, by avoiding singularity, to increase the allowable number of target modes.

Performance of this array was evaluated using two different sets of input modes: first, modes m = -1, 0, 1 at 100 dB, zero reference phase, and secondly, modes m = 10, 11, 12 at these values.

The circumferential pressure field resulting from m = -1, 0, 1 inputs is shown in Figure 10. This is a standing wave field due to the symmetry of the input. The microphone locations and corresponding pressures are indicated. Interpolated values for points midway between microphones are also shown. Because of the gradual variation of wall pressure with angle, resulting from the low order input mode selection, the interpolated pressures are very close to the true values at the midpoints, and it may be anticipated that the calculated modes will agree satisfactorily with the inputs.

The 10 microphone readings were truncated to 0.1 dB, together with the interpolated pressures, and used to form successive array signals, F_M. As in previous simulations the size of the target set was increased and the array equations were solved for the input modes and the null modes in the set.

Resulting calculations are shown in Figure 11 and indicate satisfactory performance for target mode sets through 20 in size. (The acceptable results obtained when the set size is greater than the total of actual and interpolated pressure is probably fortuitous.)

However, matters are quite different when the procedure is repeated for the high order input modes, m = 10, 11, 12. Figure 12 shows the circumferential variation of the real part of the wall pressure, together with the values at the microphone locations and the interpolated values. Due to the high order modes, there is much greater discrepancy between interpolated and true values than in the previous low order m = -1, 0, 1 case. Similar results are obtained for the imaginary part of the wall pressure.

The results of targeting successively larger mode sets are shown in Figure 13. The performance is unsatisfactory: even for the smallest set size, m = 10, 11, 12, the computed modes differ from the input values by 10 dB. Larger set sizes give still worse sensitivity. Clearly, this behavior results from several large errors in the interpolated pressures which are present when the field fluctuates rapidly with wall position.

For this reason, the concept of using an unequally spaced array supplemented by interpolated pressure readings was found to be unfeasible.

3.1.4.3 Scan of Array Signal

None of the array methods considered thus far were found to be satisfactory. For one or more reasons, in many instances the computed modal coefficients differed unacceptably from the input figures due to an excessive sensitivity to pressure errors.

In an effort to circumvent the problems with computing reasonably accurate modal coefficients, the concept of simply using the array as a scanning filter to indicate locations (in m-space) of dominant modes was examined. If the array method would just indicate the general neighborhoods of dominant modes it might at least serve the purpose of a preliminary survey of the pressure field. These results could then be used as a guide in selecting a specific array geometry to use subsequently for more detailed measurements with a limited number of microphones.

The process involves simply observing the amplitude of the array signal as it is scanned from one end of the complete set of propagating modes to the other, much as is done in sweeping a variable frequency filter applied to a time series. No modal coefficients are to be calculated so the microphone number, as such, is no problem. The question is whether the array signal, which is essentially the modal spectrum convolved with the array factor, can provide a reasonable visual indication of where the dominant modes are located in m-mode space.

Again 10 microphones were established for the array. If these are to be equally spaced, the usual minimum separation for antialiasing applies, indicating the use of only a fraction, 1/F, of the circumference. (If they are distributed evenly in 2π, the array period is 10, and for a signal at m = M, there will be identical peaks at the aliases M $\pm$10, M $\pm$20, etc. rendering the array scan useless.)

F was chosen as 4.1, giving an array factor period of 41 and allowing modes between m = -20 and +20 to be detected without aliasing. The actual mode scan ranged from m = -19 to +19, providing 39 modes to be be scanned. Of these modes, 8 were assigned equal values of 100 dB, zero phase, and the remainder were null. (Note that if but a single mode is assumed to be significant, a scan or sweep of the array signal through the mode range will simply map the array factor.) For the cases presented here, the significant, 100 dB modes were selected for m = -19, -18, -17, -12, -7, -4, -3, and +9.

Figure 14 shows the array factor, $Z(\beta)$, for this array. In Figure 15, the response of the array to the field of the 8 100 dB modes as the array is scanned over $-19 \leq m \leq +19$ is shown, together with the input mode values represented by circles.

In this instance, the array signal prominences around the neighborhoods of m = -18, -12, -3, and +9 do correctly indicate the presence of one or more significant modes in those general locations. There is no clear indication, however, of the input mode at m = -7 and of the total absence of modes between m = -2 and +8 and for m > 9.

The effect of an important change in the input is examined next. For this purpose, the phase of the 100 dB mode at m = -4 is changed to 180 degrees. The resulting array response, Figure 16, shows that the previous prominence in the neighborhood of m = -3 has been replaced with a rather sharp minimum at m = -4. The resulting response thus completely fails to suggest the presence of two consecutive dominant modes in that general location.

Similar calculations were made for these two sets of 8 modal inputs, using a modified form of the array. The modification consisted of applying different weighting values to the microphones in the array. This process, which is called windowing or tapering in digital signal processing and antenna theory, causes a reduction in the minor lobe response of the array factor and a broadening of the main lobe. A description may be found in Section 3.3. At this point it will serve the purpose merely to illustrate the array factor when a weighting schedule called the Blackman window is incorporated in the N = 10, F = 4.1 array. This array factor is displayed in Figure 17 and shows the large reduction in minor lobe response, accompanied by main lobe broadening.

When used to survey the spectrum including the 8 principal modes, all in phase, the array response is as illustrated in Figure 18. This result does not provide a very good indication of the dominant mode locations. The modes around m = -17, -3 and +9 are properly suggested by the response. However, the mode at m = -12 is missed entirely and there is a false signal of dominant modes in the neighborhood of m = +18. Even worse performance is displayed in Figure 19 which gives the array response when the m = -4 mode is shifted 180 degrees.

Finally, the unequally spaced array previously considered having the array factor shown in Figure 9 was applied to the 8 mode, in phase set of inputs. The array response, shown in Figure 20, is seen at a glance to be useless in identifying mode locations.

As a result of this exploration of a variety of array designs and conditions, it is clear that the use of the array signal scan to identify m-neighborhoods of dominant modes is not feasible.

3.1.5 Summary of Feasibility of Partial Circumferential Array Methods

The properties of several methods involving circumferential arrays for mode determination have been found and used to evaluate the feasibility of such methods in experimental programs employing a reasonably small number of microphones. The following array methods were evaluated:

1. Full circumferential array
2. Partial circumferential array
3. Array signal power
4. Irregularly spaced array with interpolated microphone signals
5. Scan of array signal

None of these methods proved feasible for a variety of reasons.

A summary of the deficiencies of the individual methods follows.

1. Full Circumferential Array

This array geometry is the simplest, involving N microphones spaced equally around the full circumference of the fan inlet duct. To prevent aliasing (the irresolvable mixing of the signals from two or more modes) requires that the spacing between microphones be less than one half the shortest circumferential wavelength of the propagating modes. In the case of twice blade passing frequency for the JT9D at approach power, for example, this requirement implies that more than 150 microphones would be needed. Such an excessive number of microphones makes the full circumferential array unfeasible in many engine and fan rig applications, and provided the motivation for exploring other array methods.

2. Partial Circumferential Array

It was found that the number of microphones could be greatly reduced by maintaining a half-wavelength separation over a fraction, 1/F, of the circumference without encountering aliasing. This initially promising concept turned out to have two serious deficiencies: 1. The largest number of modes that could be determined was limited to the actual number of microphones in the array. 2. The sensitivity of the method to small errors in microphone readings was found to be excessive, even when limited to detection of but a few modes, due to insufficient array length. These limitations led to an examination of the additional methods or concepts described below.

3. Array Signal Power

This concept was directed to improving the requirement for large microphone number. From N microphone readings of pressure amplitude and phase 2N known quantities result, and might possibly be used to determine 2N modal amplitudes. To eliminate modal phase, the square of the modal amplitude, or modal power was investigated. Modal power appears in the power of the array signal - unfortunately it was found to be contaminated by cross-power terms between modes. These unwanted terms effectively increased the number of unknown quantities in the system and made the method unfeasible.

4. Irregularly Spaced Array with Interpolated Microphone Readings

This array method was directed to solving both the problems of microphone number and array length: maximum length was achieved through use of the full circumference. Aliasing was prevented by employing an irregular spacing between microphones. The number of microphones was effectively increased by augmenting the actual microphone readings with additional interpolated values. Performance of this system was satisfactory when used in a pressure field having low order circumferential modes. However, when a moderately high order modes were present, the method failed, due to large errors in the interpolated microphone readings. This array concept, therefore, is not feasible.

5. Scan of Array Signal

This method was an attempt to circumvent the problems associated with solving for the numerical values of the modal coefficients. The problem requirements were lowered to simply locating the mode number neighborhoods of dominant circumferential modes. The method consisted of scanning or sweeping the array target through the range of propagating modes and noting where prominences in the array signal occur. Several array designs were examined for a variety of input modes. The output of the array scan did not provide a reliable indication of the dominant modes - even this limited purpose array method is not feasible.

3.2 FAN SPEED CHANGE IN ARRAY USAGE

3.2.1 Objective and Features of the Method

The objective of this study was to determine the feasibility of generating additional data for modal identification, using a limited number of microphones by replicating array information at a plurality of closely-spaced fan speeds. By this means it should be possible, in principle, to solve for a number of modes that is the product of the number of microphones in the array and the number of speeds.

There are several features of this method that differ significantly from the previously considered array systems. One feature that is evident at the outset is that circumferential-radial (m,μ) modes must be considered, and not simply the particular radial mode sum that previously defined the resultant circumferential mode coefficient at the wall in the plane of the circumferential array. To make this point clear, the wall pressure function is examined below.

From Eq. (1), on replacing $C_{m\mu} E_{m\mu}(k_{m\mu} b)$ by $B_{m\mu}$ for simplicity, the pressure for a wall microphone located at (x, θ) is

$$p(x, \theta, t) = \mathrm{Re} \sum_{m} \sum_{\mu} B_{m\mu} \exp i \, (k_{xm\mu} x + m\theta - \omega t), \tag{35}$$

where,

$$k_{xm\mu} = \sqrt{k^2 - k_{m\mu}^2} = \sqrt{(\omega/c)^2 - k^2_{m\mu}} \tag{36}$$

From these expressions it is seen that the effect of changing fan speed (frequency) is to modify the axial wave number, $k_{xm\mu}$, and thus to shift the phase of the local pressure due to the (m,μ) mode through the exponential, $\exp i\, k_{xm\mu} x$. Since the $k_{xm\mu}$ are generally different, each mode will sustain a different phase shift and the resulting sum will change in both amplitude and phase.

The next important aspect of the method is revealed by examining this phase shift in more detail. Consider the exponential or phase factor for an (m,μ) mode in Eq. (35). Changing ω will not affect pressure phase through the factor $\exp i\, m\theta$, nor will the factor $\exp -i\omega t$ alter phase since zero phase is referred to $\omega t = 0, 2\pi$, etc. The factor $\exp i\, k_{xm\mu} x$ is the sole variable affecting phase. Now, if the speed is changed so that the axial wave number changes by $\Delta k_{xm\mu}$, the phase of p changes by $\Delta k_{xm\mu} x$.

Thus the x-coordinate of the microphone enters as a multiplier in determining the local phase shift of a mode when speed changes. In most duct propagation studies x is defined with respect to any convenient, arbitrary origin. Now, since phase shifts with speed must be correctly obtained, it is necessary to replace x by the distance between receiver and mode source. This is an extremely important feature of the method.

It is also necessary to assume that modal amplitude and phase at the source location remain constant over the small speed range to be used.

To clarify matters, it is helpful to consider a simple specific example - detection of two propagating modes. Two methods will be illustrated. In the first, or standard reference case, two microphones are used at a single speed to obtain modal coefficients for two specified (m, μ) modes. The second case illustrates the subject method when applied to the detection of the same two modes by means of data obtained at two adjacent speeds from a single microphone.

Reference Case, Two Microphones, Single Speed

Let the two forward propagating (m, μ) modes have (complex) coefficients, A and B, and wave numbers $k_{xm\mu} = k_A, k_B$; $m = m_A, m_B$. The coordinate origin is downstream of all sources and microphones. The source locations of the modes are x_A, x_B. Two microphones are located at (x_1, θ_1) and (x_2, θ_2). The complex pressures at the microphones are:

$$P_1 = A \exp i \left[k_A (x_1 - x_A) + m_A \theta_1\right] + B \exp i \left[k_B (x_1 - x_B) + m_B \theta_1\right]$$

$$P_2 = A \exp i \left[k_A (x_2 - x_A) + m_A \theta_2\right] + B \exp i \left[k_B (x_2 - x_B) + m_B \theta_2\right] \qquad (37)$$

The following substitutions will greatly simplify (37):

Let $x_2 - x_1 = \Delta x$, $\theta_2 - \theta_1 = \Delta\theta$, and

Let $A \exp i \left[k_A (x_1 - x_A) + m_A \theta_1\right] = A'$

$B \exp i \left[k_B (x_1 - x_B) + m_B \theta_1\right] = B'$

Then, the pressures become

$$P_1 = A' + B'$$

$$P_2 = A' \exp i \left[k_A \Delta x + m_A \Delta\theta\right] + B' \exp i \left[k_B \Delta x + m_B \Delta\theta\right] \qquad (38)$$

Since k_A, k_B, m_A, m_B, Δx and $\Delta\theta$ are known, Eqs. (38) can be readily solved for A' and B'. Notice that A' and B' are the modal coefficients with phase evaluated at mic location 1. Most importantly, the actual source locations of the modes, x_A and x_B, have been eliminated from the problem. This will not be so for the speed change method.

Speed Change Method - Single Microphone - Two Speeds

Superscripts 1 and 2 denote the two speeds. The single microphone is at $x = x_o$, $\theta = 0$. The wave numbers k_{xmn} are $k_A{}^1$ and $k_B{}^1$ for the two modes at speed 1 and $k_A{}^2$ and $k_B{}^2$ at the second speed. Denote the source to microphone distance, $(x_o - x_A)$ by S_A and $(x_o - x_B)$ by S_B. The complex pressures at the microphone for the two speeds are:

$$p^1 = A \exp i\, k_A{}^1 S_A + B \exp i\, k_B{}^1 S_B$$
$$p^2 = A \exp i\, k_A{}^2 S_A + B \exp i\, k_B{}^2 S_B \qquad (39)$$

These would appear to be similar to the equation (38) for the reference, two microphone case. Each is a pair of linear equations in the complex modal quantities with coefficients that are unit complex numbers. However, in the speed change method the microphone to source distances S_A and S_B are involved in the coefficients. These are generally unknown quantities, in contrast to the coefficients in Eqs. (38). No manipulation will remove them from the problem, in contrast to the two microphone case.

Consequently, to solve for the four unknown quantities in Eqs. (39) requires information to be obtained at two additional speeds. For simplicity, let expi S_A be denoted by U and expi S_B = V. The pressures at each of these four speeds become:

$$p^1 = A\, U^{k_A{}^1} + B\, V^{k_B{}^1}$$
$$p^2 = A\, U^{k_A{}^2} + B\, V^{k_B{}^2}$$
$$p^3 = A\, U^{k_A{}^3} + B\, V^{k_B{}^3} \qquad (40)$$
$$p^4 = A\, U^{k_A{}^4} + B\, V^{k_B{}^4}$$

The above is a non-linear system of equations with four unknowns, A, B, U, and V. A solution can be obtained by iterative means for this case, but for larger systems, the development of an efficient iterative method would require significant effort.

Generally, since each mode has a different source location, the number of unknown variables is twice the number of propagating modes, and the number of fan speeds at which data must be taken is twice as many as would be required if the source locations were known or did not enter the problem. This means that if it can be assumed that mode amplitudes and phases remain constant at their source over some small speed range, the increments available between successive speed settings are reduced and the factors $U^{k}A$ and $V^{k}B$ do not change as much as would otherwise be the case. It may be expected that the conditioning of Eqs. (40) is adversely affected as a result.

Additional problems remain. Suppose, for illustration, that a solution for U and V in Eqs. (40) has been obtained. (This can be done by eliminating A and B algebraically and then solving the resulting pair of non-linear simultaneous equations in U and V by iteration.) Two of the Eqs. (40), say P^{1} and P^{4}, then provide a linear system from which A and B are obtained. In previous array equations the coefficients of the unknown modes were subject to very small errors compared to the pressure measurement error. In contrast, in the speed change method the equivalent coefficients, functions of U and V, will contain significant errors since they have been obtained from equations that contain the error-prone measured pressures. This new source of error will further degrade the accuracy of the resulting modal coefficients.

It remains to explore numerically some aspects of the speed change method in order to evaluate its feasibility. This investigation is described in the next section.

3.2.2 Application of Speed Change Method to the 10-inch Fan Rig

The purpose of this investigation was to develop an array method incorporating speed changes which could be used to determine the propagating mode structure in the 10-inch fan rig inlet duct. The sensitivity of this system to pressure measurement errors was evaluated by computer simulation, thus providing a measure of the feasibility of the method.

Modes of twice blade passage frequency at a rig speed of 6000 rpm are to be detected. Only those modes that propagate or decay less than 40 dB in a distance of one duct radius are included. Table III lists the number of such modes that must be identified.

TABLE III

NUMBER OF MODES IN 10-INCH RIG
(2 BPF, 6000 rpm, kb = 15.16, x/b = 1)

Circumferential Wavenumber (±) m	Number of μ modes
0	4
1	3
2	3
3	3
4	3
5	3
6	3
7	2
8	2
9	1
10	1
11	1
12	1
13	1

Total number of modes, including forward and reverse spin = 58

A total of 58 modes must be found. It has been seen that, in practice, the source locations of these modes enter into the problem as additional unknowns. To greatly simplify matters here, it is assumed that all 58 modes have a single known source location - the plane of the fan blade leading edge. This assumption causes the array equations to be linear in the unknown modal coefficients and allows a routine solution. If the sensitivity of this system is poor the method can be judged unfeasible at that point. If, on the other hand, the sensitivity is acceptable, further investigation would be needed to determine the effects of having unknown source locations in an actual test case.

For illustrative purposes the number of microphones to be used is taken as 20, about one-third the total number of modes. If these microphones were distributed arbitrarily over the duct surface, each mode would contribute to each microphone signal. There would thus be 20 equations in 58 modal coefficients. By running at 3 different speeds, 60 equations would be generated for determining the 58 unknowns. Such a large system is unattractive.

However, if the microphones are arranged in a complete, equi-spaced, full circumferential array, the system can be decoupled into a number of independent sets of equations, each such sub-set involving a comparatively small number of modes. This decoupling results from the modal filtering property of the array - only the target circumferential modes and their

possible aliases contribute to the array signal. Thus, when the circumferential array is targeted to the m = M modes, the array signal is:

$$F_M = C_{M-20} + C_M + C_{M+20}$$

$$\text{where } C_M = \sum_{\mu} B_{M\mu} \exp i\, k_{xM\mu}\, x \qquad (41)$$

$$C_{M-20} = \sum_{\mu} B_{(M-20)\mu} \exp i\, k_{x(M-20)\mu}\, x$$

$$C_{M+20} = \sum_{\mu} B_{(M+20)\mu} \exp i\, k_{x(M+20)\mu}\, x$$

and x denotes the source to array distance, assumed known and common to all modes. The aliased modes M $\pm$20 are not present for all target M, and higher aliases at M $\pm$40, etc. always decay. A common known source distance is taken as 1 radius, x = b, for all modes. The following Table IV identifies each of the forward spin target M-modes together with their aliases (where they propagate) and the associated radial modes that contribute to the array signal.

TABLE IV

MODES CONTRIBUTING TO ARRAY SIGNAL

Target M	Aliases	Number of μ-Modes For Target M	For Alias	Total
0	None	4	-	4
1	None	3	-	3
2	None	3	-	3
3	None	3	-	3
4	None	3	-	3
5	None	3	-	3
6	None	3	-	3
7	-13	2	1	3
8	-12	2	1	3
9	-11	1	1	2
10	-10	1	1	2
11	-9	1	1	2
12	-8	1	2	3
13	-7	1	2	3

Table IV clearly shows the advantage of arranging the microphones in a circular array. Except for the axi-symmetric M = 0 modes, there are at most 3 modes contributing to each array signal, in contrast to 58 for each microphone in an arbitrary arrangement. This means that only three speed settings are needed to obtain the $B_{M\mu}$ modal coefficients. To illustrate, with the array

targeted M = 8, aliased by M = -12, the array equations resulting from 3 speeds are:

$$F_8^1 = B_{8,0} \text{ expi } k^1_{x8,0}x + B_{8,1} \text{ expi } k^1_{x8,1}x + B_{-12,0} \text{ expi } k^1_{x-12,0}x$$

$$F_8^2 = B_{8,0} \text{ expi } k^2_{x8,0}x + B_{8,1} \text{ expi } k^2_{x8,1}x + B_{-12,0} \text{ expi } k^2_{x-12,0}x \qquad (42)$$

$$F_8^3 = B_{8,0} \text{ expi } k^3_{x8,0}x + B_{8,1} \text{ expi } k^3_{x8,1}x + B_{-12,0} \text{ expi } k^3_{x-12,0}x$$

The sensitivity of such array equations to errors in the signals, F_M, was explored by numerical simulation. Calculations were made for several sample sets of modes selected from Table IV. These modal sets are listed in Table V.

TABLE V

SELECTED MODE SETS

Case	(M, μ) Modes in Array Signal		
a	(1, 0)	(1, 1)	(1, 2)
b	(4, 0)	(4, 1)	(4, 2)
c	(6, 0)	(6, 1)	(6, 2)
d	(8, 0)	(8, 1)	(-12, 0)
e	(11, 0)	(-9, 0)	

Calculations were made for two ranges of speed variation - 5 percent and 10 percent, taken downward from 6000 rpm. With 3 modes per set as a typical value, calculations were made for the 10 percent range, at speeds of 6000, 5700, and 5400 rpm, and for corresponding values in the 5 percent case of 6000, 5850, and 5700 rpm.

Note that the largest number of modes in any target set determines the size of the speed increments. If, for example, a 10-microphone array were to be used, it turns out that, because of the increased M-mode aliasing, 5 or 6 (M, μ) modes would be present in each target set. Consequently, the speed differences between data points spread over a 10 percent range would drop from 300 rpm to 150 rpm. It can be appreciated that the solution accuracy would be affected adversely.

The accuracy or sensitivity of the 5 sample systems defined by cases a through e in Table V was examined in the following way:

Values of the $B_{M\mu}$ were chosen, and by means of equations corresponding to the illustrated Eq. (42), values of the array signal, F_M, were computed at each of the 3 rig speeds for speed ranges of 5 percent and 10 percent.

The effect of data errors that would be present in an actual test was simulated by adding 0.5 dB to 1 of the 3 array signals. (No phase errors were introduced.) The system of 3 equations was then solved to find the $B_{M\mu}$ values that would produce the modified array signals. The $B_{M,\mu}$ thus computed were compared with the original input values to provide a measure of the system sensitivity.

This procedure was repeated, applying the 0.5 dB error to each of the 3 array signals in turn.

Further, two types of input modal coefficient sets were selected. In the first, each of the 3 input $B_{M\mu}$ were taken equal at 74 dB (1 dyne per square cm) and zero phase. In the second set of inputs only 1 of the 3 $B_{M\mu}$ was taken as 74 dB, the others were null.

Table VI shows the results for the case of all 3 input modes equal at a level of 74 dB. The calculated $B_{M\mu}$ are listed, corresponding to successive application of 0.5 dB array signal errors at each of the 3 speeds.

TABLE VI

CALCULATED MODAL COEFFICIENTS $B_{M\mu}$ (dB) WITH 0.5 dB ERROR ADDED TO ARRAY SIGNAL

			10% Speed Range Speed at which error added to F_M			5 % Speed Range Speed at which error added to F_M		
Case	Modes	Input $B_{M\mu}$ (db)	6000	5700	5400	6000	5850	5700
	(1, 0)	74	75.5	80.4	73.4	88.5	94.0	87.6
a	(1, 1)	74	84.2	83.8	83.1	95.1	99.4	94.3
	(1, 2)	74	68.6	74.1	67.6	82.4	88.1	81.9
		(all cases)						
	(4, 0)		65.8	82.4	68.5	86.7	109.3	84.0
b	(4, 1)		80.3	81.4	78.2	92.7	113.2	90.9
	(4, 2)		72.0	77.6	72.4	74.5	101.1	71.1
	(6, 0)		74.0	74.9	74.0	73.4	76.2	73.5
c	(6, 1)		74.0	75.2	73.9	75.5	72.5	76.2
	(6, 2)		73.2	75.9	73.0	73.8	75.0	73.7
	(12, 0)		74.6	76.1	71.5	82.4	82.3	82.7
d	(8, 0)		74.2	74.1	74.2	72.5	76.7	72.4
	(8, 1)		73.9	76.8	71.8	83.3	82.7	83.0
	(-11, 0)		74.3	74.3	-	74.8	75.0	-
e	(9, 0)		74.3	74.3	-	74.2	75.0	-

If results that are within about 2 dB of the 74 dB input values are considered acceptable, 3 of the 5 sample cases are acceptable in the 10 percent speed range, and only 2 are acceptable when the speed range is reduced to 5 percent. Roughly, of the total number (27) of sets of equations that would have to be processed in a 10-inch rig test, something like one half of them would be expected to give modal coefficients that are excessively in error. Further, some of the errors would be as large as 10 dB with the 10 percent speed range, and more using the 5 percent range.

Confirmation of this unsatisfactory sensitivity is provided by the following Table VII. In these cases only 1 of the 3 possible modes contributing to the array signal is given a 74 dB input level. A suggested criterion for judging the results of the calculation is that the corresponding calculated coefficient should be roughly 74 $\pm$2 dB and, further, that the other calculated coefficients should be significantly lower, say no larger than about 54 dB.

TABLE VII

CALCULATED MODAL COEFFICIENTS $B_{M\mu}$ (dB) WITH 0.5 dB ERROR ADDED TO ARRAY SIGNAL

			10% Speed Range Speed at which error added to F_M			5 % Speed Range Speed at which error added to F_M		
Case	Modes	Input $B_{M\mu}$ (db)	6000	5700	5400	6000	5850	5700
	(1, 0)	-	75.5	80.4	73.4	88.5	94.0	87.6
a	(1, 1)	74	84.2	83.8	83.1	95.1	99.4	94.3
	(1, 2)	-	68.6	74.1	67.6	82.4	88.1	81.9
	(4, 0)	-	67.1	70.9	63.4	80.5	85.7	79.0
b	(4, 1)	74	78.1	64.6	77.3	86.5	88.0	85.6
	(4, 2)	-	56.6	61.9	55.2	71.7	77.4	71.1
	(6, 0)	-	29.6	54.2	54.6	56.1	56.8	58.9
c	(6, 1)	74	74.0	74.3	74.3	74.9	72.5	75.0
	(6, 2)	-	49.7	54.5	47.5	44.1	49.6	43.1
	(-12, 0)	-	62.5	62.2	63.1	79.3	83.6	76.4
d	(8, 0)	74	74.2	74.0	74.2	73.1	76.3	72.9
	(8, 1)	-	65.1	61.1	63.8	79.8	84.3	77.2
	(-11, 0)	74	74.2	Not	-	74.3	74.3	-
e	(9, 0)	-	74.3	Avail.	-	56.9	56.9	-

As with the previous equi-mode cases, only about half the sample cases indicate adequate accuracy.

A final supportive indication of the system sensitivity is provided by the condition numbers of the system matrices, which are listed below in Table VIII.

TABLE VIII

MATRIX CONDITION NUMBERS

Case	10% Speed Range	5% Speed Range
a	162	391
b	51	302
c	7	9
d	12	50
e	1.2	5

It will be recalled that the condition number of a matrix provides a measure of the magnification of input errors in affecting output accuracy. A comparison of the condition numbers in Table VIII with the modal coefficient solutions in Tables VI and VII shows that the unsatisfactory calculated coefficients correlate with relatively high condition numbers.

The basic reason that many of the sampled case systems are poorly conditioned may be found from an examination of the coefficients, expi $k_{xM\mu}x$, in equations (41) or (42). These unit complex numbers have the effect of rotating the modal coefficients $B_{M\mu}$ through an angle of $k_{xM\mu}x$ radians. If two or more modes in the array signal have comparable values of $k_{xM\mu}x$, then as rig speed is changed, the relative phase between these modes will not be large and it is difficult to separate accurately the contributions of these modes to the array signal. In the case of common source location, x, this ill-conditioned situation prevails when the frequency is high compared to the mode cutoff frequencies, or when the cutoff frequencies are approximately equal, as may be seen from Eq. (36), $k_{xm\mu} = \sqrt{k^2 - k_{m\mu}^2}$. In the sample case (a) tabulated above, it turns out that the relative phase between modes (1, 0) and (1, 1) changes by only about 4 degrees for each of the speed increments in the 10 percent range. It is clear that this small relative phase change leads to a poorly conditioned set of array equations.

On the basis of the sample cases evaluated for the 10-inch rig, together with a comparable application to a full-scale fan, it has been found that the array equations are prone to ill-conditioning, leading to unacceptably large errors in the modal coefficients.

Feasibility of Array With Speed Change Method

Several properties of this method have been determined and were found to have an adverse effect on the feasibility of obtaining satisfactory solutions for the modal coefficients. A summary of these properties follows:

1. In contrast to other array systems, in the speed change method the source locations of the (m, μ) modes enter into the problem as additional unknowns, thus requiring more array equations to be formed than implied by the number of unknown modes.

2. The array equations are non-linear. The coefficients of the modal amplitudes are exponential functions of the unknown source locations. Consequently, an efficient iterative method for the solution of the equations would have to be developed. By means of such a method the coefficients of the unknown modes in the array equations can be obtained. However, they will contain substantially larger errors than the corresponding coefficients in other array methods and will therefore adversely affect the accuracy of the solution for the unknown modal amplitudes.

3. In addition, after the source locations have been determined, the resulting equations for the modal amplitudes are quite likely to be ill-conditioned, even if the source locations are assumed to be error-free.

4. The foregoing results are based on the assumptions that modal amplitude and phase remain constant over the speed range used, and that the source locations also are fixed. These assumptions may not hold in practice. In principle, the method could be extended to provide for variations in source properties, but the additional unknown parameters required in such a formulation could only increase the difficulties that have been previously described.

For these reasons, the use of speed changes with circumferential arrays -- a method designed to reduce the required number of microphones -- is found to be unfeasible.

3.3 CUTOFF RATIO ARRAYS

3.3.1 Background

The cutoff ratio, $\xi_{m,\mu}$, of an acoustic mode plays a prominent role in fan noise studies. For example, at zero Mach number, the angle of peak far field radiation, $\alpha_{m\mu}$ is given simply by

$$\sin \alpha_{m,\mu} = 1/\xi_{m\mu} \tag{43}$$

Thus, all modes having an essentially common cutoff ratio combine to determine the far field at that corresponding angle. Design of sound-absorbing duct liners also depends on a knowledge of how the modes are distributed with respect to cutoff ratio. Liner performance is a function of the direction the wave makes with respect to the duct surface. The angle between modal wavefront and liner surface is given by

$$\cos \gamma_{m\mu} \approx \frac{1}{\xi_{m,\mu}} \sqrt{1 - \frac{1}{M^{*2}_{m\mu}}} \tag{44}$$

where $M^*_{m\mu}$ is the tangential wall Mach number of the (m, μ) mode at cutoff. (Ref. 12)

Thirdly, the acoustic power flux in the duct can be expressed as

$$\Pi_{m\mu} = \frac{1}{2\rho c} \pi b^2 \sqrt{1 - 1/\xi^2_{m\mu}} \left[1 - \frac{1}{M^{*2}_{m\mu}}\right] |B_{m,\mu}|^2 \tag{45}$$

where $|B_{m,\mu}|$ is the modal amplitude at the duct wall.

Thus, far field directivity, wall incidence angle, and acoustic power flux, all depend on cutoff ratio. (In addition, the characteristic Mach number $M^*_{m\mu}$ also is needed to define wall angle and power.)

Consequently, it is important to determine means for measuring the distribution of duct modes with respect to cutoff ratio. The appropriate measure of a set of modes having common cutoff ratio must be selected. From the expression for power, Eq. (45) it is seen that this measure may be taken as the sum of the $|B_{m\mu}|^2$ in a band $\Delta\xi$ wide centered on some value of ξ. The resulting distribution could be illustrated, for example by Figure 21.

It should be noted that the required quantity for which the distribution is needed is the sum of the squares of the modal coefficients, which is a measure of intensity. The sum, $\sum B_{m\mu}$ involving the complex quantities $B_{m\mu}$, is not meaningful in the context of this investigation since it involves the relative phase of the modes in the band $\Delta\xi$.

The desired quantity, $\sum |B|^2$ in a band $\Delta\xi$, will be called modal power for convenience, and to distinguish it from acoustic power flux, Eq. (45). An account of the investigation of wall-mounted microphone arrays that would define the distribution of modal power with respect to cutoff ratio is now given.

3.3.2 Derivation of Array Equations

The basic type of microphone arrangement needed to enhance the set of modes having a selected, common cutoff ratio is an axial array. This requirement may be deduced from the equation for the pressure field at the wall:

$$p\ (x, \theta, t) = \mathrm{Re} \sum_{m,\mu} B_{m\mu}\ \mathrm{expi}\ (k_{xm\mu} x + m\theta - \omega t) \tag{46}$$

where the axial wavenumber, $k_{xm\mu}$, is

$$k_{xm\mu} = \sqrt{k^2 - k_{m\mu}^2} = k\sqrt{1-1/\xi_{m\mu}^2} = ka_{m\mu} \tag{47}$$

All modes having common $\xi_{m\mu}$ thus also have common $k_{xm\mu}$. Since the axial phase velocity, $\omega/k_{xm\mu}$, will also be common, an axial array incorporating a progressive time delay will track the corresponding set of modes and will tend to filter out other modes traveling at different axial velocities.

Characteristics of the axial array will now be determined. Let the array be located at $\vartheta = \theta_o$, with the first microphone in the array positioned at $x = x_o$ and the separation between microphones = Δx, as illustrated in Figure 22.

From Eq. (46) the pressure at the n-th microphone is

$$\begin{aligned} p_n &= \mathrm{Re} \sum_{m,\mu} B_{m\mu}\ \mathrm{expi}\ \left[k_{xm\mu}\ (x_o + n\Delta x) + m\vartheta_o - \omega t\right] \\ &= \mathrm{Re} \sum_{m,\mu} B_{m\mu}\ \mathrm{expi}\ (k_{xm\mu} x_o + m\theta_o)\ \mathrm{expi}\ (k_{xm\mu}\ n\Delta x - \omega t) \end{aligned} \tag{48}$$

Let this signal be delayed in proportion to the distance from the first microphone: $\Delta t = \eta_x n\Delta x$, where η_x is the delay rate. The delayed signal, p'_n, is thus

$$p'_n = \text{Re} \sum_{m,\mu} B_{m,\mu} \exp i\,(k_{xm,\mu} x_o + m\theta_o) \exp i \left[k_{xm,\mu} n\Delta x - \omega\,(t + \eta_x n\Delta x)\right]$$

$$= \text{Re}\, \exp -i\omega t \sum_{m,\mu} B_{m,\mu} \exp i\,(k_{xm,\mu} x_o + m\theta_o) \exp i \left[(k_{xm,\mu} - \omega\eta_x)\, n\Delta x\right]$$

Also, let this pressure be weighted by a (real) factor, W_n. Then, summing over the N microphones in the array and averaging gives the array signal, $f_{\eta x}(t)$:

$$f_{\eta x}(t) = \text{Re}\, \exp -i\omega t \sum_{m,\mu} B_{m,\mu} \exp i\,(k_{xm,\mu} x_o + m\theta_o)\, Z_{m,\mu} \qquad (49)$$

where $Z_{m,\mu}$, the (complex) array factor is:

$$Z_{m,\mu} = \frac{1}{N} \sum_{n=0}^{N-1} W_n \exp i \left[(k_{xm,\mu} - \omega\eta_x)\, n\Delta x\right] \qquad (50)$$

From Eq. (50) it can be seen that when the delay rate η_x is set to target modes having a particular $k_{xm,\mu}$ by making $(k_{xm,\mu} - \omega\eta_x) = 0$ all the terms in the sum are real. If $W_n \equiv 1$ then $Z_{m,\mu} = 1$. With this η_x, modes with $k_{xm,\mu}$ different from the target will produce at each microphone a different complex number, $\exp i\,[(k_{xm,\mu} - \omega\eta_x)\, n\Delta x]$, so that their sum will be less than one.

The design objective for the array study is to determine the parameters N (number of microphones), Δx (spacing), and W_n (weighting function) such that $Z_{m,\mu}$ will be essentially unity over the target cutoff ratio bandwidth, and will be negligible outside this band.

It will be helpful to modify the argument of the exponential function in Eq. (50) by means of the following substitutions:

Let $\Delta x = L/N$, where L is the effective length of the array (51a)

$$\omega = 2\pi c/\lambda \tag{51b}$$

$$k = 2\pi/\lambda \tag{51c}$$

$$k_{xm\mu} = k\sqrt{1-1/\xi_{m\mu}^2} = k\, a_{m\mu} \tag{51d}$$

$$a_{m\mu} = \sqrt{1-1/\xi_{m\mu}^2} \tag{51e}$$

Then Eq. (50) takes the form:

$$Z_{m\mu} = \frac{1}{N}\sum_{n=0}^{N-1} W_n \exp i\left(\beta_x \frac{2\pi}{N} n\right) \tag{52}$$

where

$$\beta_x = (a_{m\mu} - c)\frac{L}{\lambda} \tag{53}$$

The advantages of this form over Eq. (50) include the following: The important parameter, L/λ appears explicitly. Secondly, the parameter $a_{m\mu} = \sqrt{1-1/\xi_{m\mu}^2}$ encompasses all propagating modes in a range from 1 for highly propagating modes, through 0 at cutoff, to -1 for highly propagating reflected modes. It has been shown (Ref. 12) that $a_{m\mu}$ is the cosine of the angle made between the normal to the modal wavefront at the duct wall and the axial direction of the array. Consequently, the array may be considered to track modes on the basis of their direction with respect to the array. A further advantage of Eq. (52) over Eq. (50) is that the closed form expression for the sum in Eq. (52) may be had by replacing β by β_x in the equation that was previously obtained for the full circular array.

In the case of uniform microphone weighting, $W_n = 1$, the closed form of the array factor, $Z_{m\mu}$, is

$$Z_{m\mu} = \frac{\sin \beta_x \pi}{N \sin \beta_x \pi/N} \exp i \frac{N-1}{N} \beta_x \pi \tag{54}$$

where $\beta_x = (a_{m\mu} - c\eta_x)\, L/\lambda$ (53)

and $a_{m\mu} = \sqrt{1-1/\xi_{m\mu}^2}$ (51e)

3.3.3 Characteristics of the Axial Array

The performance of the array in enhancing the target modes and excluding other modes may be determined by examining the expression for the array factor, $Z_{m\mu}$. The case of equal weighting, $W_n = 1$ will be considered first.

3.3.3.1 Periodicity

The periodic nature of the array factor is crucial to designing the array so that aliasing or false indications are avoided. Eq. (52) most clearly shows the periodicity: It is well known that the complex sum,

$$\frac{1}{N} \sum_{n=0}^{N-1} \text{expi}\ (\beta_x \frac{2\pi}{N} n)$$

has value 1 for $\beta_x = 0, \pm N, \pm 2N$, etc., and is zero for all other integer values of β_x. For non-integer β_x, calculation using Eq. (54) shows a set of minor peaks at approximately $\beta_x = 1.5, 2.5$, etc. Thus $Z_{m\mu}$ starts with a major peak at $\beta_x = 0$, has diminishing minor peaks intersperced with zeros as β_x increases, and returns to a major peak at $\beta_x = N$, the period of the array factor.

This behavior is illustrated in Figure 23 for the cases of 5 and 10 microphone arrays. The largest of the minor lobes is about 13 dB below the major peak. It may also be seen from Eq. (54) that there is a linear phase shift in Z as β_x departs from zero and that $Z_{m\mu}(-\beta_x) = Z^*_{m\mu}(\beta)$.

The most important property of the periodicity is that the period in β_x is exactly equal to N, the number of microphones, and can only be increased by employing more microphones in the array. To determine the significance of this period, the range of the target modes must next be examined.

3.3.3.2 Range of Target Modes

It has been mentioned that all propagating modes (both direct and reflected) lie between values of $a_{m\mu} = \sqrt{1-1/\xi_{m\mu}^2}$ of +1 and -1. No matter which value of a is targeted by selecting η_x such that $(a_{m\mu} - c\eta_n) = 0$, all the existing modes are bracketed in a range of 2 units of a. Now, from Eq. (53) it is seen that with a 2 unit range of $(a_{m\mu} - c\eta_x)$ the corresponding range of β_x is $2\, L/\lambda$. That is, all the modes lie in a range of β_x of $2\, L/\lambda$ units long.

Figure 24 illustrates how a 10-microphone array would be used to target successively modes that are highly cut on, modes near cutoff, and highly cut on reflected modes. A value of 3 is illustrated for L/λ, giving a mode range of 6 units in β_x.

It can be seen that by changing the delay rate, Ω_x, the array is made to track or enhance modes over the entire range of direction. There is some contamination of the desired signal, represented by the major lobe, by the minor lobe responses to other modes, but as will be shown later this effect can be reduced appreciably by a different selection of the microphone weighting factors, W_n.

3.3.3.3 Aliasing

The range of the target modes with respect to β_x, $2\ L/\lambda$, together with the array period, N, determine the requirement for prevention of aliasing. Aliasing is best described by means of a figure corresponding to Figure 24. The following situation will be described for illustration: An array 3 wavelengths long, as in Figure 24, will be examined. Now, however, the number of microphones will be reduced from 10 to 5. Since L/λ is the same, the range of the modes is retained at 6 units. The array period, N, is now half its previous values.

Figure 25 shows this array tracking the same types of modes as illustrated previously. In Figure 25b the delay rate is set such that $\Omega_x = 1$, causing the array to enhance those modes with $a_{m\mu} \approx 1$. However, at the same time, because the array period, N, is now 5, another major lobe at $\beta_x = -5$ is within the mode range. As shown, this major lobe enhances modes at $a_{m\mu} = -2/3$ equally well as the target modes at $a_{m\mu} = 1$. This phenomenon is called "aliasing". Figure 25c displays the situation when tracking broadside modes near cutoff with Ω_x set to zero. Here the major lobes 5 units on either side of the target fall outside the range of the modes and cause the array to transmit no aliased signal. Figure 25d shows the array being used to track reflected modes near $a_{m\mu} = -1$. As in Figure 25b, aliasing of the target signal is produced by the major lobe at $\beta_x = 5$, transmitting unwanted signals from the forward modes around $a_{m\mu} = 1$.

It is evident that aliasing will be avoided completely when the distance between major lobes - the array period - is larger than the range of the target modes. This requirement is expressed simply as

$$N > 2\ L/\lambda \tag{55a}$$

or

$$\Delta x = L/N < \lambda/2 \tag{55b}$$

Thus the separation between microphones, $\Delta x = L/N$, must be less than one half the free space wavelength to prevent aliasing.

An argument could be made that this requirement is unnecessarily severe: aliasing first occurs when the highly propagating reflected modes ($a_{m\mu} \approx -1$) contaminate the signal with the array targeted to the direct, forward modes at $a_{m\mu} \approx +1$. But, in normal inlets, highly propagating modes radiate quite freely from the inlet with very little reflection. If we assume that modes radiating to the far field at less than 45 degrees to duct axis ($a_{m\mu} = 0.707$) are not significantly reflected, then the range of $a_{m\mu}$ in which significant modes can be expected is from +1 to -0.707 or 1.707 units of range of $a_{m\mu}$. To prevent aliasing under this condition requires (roughly) that $N > 1.707\ L/\lambda$. Compared to the original requirement of $N > 2\ L/\lambda$, this relaxed requirement gives a saving of only 0.293 out of 2, or 15 percent in the number of microphones. This small saving does not justify the risk involved in getting contaminated signals.

It will be understood in all that follows that the full anti-aliasing requirement is incorporated in the array design. The question of array resolution is examined next.

3.3.3.4 Array Resolution and Modal Density Functions

The resolving power of the array or its ability to discriminate between modes having neighboring values of $a_{m\mu}$ obviously depends on the sharpness of the main lobe of the array factor. Further, the width of the main lobe is not in itself the criterion but rather the width as a fraction of the range of the entire set of modes. Since the width of the main lobe is always 2 units in β_x and the target mode range is $2\ L/\lambda$ in β_x the ratio, r, is just

$$r = \frac{\lambda}{L} \tag{56}$$

This ratio is somewhat more convenient than its reciprocal since it gives directly the fraction of the target mode range that is enhanced by the array.

It is thus seen that for a given operating frequency, corresponding to the wavelength, λ, the only way to improve resolving power is to increase the length of the array. At the same time, however, the number of microphones must be increased so that their density is not reduced, which would produce aliasing. Thus, increased resolution requires both added length and proportionally more microphones.

Array factors of increasing resolution are illustrated in Figure 26. In each case, as L/λ is increased, the minimum number of microphones required to prevent aliasing $N = 2\ L/\lambda + 1$, is used.

It might appear that the $L/\lambda = 8$ array, employing 17 microphones, has a reasonably sharp response since $r = 1/8$. However, the following considerations should be examined.

First, half of the mode range, from $a_{m\mu} = 0$ to -1 is occupied only by modes reflected back from the inlet. These modes are of very little interest compared to the direct forward propagating modes from $a_{m\mu} = 0$ to +1. Consequently the array resolution r is more realistically 1/4 rather than 1/8.

Secondly, the way the forward modes are distributed with respect to the parameter $a_{m\mu}$ is significant. Rice has shown (Ref. 13) that the fractional density of propagating modes with respect to cutoff ratio can be approximated by

$$D_\xi = 2/\xi^3 \tag{57a}$$

The modal density function D_ξ is defined such that:

Fraction of modes between cutoff ratios ξ_1 and ξ_2 =

$$\int_{\xi_1}^{\xi_2} D_\xi \, d\xi \tag{57b}$$

As has been seen, the behavior of the axial array is not a direct function of ξ but rather of a, where $a = \sqrt{1-1/\xi^2}$. Consequently an estimate is required of how the forward propagating modes are distributed with respect to a rather than ξ.

This distribution, the density with respect to a, may be obtained from D_ξ, the density with respect to ξ, by use of the chain rule:

$$D_a = D_\xi \left[\frac{d\xi}{da} \right] \tag{57c}$$

Since $a^2 = 1 - 1/\xi^2$

$$2a = 2/\xi^3 \frac{d\xi}{da} \quad , \quad \frac{d\xi}{da} = a\xi^3$$

Thus, from Eq. (57a) and Eq. (57c)

$$D_a = \frac{2}{\xi^3} \cdot a\xi^3 = 2a \tag{57d}$$

This is a very simple linear density function showing that for a bandwidth Δa near cutoff ($a = 0$), there are very few modes compared with the number of modes in a Δa bandwidth near $a = 1$. In fact, 3/4 of the forward propagating modes lie between $a = 1/2$ and $a = 1$.

Because of this concentration of modes in the range $1/2 < a < 1$, it is reasonable to stipulate that an array provides "reasonable" resolution over the range $1/2 < a < 1$ rather than defining resolution with respect to the full forward range, $0 < a < 1$, or the total range of 2 for both forward and reflected modes.

The $L/\lambda = 8$ array of Figure 26, therefore, may be said to have the following resolutions in terms of the full set of modes and the more restricted sets:

Mode Set Range, Δa		Resolution: $\frac{\text{Main lobe width}}{\Delta a}$ for $L/\lambda = 8$ array
All modes	2	1/8
Forward modes	1	1/4
3/4 majority	1/2	1/2

These figures clearly show that the $L/\lambda = 8$ array, which might be considered to have reasonably good resolving power based on the range of all modes, has a resolution of only 1/2 in the range over which 75 percent of the forward propagating modes exist.

Accordingly, if an "effective" resolution of 1/8 is considered "reasonable", the array should have an L/λ of 32 rather than 8 and the microphone requirements, $N > 2L/\lambda$, increase from 17 to 65!

These requirements should be examined in the context of the 10-inch fan rig geometry: At a speed of 6000 rpm, the frequency of twice blade passage rate is approximately 6000 Hz, corresponding to a wavelength, λ, of about 2 inches. With an L/λ of 32, the array length required for 1/8 effective resolution is thus 64 inches or about 6 diameters long. To accommodate this length would require a special long inlet (far from a representative geometry) which might affect the inflow to the fan in an uncharacteristic way. Further, with a $\lambda/2$ microphone spacing, this array requires about 65 microphones.

In a larger scale machine, such as the JT9D, the length problem would not be as severe. At 2400 rpm, the 46 blade fan 2 BPF frequency is about 3600 Hz giving $\lambda \approx 4$". The corresponding array length is then 128". This is about 40 percent longer than one fan diameter. If the resolving power of the array were to be accepted at 1/2 that used in this example, an array length of about 5 feet would result which might, under certain conditions, be considered feasible for test purposes. With a $\lambda/2 = 2$" spacing, about 30 microphones would be needed.

In both these examples, if BPF rather than 2 BPF is considered, λ will double and the array length must also double for the same resolution. Since the minimum microphone spacing also doubles, no added microphones are needed.

It will now be shown, that even these long array lengths are insufficient to provide entirely satisfactory information.

3.3.3.5 Use of the Weighting Function, W_n

If an array with sufficient length and microphone density to provide adequate resolution were used, it would still have a serious defect: Due to the excessive minor lobe response (-13dB), the array signal would be contaminated by modes lying outside of the main lobe target. It is well-known (Refs. 14, 15) that these lobes may be reduced by modifying the microphone weighting function, W_n, which has been taken as unity thus far in the present treatment.

A systematic way of representing a class of weighting functions that are symmetrical about the midpoint of the array is by means of the function:

$$W_n = a_o + a_1 \cos \frac{2\pi}{N-1} n + \ldots + a_p \cos \frac{2\pi p}{N-1} n + \ldots \qquad (58)$$

If the number of microphones, N, is even, there will be N/2 distinct coefficients, a_p, that can be determined uniquely for an arbitrary (symmetrical) set of W_n. When N is odd, there is a microphone at the center of the array, and N/2+1 coefficients can be found. It turns out, however, that the use of only the first two or three terms in Eq. (58) is sufficient to achieve very substantial reductions in minor lobe response.

The advantage of using Eq. (58) as the generating function for the weighting schedule is that it allows a closed form expression to be obtained for the array factor: Substitution of (58) in (52) gives

$$Z(\beta_x) = \frac{1}{N}\sum_{n=0}^{N-1} a_o \exp i\, \beta_x \frac{2\pi}{N} n + \frac{1}{N}\sum_{n=0}^{N-1} a_1 \cos\frac{2\pi}{N-1} n \exp i\, \beta_x \frac{2\pi}{N} n +$$

$$+ \frac{1}{N}\sum_{n=0}^{N-1} a_p \cos\frac{2\pi p}{N-1} n \exp i\, \beta_x \frac{2\pi}{N} n + \ldots$$

After some reduction $Z(\beta_x)$ can be expressed as follows:

$$Z(\beta_x) = \sum_{p=0}^{P-1} a_p Z_p(\beta_x)$$

where

$$Z_p(\beta_x) = (-1)^p \frac{1}{2}\left[\left\{Z_o(\beta_x + p\frac{N}{N-1})\right\} + \left\{Z_o(\beta_x - p\frac{N}{N-1})\right\}\right] \exp i\, \frac{N-1}{N}\beta_x \pi \qquad (59)$$

and

$$\left\{Z_o(\beta_x)\right\} = \frac{\sin \beta_x \pi}{N \sin \beta_x \pi/N} \exp i\, \frac{N-1}{N}\beta_x \pi$$

Examination of Eq. (59) shows that the new (general) array factor $Z(\beta_x)$, is the weighted sum of the original (uniform) factor, $Z_o(\beta_x)$ and factors, $Z_p(\beta_x)$, which are pairs of the original $Z_o(\beta_x)$ shifted $p \cdot N/(N-1)$ units in β_x to the right and left of $\beta_x = 0$. The effect of such weighting is to allow (with proper selection of the a_p coefficients) the side lobes to substantially cancel each other. Another effect, which is undesirable, is an increase in the width of the main lobe.

In digital filtering of time series, where the filter response has a mathematical structure identical to the array factor under consideration here, several weighting functions in the category of Eq. (58) are commonly used (Refs. 15, 16). Three of these are called Hanning, and Hamming (two-terms), and Blackman (3 terms). The coefficients appropriate to calculating these weighting functions (Eq. 58) and the array factors (Eq. 59) are:

Hanning:	$a_o = 0.5$	$a_1 = -0.5$	
Hamming:	$a_o = 0.54$	$a_1 = -0.46$	
Blackman:	$a_o = 0.42$	$a_1 = -0.50$	$a_2 = 0.08$

Figure 27 represents the variation of array factor with β_x for a 12-microphone array employing rectangular (uniform), Hamming, and Blackman weighting schedules. The very significant reduction in the -13 dB of the rectangular side lobe resulting from the Hamming and Blackman weighting is evident. The undesirable broadening of the principal lobe also stands out. The significance of this broadening is examined next.

A comparison of the operating features of the Hamming and rectangular arrays in Figure 28 will illustrate the main features. (The Blackman array produces, at the expense of more main lobe broadening, greater side lobe suppression than is needed in this application). The reference rectangular (uniformly weighted) array is illustrated with $L/\lambda = 8$. As discussed previously this provides a resolution of 1/8, with the main lobe spanning 1/8 of the entire range of forward and reflected modes or only 1/4 of the range of the forward modes. The number of microphones, N, must exceed $2\ L/\lambda$ or 16 to avoid aliasing. N is selected as 18 to completely eliminate any main lobe aliasing. Figure 28a shows the target mode range and Figure 28b displays the array factor with the reference rectangular array targeted to the extreme range of the highly propagating forward modes.

The corresponding array with a Hamming weighting is shown in Figure 28c. All minor lobes are at least 40 dB below the main lobe and are not shown. The -40 dB point on the principal lobe occurs at $\beta_x = 2.1$ (the first zero is at $\beta_x = 2.334$). Consequently the effect of the main lobe broadening is to diminish the resolving power by slightly more than a factor of two compared with the rectangular array. With the resulting resolution of 1/4, the array now contains within its main beam one-half of all the forward propagating modes. (It may also be noted that the anti-aliasing margin has been reduced as a consequence of the main beam broadening.)

To restore the resolving power of the Hamming weighted array to that of the original rectangular configuration requires doubling the length and number of microphones. The resulting $L/\lambda = 16$, $N = 36$ Hamming array is shown in Figure 29, together with the rectangular array of equal resolving power. As previously described, the resolution of 1/8 of the total mode range implies resolution of only 1/4 of the forward modes, and only 1/2 with respect to the range of β_x in which the 3/4 majority of these modes lie. Consequently this $L/\lambda = 16$, $N = 36$ Hamming weighted array can provide, at best, only a very crude measure of the modal distribution. In brief, whatever array length and

number of microphones are required for a rectangular weighted array to provide a specified measure of resolution, when side lobe suppression requirements are incorporated the length and number of microphones are essentially doubled.

Another feature of the array factor should be examined - the shape of the main lobe between $\beta_x = 0$ and its first zero. Ideally $Z(\beta_x)$ should be substantially one over an interval about $\beta_x = 0$ and then fall rapidly to a negligible value. This property would assure that all modes lying within the target window are completely transmitted, and all other modes are completely rejected. The non-equal weighting schedules just examined provide this off-target rejection satisfactorily in principle. However, the detailed shape of the main lobe leaves much to be desired, as seen in Figure 30.

Figure 30 presents $|Z(\beta_x)|$ for the two previously considered arrays providing essentially equal resolution - a rectangular N = 18 array and a Hamming weighted array with N = 36. The array factors are plotted against a fraction of the main lobe width.

It may be seen that neither response is satisfactory - at 1/2 the window width the rectangular array response is 4 dB down and the Hamming is 7 dB down. At 3/4 of the main beam width the corresponding responses are about -10 and -18 dB. So, although the rectangular array response falls at an excessive rate in the main lobe, the Hamming array main lobe response is even worse. (The Blackman weighting gives main lobe response that falls even more rapidly.)

In the design of digital filters, procedures exist and are under development (Ref. 15) for selecting weighting schedules such that the shape of the main lobe is subject to control as well as providing suppression of side lobe response. This area of array design has not been pursued further in this investigation.

The essential conclusion about the requirements for an array to provide adequate resolution and side lobe suppression is that very long arrays with large numbers of microphones are needed. Control of side lobes essentially doubles the length and microphone number needed in a rectangular weighted array. Adequate shaping of the main lobe response may further increase these requirements.

3.3.3.6 Effect of Decaying Modes

Additional requirements for array design are imposed by the need to prevent contamination of the array signal by significant decaying modes, and to verify the absence of such contamination.

The equations for the array signal, Eq. (49) and the array factor, Eqs. (50) or (52), apply equally well to decaying modes. In this case $k_{xm\mu}$ and $a_{m\mu}$ are imaginary.

Let $a_{m\mu} = \sqrt{1 - 1/\xi^2_{m\mu}}$ be represented by $i\, a'_{m\mu}$, where

$$a'_{m\mu} = \sqrt{1 - 1/\xi^2_{m\mu}} \quad \text{when } \xi_{m\mu} < 1 \tag{60}$$

From Eq. (49) the array signal due to the presence of a single decaying (m,μ) mode is

$$f_x(t) = \text{Re } B_{m\mu} \exp(-k\, a'_{m\mu}\, x_o) \exp i\,(m\theta_o - \omega t)\, Z_{m\mu} \tag{61}$$

where

$$Z_{m\mu} = \frac{1}{N} \sum_{n=0}^{N-1} W_n \exp\left(-a'_{m\mu} \frac{L}{\lambda} \frac{2\pi}{N} n\right) \exp i\left(-c\eta_x \frac{L}{\lambda} \frac{2\pi}{N} n\right) \tag{62}$$

The presence of the real factor, $\exp(-a' L/\lambda \cdot (2\pi/N) n)$ in the expression for Z destroys the basis for design and use of the array in detecting selected propagating modes and excluding non-target propagating modes. When η_x is set to target a propagating mode, the signal is contaminated by the presence of this decaying mode which is not rejected by the array factor.

In principle, decaying modes can be excluded from the array simply by arranging the microphone in the array closest to the source so that all decaying modes attain negligible levels at that microphone. This is shown clearly in equation (61) for the array signal by the attenuating factor $\exp(-ka' x_o)$. Moving the array forward is a necessary procedure but entails these problems: further lengthening of the constant diameter inlet duct and the uncertainty of how far away from the source to locate the nearest microphone.

For an existing array on test, there is a way to determine whether or not decaying modes are significantly contaminating the array signal. It consists of deliberately setting the delay rate η_x such that $c\eta_x$ lies outside the range of -1 to 1. This approach amounts to targeting modes that lie beyond the physically realizable range of axial phase velocities and is sometime called "overscan" in array terminology. Referring to Figure 29, for example, which shows two arrays targeted to highly propagating direct modes with $c\eta_x$ set equal to 1, if η_x is increased slightly the major lobe is shifted to the right, outside of the propagating mode range. The periodic major lobe at the left moves toward the extreme of the reflected mode range, but will not intrude if, as shown, N is large enough. In this mode of operation all coherent propagating modes are filtered out of the array signal. Consequently, if the array signal level is not satisfactorily small the presence of significant decaying modes is indicated.

The correction of this situation might involve slight speed changes to reduce decaying mode levels. A more straightforward process would eliminate the first few microphone signals to provide a greater length for modal decay before active microphone elements are encountered.

In summary, decaying modes must be eliminated from the array microphones before the system can be used to track propagating modes. The design requirements cannot be established completely in advance of testing, but the need for sufficient axial distance between the first microphone and the source is clear. A procedure is given for determining whether or not excessive levels of decaying modes are present at the start of a test program.

3.3.4 Determination of Acoustic and Modal Power Distributions

3.3.4.1 Array Signal Power

The ability of axial arrays to enhance modes having a substantially common cutoff ratio and therefore, to reject other modes has been determined in some detail. Assuming that the required length and number of microphones can be provided to allow adequate resolution, it remains to examine how the array could be used to obtain the distribution of power with respect to cutoff ratio, $\xi_{m\mu}$, or with respect to the parameter $a_{m\mu} = \sqrt{1-1/\xi_{m\mu}^2}$.

The acoustic power flux in a duct with negligible axial air velocity, for a set of propagating modes of common frequency, can be written in the following form, from Eq. (45):

$$\overline{\Pi} = \frac{1}{2\rho c} \sum_{m\mu} a_{m\mu} \, \bar{A}_{m\mu} \left| B_{m\mu} \right|^2 \tag{63}$$

Here $\bar{A}_{m\mu}$ is the power-effective modal area. For high hub-tip ratio ducts and for all but high m, low μ modes in plain cylindrical ducts $\bar{A}_{m\mu}$ is substantially equal to the geometric cross-section area, A.

Now if $\bar{A}_{m\mu}$ is taken simply as A, and if the array is targeted to a value $\bar{a}$, the acoustic power of the set of modes in bandwidth Δa is

$$\overline{\Pi}(\bar{a}, \Delta a) = \frac{1}{2\rho c} A \, \bar{a} \sum_{(m\mu)\bar{a}} \left| B_{m\mu} \right|^2 \tag{64}$$

where $\sum_{(m\mu)\bar{a}} |B_{m\mu}|^2$ denotes summation over those modes lying within the bandwidth Δa, centered at $\bar{a}$.

The objective is to obtain $\sum_{m\mu} |B_{m\mu}|^2$, defined as modal power, from the array signal when targeted to $\bar{a}$.

From Eq. (49) the array signal may be expressed as

$$f_\eta(t) = \mathrm{Re}\ \exp(-i\omega t)\ \mathrm{expi}\ \bar{k}_x x_o \sum_{(m,\mu)\bar{a}} B_{m\mu}\ \mathrm{expi}(m\theta_o) z_{m\mu} \qquad (65)$$

Here, the factor expi $k_{xm\mu}\ x_o$ is essentially common to all terms passed by the array and has thus been factored out as expi $\bar{k}_x x_o$.

Now the average power of any signal, $y(t) = \mathrm{Re}\ E\ \mathrm{expi}\omega t$ is

$$\overline{y^2(t)} = \lim_{T\to\infty} \frac{1}{T} \int_o^T y^2(t)\,dt = \frac{1}{2} EE^*$$

Applied to the array signal, Eq. (65), gives

$$\overline{f_n^{\,2}(t)} = \frac{1}{2} \left[\mathrm{expi}\ \bar{k}_x x_o \sum_{(m\mu)\bar{a}} B_{m\mu}\ \mathrm{expi}(m\theta_o) z_{m\mu} \right] \left[\mathrm{expi}-\bar{k}_x x_o \sum_{(m\mu)\bar{a}} B^*_{m\mu}\ \mathrm{expi}(-m\theta_o) z^*_{m\mu} \right] \qquad (66)$$

For a given (m,μ) mode passed by the array it will be assumed that $z_{m\mu}\ z_{m\mu}{}^* = 1$ with sufficient accuracy. (However, $z_j\ z_k{}^*$ is complex). The above product may be segregated into a sum of terms for equal values of m and a sum for different values, say m = j and m = k. Provided the array factor is sharp enough to pass but a single radial mode for each m:

$$\overline{f_n^{\,2}(t)} = \frac{1}{2} \sum_m B_m B_m{}^* + \frac{1}{2} \sum_{j\neq k} B_j B_k{}^* \mathrm{expi}\left|(j-k)\ \theta_o\right| z_j z_k{}^* = S_1 + S_2 \qquad (67)$$

The first sum, S_1, is exactly the quantity sought for the sum of the squares of the modal coefficients passed by the array. The mean square of the array signal, however, is grossly contaminated by the S_2 sum and cannot be used as it stands. S_2 is a sum of "cross power" terms, $B_jB_k{}^*$, modified by the factors expi $(j-k)\ \theta_o$. Because of the θ_o-dependence, S_2 is a local function of the angular position of the array.

Due to the contamination by S_2, the mean square array signal is totally useless as a measure of modal power, except in the trivial and improbable case where there is but a single mode in the array pass band. Means for eliminating or reducing S_2 are examined next.

3.3.4.2 Circumferential Integration

Since S_2 depends on θ-location of the axial array no form of manipulation of the array parameters or processing of the array signal for a particular θ-location can remove this essential and undesirable dependence. However, there is a possibility of obtaining the desired S_1 result by employing a plurality of axial arrays at different θ-locations. (Because the data are acquired by synchronous detection methods it is not necessary to have all the axial arrays on line simultaneously - a single array, re-located to successive θ-positions, may be used.)

To indicate that the array mean square signal, $\overline{f_n^2(t)}$, depends on the location, θ_o, let it be denoted simply by F_o. If similar quantities are obtained from axial arrays at a succession of locations θ_o, θ_1 ... θ_n, ... θ_{N-1} spaced $\Delta\theta = 2\pi/N$, the typical signal at θ_n will be

$$F_n = \frac{1}{2} \sum_m B_m B^*_m + \frac{1}{2} \sum_{j\neq k} B_j B^*_k Z_j Z^*_k \exp i\,(j-k)\,\frac{2\pi}{N}\,n$$

Summing and averaging the N quantities gives

$$\overline{F_n}^{\theta} = \frac{1}{N} \sum_{n=o}^{N-1} F_n = \frac{1}{2} \sum_m B_m B^*_m +$$

$$\frac{1}{2}\left[\sum_{j\neq k} B_j B^*_k Z_j Z^*_k \right]\left[\frac{1}{N} \sum_{n=0}^{N-1} \exp i\,(j-k)\,\frac{2\pi}{N}\,n \right] \qquad (68)$$

It will be recognized that the n-sum on the right vanishes for all (j-k) that are not multiples of N. Consequently, if the number of θ-locations, N, is taken a bit larger than the maximum value of |j-k|, Eq. (68) reduces to:

$$\overline{F_n}^{\theta} = \frac{1}{2} \sum_m B_m B^*_m \qquad (68a)$$

The largest |j-k| will exist for high m of opposite sign. That is, the number of array locations required is

$$N > 2m^*, \qquad (68b)$$

where m^* is the highest circumferential mode number that propagates.

In the case of the 10-inch rig, previously cited, m* is about 13. Thus at least 26 replications of axial array data would be required to obtain modal power in each target band of cutoff ratio. If the axial array employs Hamming weighting it was previously shown that to obtain a resolution of only 1/4 of the forward modes requires 36 microphones in a length of 16λ. The two figures 36 and 26 combine to give a value of about 940 for the number of microphone locations requiring data acquisition and processing.

There is still another difficulty to be overcome that increases further the microphone requirements, as will be seen in the next section.

3.3.4.3 Axial Integration Requirement

The foregoing features of array usage reflect the magnitude of the task of obtaining modal power. However, there are still other requirements to meet. In order to illustrate how cross power terms from different circumferential modes contaminate the mean square array signal it was specifically assumed that the array was sharp enough so that only a single μ-mode was present in the array signal for any m-mode. If more than one μ-mode is present Eq. (67) does not apply.

To examine the effect of several μ-modes for a given m, passed by the array, it will be sufficient to consider a single m. From Eq. (49), and putting $\theta_0 = 0$ for simplicity, the array signal is:

$$f_\eta(t) = \mathrm{Re}\ \exp -i\omega t \sum_\mu B_\mu \exp i\left(k_{x\mu} x_0\right) z_\mu \tag{69}$$

The μ-summation extends only over the bandwidth of $k_{x\mu}$ passed by the array. Instead of factoring out the approximately common quantity expi $k_{xm} x_0$ it will be retained along with B_μ for reasons that will become clear. The mean squared value of the signal is

$$\overline{f_\eta^{\,2}(t)} = \frac{1}{2}\left[\sum_\mu B_\mu \exp i\left(k_{x\mu} x_0\right) z_\mu\right]\left[\sum_\mu B^*_\mu \exp\left(-ik_{x\mu} x_0\right) z^*_\mu\right]$$

$$= \frac{1}{2}\sum_\mu B_\mu B^*_\mu + \frac{1}{2}\sum_{j\neq k} B_j B^*_k z_j z^*_k \exp i\left|\left(k_{xj} - k_{xk}\right) x_0\right| \tag{70}$$

$$= S_3 + S_4$$

As in the former case, $\overline{f^2_\eta(t)}$ contains the desired modal power, S_3, plus contaminating cross power terms, S_4. To eliminate these terms requires integration (summation) over x, just as previously, summation over θ was

required. However the required range of integration is not as clear. For the θ-integration it was obvious that a 2π range was needed since it is the base period of the set of functions $\exp im\theta$. In this case the k_{xj} are irrational numbers. For a given j and k pair the period of $\exp i\,(k_{xj} - k_{xk})x_o$ is $2\pi/(k_{xj}-k_{xk})$. But for any other pair of modes in the sum of Eq. (70) the corresponding period will be a different irrational number that is not generally an integral multiple of the first.

In principle, this difficulty is overcome by integration over a sufficiently long interval. Consider the operation:

$$\overline{\overline{f_h^2(t)}}^{x} = \lim_{X\to\infty} \frac{1}{X} \int_{x_o}^{x_o+X} \overline{f_h^2(t)}\, dx_o$$

$$= \lim_{X\to\infty} \left\{ \frac{1}{2} \sum_{\mu} \frac{1}{X} \int_{x_o}^{x_o+X} B_\mu B_\mu^*\, dx_o + \right.$$

$$\left. \frac{1}{2} \sum_{j\neq k} \frac{1}{X} \int_{x_o}^{x_o+X} B_j B^*_k Z_j Z^*_k \exp i\left[(k_{xj} - k_{xk})\, x_o\right] dx_o \right\} \qquad (71)$$

After some manipulation this may be put in the form:

$$\overline{\overline{f_h^2(t)}}^{x} = \frac{1}{2} \sum_{\mu} B_\mu B^*_\mu + \lim_{X\to\infty} \sum_{j\neq k} S_{jk} \frac{\sin (k_{xj} - k_{xk})\, X/2}{(k_{xj} - k_{xk})\, X/2} \qquad (72)$$

Here the quantity S_{jk} is the cross-power between modes j and k evaluated at the midpoint of the integration range:

$$S_{jk} = \frac{1}{2} B_j B^*_k Z_j Z^*_k \exp i\left[(k_{xj} - k_{xk})\,(x_o + X/2)\right] + \frac{1}{2} \text{ conjugate} \qquad (72a)$$

Since a variety of k_{xj} are involved during the use of the array the zeros of the (sin V)/V function in Eq. (72) cannot be exploited to reduce the cross-power contamination. Instead, a value of X must be selected so that local maxima of (sin V)/V do not exceed an acceptable value. If a typical cross term of 1/10 the value of a direct modal power term is used for illustration this requires an integration length given by

$$(k_{xj} - k_{xk}) \frac{X}{2} = 10$$

$$\text{or} \quad X = 20/(k_{xj} - k_{xk}) \quad \text{or} \quad \frac{X}{b} = \frac{20}{(k_{xj}b - k_{xk}b)}$$

Clearly, the modes with closest k_{xj} are the highly propagating low m, low μ modes. For example, comparing the (m = 1, μ = 0) and (m = 1, μ = 1) modes, for 2 BPF in the 10-inch rig at 6000 rpm gives $k_{x1,0}b = 15.1$, $k_{x1.1}b = 13.9$ for a difference of 1.2. Thus $X/b \approx 17$.

An integration length of 17 duct radii is thus needed to assure that cross power contamination is less than -10 dB. For the fundamental BPF of the JT9D at approach the requirements are even more unrealizable - about 45 radii. If the contamination requirement were greatly relaxed to a value of 1/2 (-3 dB) this would reduce the integration length requirement by a factor of 5, giving about 3 radii for the 10-inch rig and 9 radii for the JT9D.

Even this lowered value of 3 radii for the 10-inch rig imposes an unacceptable design requirement, for the entire array must be extended by this amount in the integration. The array length, L, providing $\Delta a = 1/4$ resolution of forward modes has been seen to require $L = 16\lambda$ with Hamming weighting or about 32 inches or 6 radii. To allow minimum x-integration adds 3 more radii giving a section required for microphones 9 radii long. With a maximum microphone location spacing of $\lambda/2$ or 1 inch there are thus 9 x 5 = 45 microphone locations required axially. This figure must be repeated for each of the 26 circumferential stations needed for θ-averaging. The total number of microphone locations is thus on the order of 1200.

(It may be observed that, in principle, the θ-integration may be omitted, since its purpose can also be accomplished by x-integrations. The x-integration reduces modal cross power contamination by a factor of $(k_{xj} - k_{xk})$ X/2, regardless of whether the axial wavenumbers k_{xj} and k_{xk} are for two radial modes of common m or for two different circumferential modes. However, because of the great difficulty in obtaining sufficient length for adequate x-integration, the θ-integration, which completely eliminates cross power for different m-modes should be retained.)

3.3.5 Assessment of Cutoff Ratio Array

An assessment of the method described can be facilitated by using information for 2 BPF noise in the 10-inch rig when specific figures are helpful. The method suffers from the following deficiencies:

1. Resolution with respect to cutoff ratio or axial direction cosine is poor: To provide a resolution no finer than 1/4 of the forward propagating modes requires an array 6 inlet radii long. (For comparable resolution of fundamental BPF noise an array twice as long or 6 diameters is required.)

2. Elimination of cross power terms between μ -modes of common circumferential wavenumber requires an extension of this basic array length so that the cross terms can be be reduced by x-averaging. A modest 3 dB cross power reduction requires an added 3 radii of inlet section length. Thus, the total instrumentation section of the inlet must be at least 9 radii or 45 inches long.

3. The number of microphones is governed by this length and the antialiasing requirement that spacing be less than 1/2 wavelength. For 2 BPF at 6000 rpm, $\lambda \approx 2$ inch giving a spacing less than 1 inch. Thus,more than 45 microphones are needed in the axial array.

4. To eliminate cross power terms corresponding to modes of different circumferential wavenumber (m) requires replicating the axial array in a number of circumferential locations to allow θ -averaging. The number of replications is at least twice the highest circumferential wavenumber or 26 for the 10-inch rig.

5. The total number of microphone locations in this example is thus greater than 45 x 26 or about 1200.

6. Even with this large number of microphones there remain these deficiencies:

   a. Resolution is poor
   b. Radial mode cross power is not completely eliminated.
   c. Modal power-effective areas have not been incorporated.

7. In the 2 BPF 10-inch rig case, there are only about a total of 60 (m, μ) modes. Thus, in effect, 20 microphone locations per mode are employed to obtain very approximate information. If the power distribution is taken in 4 parts, consistent with the array resolution, there are then 1200/4 or 300 microphone locations required for each of the 4 average cutoff ratios selected for sampling the distribution.

Clearly, even if employing 1200 microphone locations presented no logistical problems, use of the cutoff ratio method, as described, would be seriously inefficient.

A simpler, more accurate, direct, and economical procedure is described in the next section.

3.3.6 Circumferential - Axial Arrays

3.3.6.1 Basic Properties

In the process of θ-averaging to eliminate cross power terms it was previously found that at least $2m^*$ θ-locations of the axial array were required. Now it may be recalled that this requirement corresponds exactly to the capability of tracking circumferential modes without aliasing in a circular array. The output of the circular array is a signal corresponding to the sum of the radial modes at x_o, associated with the target value m (The array factor is unity for the target and zero for all other modes). Consequently, it would be very much more efficient to employ the circumferential mode filtering capability of the array to eliminate in one operation all modes except those radial modes associated with the target circumferential mode. These modes may have a wide range of cutoff ratio if the axial array resolution is poor, but this feature will not necessarily be a disadvantage.

This array configuration may well be classified as a repeated set of full circumferential arrays - tracking is performed with respect to circumferential mode number and no cutoff ratio targeting is involved. However it significantly reduces the number of microphones that were found to be required in the cutoff ratio array. This method bears a close resemblance to the circumferential array with speed changes, described previously in Section 3.2. It requires more microphone locations, but provides a better system of equations, dispenses with the need to solve for unknown source locations, and does not depend on assumptions about source behavior during speed change. The appropriate equations are obtained very simply, based on the information developed for circumferential arrays.

A full circumferential array without aliasing will produce the array signal when targeted to the m = M circumferential mode.

$$f_M(t) = \mathrm{Re}\, F_M \exp i(-\omega t),$$

where

$$F_M = \sum_{\mu} B_{M\mu} \exp i\,(M\theta_o + k_{xM\mu}\, x_{M\mu o}) \qquad (73)$$

Here θ_o is the reference angle of the zeroth microphone. $x_{M\mu o}$ is the location of the plane of the array ($x = x_o$) from the source of the (M, μ) mode.

For a similar circular array, located $n\Delta x$ forward of x_o, the array signal is:

$$F_M^n = \sum_\mu B_{M\mu} \exp i \left[M\theta_o + k_{xM\mu} (x_{M\mu o} + n\Delta x)\right]$$

$$= \sum_\mu \left\{B_{M\mu} \exp i (M\theta_o + k_{xM\mu} x_{M\mu o})\right\} \exp i (n\Delta x\, k_{xM\mu})$$

This can be written as

$$F_M^n = \sum_\mu C_{M\mu} \exp i (n\Delta x\, k_{xM\mu}) \qquad (74)$$

where $C_{M\mu} = B_{M\mu} \exp i (M\theta_o + k_{xM\mu} x_{M\mu o})$ is the (M, μ) mode coefficient at the wall, at $x = x_o$, $\theta = \theta_o$.

If, for a particular M, there are N μ-modes then N circumferential arrays spaced Δx apart provide information for solving the system:

$$F_M^o = C_{(M,o)} + C_{(M,1)} + \ldots + C_{(M,N-1)}$$

$$F_M^1 = C_{(M,o)} \exp i\Delta x k_{x(M,o)} + C_{(M,1)} \exp i\Delta x k_{x(M,1)} + \ldots + C_{(M,N-1)} \exp i\Delta x k_{x(M,N-1)}$$

$$\vdots \qquad \vdots \qquad \vdots \qquad \vdots$$

$$F_M^{N-1} = C_{(M,o)} \exp i\left|(N-1)\Delta x k_{x(M,o)}\right| + C_{(M,1)} \exp i\left|(N-1)\Delta x k_{x(M,1)}\right| + \ldots +$$

$$C_{(M,N-1)} \exp i\left|(N-1)\Delta x k_{x(M,N-1)}\right| \qquad (75)$$

The required number, N, of circumferential array stations is governed by the largest number of propagating μ-modes for any circumferential wavenumber, M. This will be the set of axisymmetric modes $(0, \mu)$. It may be desirable to provide two additional stations so that the least decaying (M, μ) mode and the reflected wave of the lowest cutoff ratio propagating (M, μ) mode can be incorporated in Eq. (75).

For 2 BPF in the 10-inch rig there are 4 propagating $(0, \mu)$ modes, all other circumferential modes have at most 3 μ-modes. If 3 modes are taken, together with a requirement for a decaying mode and a reflected mode, 5 array locations are needed. Using 26 microphones in each circumferential array gives a figure of 130 microphone locations. This figure, compared to the 1200 needed with the cutoff ratio array, represents a reduction of more than 9 to 1.

Knowing each mode amplitude unambiguously allows the acoustic power flux to be computed accurately, including the modal power effective area, $\bar{A}_{m,\mu}$. The distribution of the true acoustic power can then be obtained accurately with respect to cutoff ratio, wall incidence angle, or any parameter of interest.

It could be argued that the above 130 microphone location figure is too high since there are only about 60 propagating (m, μ) modes for 2 BPF in the 10-inch rig. But the 130 figure includes 2 extra array locations - one for reflected modes and one for decaying modes not in the 60 figure. A strictly comparable figure would then be 3 times 26 or about 75 microphones. The additional (75 - 60 = 15) microphone locations are not an excessive price to pay for having a highly decoupled set of equations - the m-modes are completely decoupled from each other and the sets of μ modes for each m will include progressively fewer members as $|m|$ increases.

It remains to examine the conditioning of Eq. (75). The worst cases will be for low m modes where the number of μ-modes is highest and where two or more of these are well cut-on and thus have $k_{xm,\mu}$ that are not too different.

Before discussing trial calculation results it is worth pointing out that the repeated circumferential array provides more accurate results than the single circumferential array with speed changes. This improvement can be seen by examining the relative phase change between two highly cut on modes in going between two successive array locations in this case and two neighboring speeds in the speed change method. This change in relative phase between successive equations of type Eq. (75) is a measure of the independence of the equations and is simple to estimate.

First, for the repeated circumferential array, using the (1, 0) and (1, 1) modes:

$$\text{Rel phase change,} \quad \Delta\phi = (k_{x1,0} - k_{x1,1})\,\Delta x = (k_{x1,0}b - k_{x1,1}b)\,\frac{\Delta x}{b} \qquad (76a)$$

For the circumferential array distant x from the source with speed change giving dk:

$$d\phi = \left[d(k_{x1,0}b) - d(k_{x1,1}b)\right]\frac{x}{b} = \left[\frac{1}{k_{x1,0}b} - \frac{1}{k_{x1,1}b}\right] kb \cdot \frac{x}{b}\, d(kb)$$

$$= - (k_{x1,0}b - k_{x1,1}b)\,\frac{(kb)^2}{(k_{x1,0}b)\,(k_{x1,1}b)}\,\frac{d(kb)}{kb} \cdot \frac{x}{b} \qquad (76b)$$

Comparing Eqs. (76a) and (76b) and recognizing that $(kb)^2/\left[(k_{x1,0}b)(k_{x1,1}b)\right] \approx 1$ for highly propagating modes gives:

Ratio of relative phase change: (repeated circumferential array method) to (circumferential array plus speed change method)

$$\text{ratio} = -\frac{\frac{\Delta x}{b}}{\frac{d(kb)}{kb} \cdot \frac{x}{b}}$$

In the speed change method illustration x/b was taken = 1, resulting in

$$\text{ratio} = -\frac{\frac{\Delta x}{b}}{\frac{d(kb)}{kb}}$$

If there are N modes then there must be N stations in one method and N speeds in the other. If L is the axial length of the repeated circumferential array and f is the total fractional speed change allowed (0.1), Δx is L/(N-1) and d(kb)/kb is f/(N-1). The above ratio reduces to

$$\text{ratio} = \frac{\frac{L}{b}}{f}$$

Using a section L = b units long for distributing the circumferential arrays and a speed ratio of 0.1 in the speed change method gives

ratio = 10

3.3.6.2 Sensitivity Evaluation

Calculations were made for the sensitivity of a system of three circumferential arrays located at x/b = 1, 1.5, and 2. Circumferential mode numbers, m = 1, 4, and 6 were selected, each of which support 3 radial modes. In one set of calculations all three radial mode coefficients were assumed equal at 74 dB. A second series of runs was made with the second radial mode at 74 dB, the other two being null. The procedure involved computing the three

array signals for the known modal coefficients, then adding 0.5 dB errors to each of the array signals in turn. These signals, containing errors, were then used to compute the modal coefficients, which were compared with their postulated values.

Table IX gives the results for the cases of three equal radial modes.

TABLE IX

CALCULATED MODAL COEFFICIENTS WITH 0.5 dB ERROR ADDED TO ARRAY SIGNAL

Modes	Coefficient	Array Signal to which Error Added		
		No. 1	No. 2	No. 3
(1, 0)	74 dB	73.9	74.5	74.1
(1, 1)	74	73.6	73.4	75.4
(1, 2)	74	74.0	74.6	73.9
	(all cases)			
(4, 0)		73.6	74.1	73.5
(4, 1)		73.8	73.8	73.8
(4, 2)		74.4	72.4	73.5
(6, 0)		73.8	73.0	73.4
(6, 1)		73.9	74.2	73.0
(6, 2)		73.5	73.7	73.6

An inspection of Table IX shows that the greatest error is on the order of 1.5 dB. This is a vast improvement over comparable cases in Table VI for the speed change method. The following Table X gives results for cases in which only the middle radial mode coefficient, (m, 1) was postulated as 74 dB, the other two being null.

TABLE X

CALCULATED MODAL COEFFICIENTS WITH 0.5 dB ERROR ADDED TO ARRAY SIGNAL

Modes	Coefficient	Array Signal to which Error Added No. 1	No. 2	No. 3
(1, 0)	-	44.3	45.2	44.3
(1, 1)	74 dB	74.4	73.7	74.4
(1, 2)	-	43.6	49.2	43.6
(4, 0)	-	47.5	46.5	47.5
(4, 1)	74 dB	73.6	73.1	73.6
(4, 2)		46.3	51.3	46.3
(6, 0)	-	-41.4	-36.4	-29.6
(6, 1)	74 dB	73.6	73.6	73.6
(6, 2)	-	-29.0	-34.0	-27.5

Again, the results presented in Table X are reasonably good - the greatest error in the input mode is about 1 dB and the null modes are more than 20 dB down. Improvement over the speed change method also may be seen by comparing Table VII with the above figures.

Condition numbers for the three sets corresponding to m = 1, 4, and 6 were found to be 2.4, 1.8, and 1.6. These are seen to be significantly lower than the values 162, 51, and 7 obtained in the 10 percent speed change process as tabulated in Table VIII.

It would then appear that this repeated circumferential array method has a reasonable chance of working on the 10-inch rig for 2 BPF mode detection. Other applications would have to be examined to see if the method is equally promising.

One way of assessing feasibility for a range of applications is to examine the sensitivity of the repeated circumferential array system as the number of propagating modes increases. Each additional radial mode associated with a particular m-mode requires another circumferential array to be used in the system. For an allowed installation length, the distance between circumferential arrays decreases as the number of propagating modes grows, so that the relative phase of a mode between array stations changes less. It can therefore be anticipated that the method will become progressively more sensitive to small input errors as the number of radial modes increases.

The following way was chosen to illustrate the variation of sensitivity. Two array systems were evaluated - one had the first circumferential array at x/b = 1 and the last at x/b = 2. The second system started at x/b = 1 but had twice the previous axial extent, terminating at x/b = 3. By increasing frequency (actually dimensionless wavenumber, kb) the number of propagating

radial modes associated with m = 1 took on the values 3, 8, and 13. The number of circumferential arrays required to determine these modes were provided between the extreme locations cited above. Postulated inputs of 74 dB were assigned to the modes (1,0), (1,1), and (1,2) and the resulting circumferential array signals were computed. These were then rounded to the nearest dB and used to solve for the (m,μ) modal coefficients.

Results are shown in Figure 31. As was found previously, the 3 mode array results are satisfactory. For 8 modes the 1 radius long array becomes totally unacceptable. Making the array 2 radii long improves performance to a reasonable level. However when 13 modes must be accommodated, both arrays fail to give the postulated inputs.

From these sample sensitivity calculations, it is seen that while the circumferential-axial array method may work for a small number of modes, its use for larger systems must be preceded by a careful examination of sensitivity for the specific application to determine whether the accuracy is acceptable.

3.3.7 Cutoff Ratio Arrays for Random Noise

In the previous study of the distribution of modal power with respect to cutoff ratio using axial arrays, it was found that the required number of microphones increased by a large factor due to the need for θ - and x-averaging. This averaging was required to eliminate the cross power terms in the array signal. The cross power terms depend on the intermodal phase angles which are functions of position. Since only coherent harmonics of blade-passage frequency were considered, the intermodal phase angles maintain constant values with time.

There is a category of broadband or random noise field in a duct where this situation is different and may possibly be exploited. If a random time signal is narrowband filtered, the mean square output can be obtained, and, when divided by the bandwidth gives the power spectral density at the filter frequency. "Phase", however, is constantly changing and is randomly distributed over 2π. If the sum of two such random signals is considered, the power spectral density will be the sum of the psds of the components plus (or minus) the cross power spectral density between the signals $(\overline{f_1(t) \cdot f_2(t)})$. This cross psd is the Fourier transform of their cross correlation function.

In the important special case where the signals are uncorrelated, the psd of their sum is exactly the sum of the individual psds.

An analogous situation holds between modal powers. If the modes are uncorrelated, the power of the signal at any point in the duct is the sum of the powers of the signals produced at that point due to the individual modes. At a fixed radial location, in particular at the wall, the power of the signal remains constant with circumferential and axial location for a single propagating mode. Thus with a plurality of modes, the power spectral density at all wall locations is the same if the modes are uncorrelated.

Consequently there is no need to average array signals over θ or over x to eliminate cross power spectral density contributions to the array signal. These cross psd terms are zero or negligible when the modes are uncorrelated or weakly correlated. To determine prior to array measurements whether or not the modes are, in fact, sufficiently uncorrelated, a few measurements of local psd at different wall positions will suffice - equal or closely similar local power spectral density functions will indicate the state of affairs.

In this case of uncorrelated modes, the resulting field has been called homogeneous (Ref. 1). Consequently the axial array may be placed at any θ-location. It will be necessary, however, to ensure that no decaying modes affect any array microphones significantly. Two items are involved. First, the separation between the first array microphone and the closest source, such as the fan, must be reasonably large - one duct radius for example. Secondly, since decay of each mode depends on frequency, the values of frequency for which the signal psd are obtained should correspond to satisfactory decay rates for those decaying modes closest to cutoff.

In operation the frequency range of interest may extend from about 2 BPF down to perhaps 1/2 BPF. Since both array resolution and antialiasing depend on wavelength it is clear that a single array configuration cannot efficiently accommodate this 4 to 1 frequency range. To cover this range a sequence of tests would be required, using a different array length in each test to provide comparable resolution. The total number of microphones required to ensure antialiasing will remain constant since as wavelength increases both intermicrophone spacing and overall length increase linearly.

The number of microphones is subject to a further constraint, not present in the coherent case. In the coherent case, data for a large number of microphone locations can be obtained through re-positioning of a limited number of microphones and use of synchronous detection to provide amplitude and phase for each location. The array target delay corresponds exactly to a phase shift between microphone signals in the coherent case, and the data are in fact processed using phase shifts rather than time delays in the array summations. Phase has no meaning in the random noise field case. All microphones in the array must be operating simultaneously and recorded simultaneously so that real inter-channel time delays can be made in the data processing.

So although the homogeneous random field case allows very large reductions in the number of microphone locations through the elimination of the θ and X-averaging operations needed in the coherent case, it nevertheless requires the availability of a significant number of microphones and recording channels.

Since microphone separation must be less than a half wavelength to prevent aliasing, the number of microphones can only be reduced by decreasing array length. (This reduction would also tend to make the required inlet measurement section length more acceptable). The reduced array length, of course, adversely affects resolution. However, it may be that data reduction techniques using deconvolution can provide satisfactory definition of the power spectral density with respect to cutoff ratio using an array with

relatively broad response. Further study, beyond the scope of this investigation, would be needed to establish these relations and to explore other relevant factors such as hydrodynamic noise, so that the feasibility of the cutoff ratio array method applied to homogeneous random noise fields could be assessed.

3.3.8 Summary of Feasibility of Cutoff Ratio Arrays

It was found that the basic array geometry required to enhance the set of modes propagating at essentially common cutoff ratio was an axial array. Microphone spacing must be less than one-half the natural wavelength to prevent aliasing. Sharpness, bandwidth, or resolution of the array depend on the ratio of array length to acoustic wavelength.

These properties lead to array design requirements and characteristics that are unsatisfactory:

1. The array length - and, consequently, the length of the inlet - must be large to provide even modest resolution. For example, in the 10-inch rig at twice blade passage frequency, one particular design required an array about 30 inches long, containing over 30 microphones.

2. The resolution of this array is quite poor: the bandwidth includes 1/4 of all the forward propagating modes. To improve performance by a factor of 2 would require an array length of 6 feet and use of over 60 microphones.

3. Even this hypothetical, extended array would suffer from a grave deficiency - the output signal would not provide a meaningful measure of the set of modes targeted by the array. This circumstance results from contamination of the array signal power by cross-power terms from the modes passed by the array.

4. To remove these contaminating terms would require replicating the array in a large number of circumferential locations (θ-integration) and also extending the array to a succession of axial locations (X-integration). The result is a completely unmanageable number of microphone locations - on the order of 1200 for the 10-inch rig.

5. Since this microphone number is so much larger than the number of propagating modes (about 60 in the 10-inch rig), it is obvious that the method is grossly inefficient compared to other methods that simply produce all the modal coefficients.

6. One such straightforward method uses a set of full circumferential arrays spaced apart axially. The required number of microphones in each circumferential array is a bit more than twice the highest propagating mode circumferential wavenumber. For the 10-inch rig 3 circumferential arrays of 26 microphones, or about 75 microphones would do a very much better job than the 1200 microphones needed in the cutoff ratio method.

7. There is a possibility, however, that the cutoff ratio array could be used efficiently to measure the distribution of broadband, random noise in the fan duct. If the broadband noise field is homogeneous, having the same spectrum at all axial and circumferential locations, the modes at any frequency are uncorrelated and all cross powers are zero. Consequently the axial and circumferential integrations are unnecessary and a single axial cutoff array would suffice. This application, lying outside the field of coherent blade passage harmonic noise, has not been examined further here.

4.0 EXPERIMENTAL STUDIES

4.1 SPEED WINDOWING PROCEDURE

4.1.1 Background and Objectives

All of the previously discussed techniques as well as the method presented in Reference 1 for determining coherent mode structure from wall pressure data depend on an accurate determination of local pressure amplitudes and phases. During a preliminary analysis of JT9D full-scale engine data, which was performed outside the scope of this contract, difficulties were encountered in assigning an amplitude value to the recorded data. These difficulties raised questions concerning the validity of the data reduction procedure which was then being used. It was determined that the problem was related to engine speed fluctuations which occurred during data acquisition. This fluctuation causes microphone readings to vary in amplitude and phase due to the effects of modal superposition. An improved procedure for dealing with this problem was developed under the current contract. Tests were performed to aid in the evaluation of this procedure.

The data reduction method for which the above problems occurred is called signal enhancement. It is a process that produces an average pressure-time history. In this process an ensemble average is performed at many instants over a period of time for noise filtered at some desired harmonic of blade passing frequency. The averaging process is synchronized by a signal called a block sync which is derived from the rotor position. In this process, the random component of the signal tends to average to zero and, ideally, the remaining signal is a sinusoid of constant amplitude. From a plot displaying a small number of cycles, the coherent amplitude and phase can be determined at each microphone.

Difficulty with the full-scale engine data analysis was first encountered when a large number of cycles of the enhanced signal was displayed. Although a large portion of the time histories showed nearly constant amplitude, a significant number appeared as in Figure 32. Here the amplitude derived from the center of the curve is about 2.7 dB higher than that derived from the initial portion of the curve. Although this might be considered an acceptable error in some cases, a few time-history enhancements were found where the differences in amplitude were as much as 6 dB over the range of the plot. Further work revealed that large amplitude variations in the signal enhancements were associated with large speed variations in the data record. Based on this, it was decided to attempt to analytically simulate the effect of engine speed change.

The equations which formed the basis of the simulation were:

$$P(x, t) = \sum_{m} \sum_{\mu} A_{m,\mu} \, e^{i\phi_{m\mu}} \, e^{ik_x x} \, e^{-i\omega t}$$

where

$$k_x = \left[M_x \frac{\omega}{c} \pm \sqrt{\left(\frac{\omega}{c}\right)^2 - (1 - M_x^2) \quad k_{m\mu}^{\sigma\ 2}} \right] \left[\frac{1}{1 - M_x^2} \right]$$

The notation used here is consistent with that used in Reference 1.

During the simulation study, the angular frequency, ω, was made a linear function of time which increased until a selectable time was reached and then decreased. A similar variation was allowed for phase angle, ϕ. The signal enhancement process was simulated by calculating a series of pressures at equal time increments. The block sync signal, which also contained the varying ω, was then used to determine the time of the next synchronizing pulse. Another pressure vs. time series was then calculated, using as an initial time, the value just determined, and using the same time increments used for the first series. This process was repeated until the desired number of series was obtained. The set was then ensemble averaged and plotted using computer graphics.

A study of the variable parameters was made to determine their effects on a signal enhanced time history. Typical results are shown in Figures 33-a and 33-b. The first of these has an envelope which is quite similar to the JT9D full-scale data. It was obtained by allowing the frequency to vary together with a substantial variation in the phase angle, ϕ. The second curve contains no phase variation and demonstrates a cancellation effect which occurs when many time series, associated with slowly varying frequencies, are added. The apparent randomness seen on Figure 33-a and the apparent high frequency modulation of Figure 33-b are results of the density of the sampling points. These results occur when the number of samples taken in each period of a wave is small and the period of the wave is not equal to an integral number of sampling intervals. Using these three effects, it was possible to explain all of the previously unexplained features seen thus far in full-scale engine data reduction.

The experimental portion of this contract undertook to reduce these effects of speed fluctuation by developing an improved data reduction procedure using existing electronic equipment. Since speed fluctuation was the problem, a method called speed windowing was considered which attempted to coordinate the sampling of the data so that it was only accumulated for averaging when the speed was in some selectable narrow range. The procedure was then evaluated using data obtained from the Pratt and Whitney Aircraft 10-inch compressor rig.

4.1.2 Description and Use of Speed Windowing Instrumentation

The speed windowing technique can be described with reference to the functional block diagram, Figure 34, and the timing diagram, Figure 35, which show the electrical signal which appears at various points in the circuit. A signal conditioner is shown as the first element following the speed tach

signal input. Its function is to operate on the incoming tach signal and produce rectangular pulses with heights and widths appropriate for input into the remaining components. The output of the signal conditioner is shown in Figure 35-a as a series of rectangular pulses. As the speed increases, these pulses become more closely spaced and as speed decreases, the pulses become more widely spaced. In the absence of speed fluctuation, this signal would be the appropriate input to the block sync of the signal enhancement device. In the windowing system, this signal is applied as one input to an AND gate which produces an output pulse for the block sync when its second input is similarly pulsed.

The signal at (a) in Figure 34 is also diverted through two additional paths. In the first path, a voltage proportional to speed is produced. Provision is also included in this path to remove the average value of the voltage ("offset" block) and to amplify its time varying part (Amplifier 1). This improves the sensitivity of the circuit to small changes in speed. The ability to change the amplitude of the pulse train is provided in the second path (Amplifier 2). The signals from these two paths are then added and the result is shown in Figure 35-b. By adjusting the pulse height and level of the D.C. voltage proportional to speed, the leading edge of the pulses can be made to trigger the zero crossing detector for the desired range of speeds. Output of the zero crossing detector, if met by a pulse from the original pulse train, causes a pulse to be emitted from the AND gate to synchronize pressure data sampling. This check for two simultaneous pulses is done to insure that zero crossings which might occur between the rises of successive pulses do not cause an erroneous synchronizing signal.

The complete signal enhancement system is formed by inserting the speed window circuitry described above into the path of the speed tach signal to form a block sync signal and inserting a narrow band filter into the path of the pressure data signal before they reach the enhancing analyzer. This system is described in more detail in Section 4.2.3.

Because there is a wide range of differences possible between sets of data obtained from various noise sources and facilities and also a large variety of data reduction equipment, the procedure for selection of appropriate speed window parameters must be based on an analysis of each individual set of circumstances. Important factors in this selection, which are related to the properties of the data itself include:

1. the number of modes producing pressure variations at the experimental microphone locations and the proximity of these modes to cutoff;

2. the severity and nature of speed fluctuations present in the data;

3. frequency spacing of the dominant coherent tones;

4. levels of the random noise components relative to the coherent levels at the frequencies of interest; and

5. available data record length.

The first of these helps to determine the amount of variability which might be expected in the coherent amplitude and phase of a microphone signal for slight variations in speed. If few modes are present, cancellations and reinforcements can be expected to cause larger variations for some mike locations than if many modes are present. Near cutoff of any mode, coherent microphone signals are strongly dependent on speed, but the dependence becomes weaker away from cutoff. Large speed fluctuations imply that the speed spends a small amount of time in any given window. For these cases, larger record lengths and analysis times are required than for cases where the speeds are constant. This assumes that the speed fluctuates around some value of interest. If the speed fluctuation is more or less monotonic, very little improvement will be possible from windowing, since very few samples are avialable for any given window. The spacing of the dominant coherent tones in the noise spectra imposes some requirements of the filter bandwidth used in the analysis, while the level of the random component influences the number of ensemble averages required to reduce the variance of the enhanced data to a desired level. Finally, if the data is recorded on magnetic tape or some other medium, the record length available, together with the speed fluctuations, determine the maximum amount of samples available for averaging.

Factors related to the characteristics of data reduction equipment which should be considered when planning a test program include:

1. amplitude response and delay characteristics of equipment;

2. filter bandwidths available and tracking ability of filter;

3. input digitizing resolution, cycle time, and number of averages permissible on the signal enhancement device; and

4. characteristics of the windowing system.

To conform with good instrumentation practice, means must be provided to evaluate the amplitude and phase response of all instrumentation in the data processing system. In addition, since the phase shift of a filter depends on the distance of a test frequency from the center frequency of the filter, it is recommended that a tracking filter be used in an attempt to keep the frequency tuned properly and phase shift due to the filter at zero. If the speed change is such that the filter is unable to track the signal effectively, a phase shift will occur when the frequency increases which will be different from the phase shift which occurs when the speed is decreasing. This effect will be more pronounced for narrow filters than for wide.

Several characteristics of signal enhancers themselves were also found to be important. Machine cycle time is the minimum amount of time which must elapse from the time one synchronizing pulse initiates the collection of a time history until another pulse can be accepted to initiate the next history. This sometimes acts to limit the number of samples available in a data window to an amount which is smaller than would be expected from a consideration of the other enhancement parameters. The input digitizing resolution is usually related to the number of permissible averages. Large input resolution machines are more appropriate for data with a large coherent component. Under these circumstances, accurate results can be obtained with relatively few samples. Small input resolution is appropriate for data with large random components. Here large numbers of samples are required and the lack of resolution is not a problem.

Because of all the factors mentioned previously that go into the selection of the window width, it is not possible to specify here what should be used in a particular application. It is expected, however, that in most cases, an appropriate window width can be determined in a trial-and-error fashion by fixing all parameters except the window width at convenient values based on the previous discussion and varying the window width until satisfactory repeatability is obtained.

4.2 EVALUATION OF THE SPEED WINDOWING PROCEDURE

4.2.1 Approach

The procedure previously described for windowing data was implemented and evaluated using data from the Pratt and Whitney Aircraft 10-inch fan rig. One configuration of blades and vanes was selected to produce a variety of modes such that some were well above cutoff and others were near cutoff for the speed range tested. Five steady speeds were run. The rig speed was then cycled continuously throughout the range covered by the steady speeds. Enhancement of microphone signals was conducted to provide pressure amplitudes and phases at the steady speed conditions and narrow speed windows were used to obtain corresponding information from the variable speed data. Besides direct comparison of the pressure information, modal information using these data and the Modal Calculation Program (MCP) reported in Reference 1, was compared to provide the evaluation of this method.

4.2.2 Test Facilities

The Pratt & Whitney Aircraft 10-inch fan rig consists of a 32-blade rotor cantilevered from a flaired flange 38 cm (15 inches) downstream. A photograph looking into the inlet is shown in Figure 36, and a schematic drawing is given in Figure 37. The fan is enclosed in a cylindrical tube 25.571 cm (10.067 inches) in diameter with bellmouth opening. The distance from the face of the bellmouth to the face of the fan was 74.2 cm (29.2 inches). In order to form an annular duct, an 11.2 cm (4.4 inch) diameter centerbody was positioned concentrically in the duct. The centerbody extended 2.8 meters ahead of the rotor and was supported 1.8 meters upstream of the rotor. A single stator rod,

0.396 cm (0.156 inch) in diameter was positioned upstream of the rotor at bottom dead center. The spacing between the fan face and the downstream edge of the rod was 3.566 cm (1.404 inch).

The operating speed range of this fan rig is between approximately 2800 and 5800 rpm. The fan tip Mach number operating range is approximately 0.12 to 0.24. In this range, axial flows of up to 25 meters/second (80 ft/sec) result.

To reduce both steady inflow distortion and unsteady inflow turbulence, the wire mesh screen described in Reference 1 was installed. The screen consisted of a 76.2 cm (30 inch) cube formed from 0.635 cm (0.25 inch) diameter rods covered with domestic wire screen.

A constant speed motor was used to power the rig. The fan speed was varied by the use of a belt-driven system of variable diameter pulleys. The rig accelerated or decelerated at a constant rate which was determined by the speed of an auxiliary motor which changed the pulley diameters. The rate of this rpm change is approximately 180 rpm/second. During constant speed operation, the speed was maintained constant to within ± 4 rpm. This speed was measured by counting the output pulses from a proximity transducer which sensed the passage of teeth on a 32-tooth gear which was attached to the shaft driving the rotor.

In order to provide sound mode stability, rig inlet temperature was controlled during testing. Space heaters were installed in the rig inlet plenum to raise the ambient temperature to $20.5^{\circ}C \pm 0.5^{\circ}C$. Thermocouples were located on the inlet screen to monitor inlet temperature which was then adjusted by means of an air bypass gate located in the roof of the test cell.

A total of 11 microphones were flush mounted in the OD wall of the rig inlet. Since the test geometry and two of the speeds in the current program were the same as described in Reference 1, microphones were installed in the locations determined for the referenced program. Figure 38 shows the locations of the microphones relative to top dead center for the circumferential coordinate and relative to the microphone numbered 1 for the axial coordinate. The microphone locations were measured in the P&WA experimental inspection laboratory and are accurate to 0.0025 cm (0.001 inches) axially and 1.0 minute of angle. Included on this figure are the values of axial and circumferential coordinates used in the MCP computer program (Reference 1) to process the microphone data, together with the values of other computer inputs required by the program. All data was processed using the English units although the program can also be run in a consistent set of metric units.

4.2.3 Instrumentation

Instrumentation used to acquire the desired pressure and speed data is shown in Figure 39. Sound pressures were obtained using 1/8 inch diameter microphones, model 4138, from B&K. These microphones were certified acceptable for sensitivity and frequency response in the P&WA standards laboratory prior to the test. The microphones were calibrated for output sensitivity

immediately preceeding the test with a B&K, model 4220, pistonphone calibrator, which was also certified for an output of 124.0 ±0.2 dB (re. 0.0002 dynes/sq.cm.) at the P&WA standards laboratory. All microphones were normalized at 1.0 volt equal to 124.0 dB.

The 32E tach signal, obtained from a proximity transducer responding to the passage of a 32-tooth gear, was conditioned using a P&WA, model E2772, speed normalizer. This device is armed by a positive going signal of selected amplitude and produces a rectangular pulse at the next zero crossing. The pulse train produced by this method accurately reflects the passing of the gear teeth, but has the electrical ringing transients removed. The pressure and speed signals were then routed to a P&WA, model 1480-27, signal conditioner, which allows the amplitudes to be monitored and adjusted to proper recording levels. Recording was done on a Honeywell, model 96, fourteen channel tape recorder. This wideband group I recorder was set up in the FM mode at 30 IPS, 108 KHz center frequency. Mikes 1 through 11 were recorded in order on channels 1 to 11. The conditioned tach signal (rectangular pulse) was recorded on channel 13 and the unaltered tach signal was recorded on channel 12. Other peripheral monitoring and calibration equipment used are shown in the figure.

An advantage of recording the data on tape is that signals can be analyzed from the same time period. This is particularly important for the transient data where recording insures that the data is not changing while various analysis methods are tried. The disadvantage of recording is the careful calibration required to preserve proper phase relationships.

The procedure for signal enhancement with speed windowing, described earlier, was exercised using the equipment shown in Figure 40. Mike pressure and speed signals, recorded at the test stand, were obtained using a Bell and Howell VR 3700B tape playback unit. The conditioned speed signal from channel 13 was reshaped using a P&WA, model 2577-1, pip shaper. This unit triggered on the leading edge of the speed signal which was slightly distorted from the tape recording process and produced a rectangular pulse. The signal was then routed to a P&WA, model 2618-1, trigger delay timer. This unit delayed the impulses by a calibrated amount to compensate for signal delays in other legs of the circuit. This pulse was then widened by a Spectral Dynamics, model SD103, dynamic input - sine converter to a width suitable for the block sync input of the Nicolet, model 411B-401B signal enhancement system before it was fed to one side of the AND gate which is part of the P&WA, model 2676-2, armed-gate pulse generator.

The channel 13 speed signal was also routed to a Spectral Dynamics, model SD103, dynamic input - sine converter which produced a voltage proportional to frequency and a sine wave to tune the Spectral Dynamics, model SD121, tracking filter. Microphone data was filtered with a 50 Hz constant bandwidth filter before reaching the data input jack of the 411B. The voltage proportional to frequency was amplified by two Kistler, model 561A, D.C. amplifiers and was added in a P&WA, model 900-17, sum and difference amplifier, to the original shaped pulse. The composite signal was fed to the P&WA 2676-2 which detected

positive going zero crossings and pulsed the second input of the AND gate. The process was monitored as shown in the figure using a Tektronix 561A oscilloscope and the signal enhanced sine waves were plotted on a Hewlett-Packard, model 700, x-y plotter.

Amplitude calibration was obtained from a recorded sine wave. A cross-spectral density between channel 13 and the data channels was obtained using recorded white noise. This provided phase calibration of the recording-playback system. The time delay through the windowing circuitry was measured during each reduction session. The sum of the two phase corrections was applied to correct the apparent phase of the pressure signal.

Spectral plots were obtained with a Nicolet, model UA-6B, Ubiquitous Spectrum Analyzer and Nicolet, model 129B, spectrum averager system. Spectrum analysis was over a frequency range from 0-10 KHz using a 32-Hz bandwidth filter. Plots of speed versus time were obtained using a Spectral Dynamics, model SD134A, tracking ratio tuner while plots of blade passing frequency versus speed required an additional Spectral Dynamics, model SD121, tracking filter equipped with a 50-Hz constant bandwidth filter.

4.2.4 Test Program

Since the objective of the test program was to compare modes obtained from steady and variable speed data, a rig configuration and speed range was desired for which the mode structure could be completely defined with a single, reasonably small, set of microphones. At a speed of 3400 rpm, it was shown in Reference 1, that 7 incident modes are supported by the duct at blade passing frequency. It was also shown that the set of microphones used in that test produced a low conditioning number of 2.1 which increased to 3.1 when the speed was increased by 10 percent. At a 10 percent lower speed, two of the circumferential modes present at 3400 rpm are below cutoff. Having modes near cutoff was expected to result in larger pressure variations at a microphone when there is a change in speed. This is due to the sensitivity of the axial wavenumber to frequency near cutoff. For these reasons it was decided to continuously vary rig speed 15 percent to each side of 3400 rpm and to also run steady-state points at 3400 rpm and 3400 rpm $\pm$5 percent and $\pm$10 percent.

Following recording of the microphone calibration signals, acoustic tests were initiated, during which 11 microphone signals and the speed signal were recorded during a single, decreasing speed transient. The rig was set near the maximum speed of 5813 rpm and decelerated through its operating range to its minimum speed of 2800 rpm. It was then allowed to coast slowly to zero. This test was followed by 5 steady-state records, each approximately 5 minutes long, taken at speeds of 3735, 3570, 3394, 3229, and 3060 rpm. Blade passing frequencies corresponding to these speeds are 1992, 1904, 1810, 1722, and 1632 Hz, respectively. The rig was then cycled back and forth 75 times between 2800 rpm and 4125 rpm. Each complete cycle required about 20 seconds. This provided 150 speed sweeps through the 5 steady-state values. To check repeatability, an additional steady-state record was then taken at 3394 rpm.

4.2.5 Test Results and Discussion

In order to determine how constant the rig speed was maintained during the steady speed portion of the test program, speed histories were made for each of the 6 steady records and are shown in Figure 41. During the first minute of each record, which was the portion later used for signal enhancement, 4 of the speeds and the repeated speed were held to within 2 rpm of the nominal speed. Record 3, 3060 rpm shows a somewhat larger deviation of about 7 rpm.

A sample transient speed history, taken over several cycles of speed change is shown in Figure 42. Since the speed cycling was performed by manually starting and reversing a motor which changes pulley diameters, portions of the history near the highest and lowest speeds vary from cycle to cycle. The central portions, however, between the speeds of about 3056 rpm and 4012 rpm are seen to be approximately straight lines with slopes of 180 rpm/second. The five steady speeds occur within these straight line portions of the speed history curve.

Curves of blade passing frequency level versus rig speed were prepared to determine the ranges which might be expected to show sensitivity to speed change. A sample of these curves from one microphone is shown in Figure 43, covering the entire operating speed range of the rig and proceeding down through the range where the rig is coasting to zero. Calculated cuton frequencies for the first 8 possible propagating modes are shown on the figure and it can be seen that amplitude spikes in excess of 10 dB above the background can occur at these modal cuton frequencies. It is also seen that the spikes are higher above the background and sharper at the lower speeds where fewer modes are propagating and they reduce in significance at the higher speeds where more modes propagate. For the transient range of speeds used in this test program, only the cuton frequency of the (3,0) mode is seen to be important. The steady speed of 3239 rpm (1722 Hz) is very close to this frequency and can therefore be expected to cause more difficulty than the others. Data from the other microphones were similar to that shown.

Pressure amplitudes and phases required for mode structure determination were next obtained from steady state and windowed transient data records using the signal enhancement procedure described earlier. A signal enhanced pressure history, which is typical of both steady-state and windowed analyses is shown in Figure 44. Peak-to-peak amplitudes plotted in units of pounds per square inch were multiplied by 0.353 to convert them to RMS amplitudes and further multiplied by 68144.14 to convert them to dynes/sq.cm, before converting them further to decibels referenced to 0.0002 dynes/sq.cm. Phases were computed by dividing the time to the first negative going zero crossing by the time required for one period of the wave and multiplying the result by 360 degrees. This value was then corrected for tape recorder and reduction equipment phase shifts. Thirty-two ensemble averages were found to be adequate to remove the incoherent noise from the highly coherent data which was characteristic of this test configuration. This number was used in the analysis of transient data, while 1024 averages were performed for the steady-state data because of the relative ease of implementing this improvement.

The speed window size used for analysis of the transient records was determined by comparing signal enhancements produced using various window widths. Figure 45 shows the effect of the window width on the amplitudes and phases of the signal enhanced pressures of microphone number 5 at 1810 Hz. Six enhancements were made for window widths between 20 and 200 Hz. At smaller widths, fewer samples were obtained since repeatability was seen to be improving. At the speed window width of 2 Hz (nominal $\pm$1 Hz) two types of data were taken. The first, designated by circles, corresponded to the type used in all larger windows where data was accumulated during both the increasing and decreasing portion of the speed change cycle. It was desired to narrow the window below this width in an effort to improve repeatability further, but noise which developed in one of the electronic components made this impossible. An alternative reduction, designated by squares, consisted of using this same window, but processing the data only during the increasing portion of the speed change cycle. The results of using this second technique were found to be more repeatable than the first technique and, for this reason, it was believed to provide a better basis for mode evaluation. All subsequent transient data were analyzed with the 2 Hz speed window with samples taken only during the increasing portion of the speed signal cycle.

To provide an upper limit for checking signal enhanced mode amplitudes, narrow band spectra were obtained for all steady-state records and blade passing frequency levels were recorded. Typical spectra are shown in Figure 46 for microphones 2 and 6 at 3229 rpm. In these figures, blade passing frequency can be seen to be the dominant tone and is well above the broadband background. Comparison of these blade passing tone levels with signal enhanced levels shows they are largely coherent. Their large change in level with microphone location indicates that the modal structure is probably dominated by relatively few coherent modes. Details of the spectrum other than at BPF and 2 BPF were found to be constant with location and speed and are, therefore, assumed to be part of the background machinery noise of the drive motor and broadband aerodynamic noise.

Spectral levels at the various blade passing frequencies are compared with steady-state signal enhanced levels and windowed transient levels in Figure 47 for microphones 1 through 7. Levels plotted here are also tabulated in Appendix A (Tables A1 through A14). These microphone data are the ones used with the MCP computer program of Reference 1 to determine the mode structure present in the duct. Steady state enhanced levels are seen to be in reasonably good agreement with those reported previously in Reference 1, where equivalent rig geometry and two nearly identical speed conditions were run. They are also slightly lower than the spectral levels at all points, but their close proximity indicates a high degree of coherence in the microphone signals. Steady-state enhanced levels are also in good agreement with narrow windowed transient levels for most cases. For those cases which differed by more than 3 dB from each other, both types of reduction were repeated and the results of each repeated within 1 dB. This indicates that a slight error remains which might be reduced with a narrower window or more exacting speed control during the recording and reduction process.

or narrow window transient levels because of cancellations associated with adding many signals with varying phases. Since the wide window levels are not representative of the steady state levels at any speed, their use would not likely result in a reasonable estimate of the mode structure.

Figure 48 shows phase angles which correspond with the enhanced levels shown in Figure 47. These angles are also tabulated in Tables A2 through A14 for reference. The agreement between the steady-state and narrow windowed data is seen to be good for most points. However, agreement with the data from Reference 1 is seen to be poor. This is believed to be the result of differing stator alignments between the two test programs or changes in the tach signal generator and not the result of faulty calibration of electronic equipment. As was seen with the amplitudes, phase data taken with a wide window are not representative of the data at any speed.

Mode amplitudes obtained at the five test frequencies are shown in Figures 49-53. Tabulated amplitudes and phases are also given in Tables A15-A27. Seven modes which include the (0,0), ($\pm$1,0), ($\pm$2,0), and ($\pm$3,0) propagate at the four highest speeds. The ($\pm$3,0) modes are, however, cutoff at the lowest speed. The mode amplitudes derived from steady-state data are shown with a standard deviation band based on estimated errors in microphone location, pressure amplitude and phase. The standard deviations used with the MCP computer program to produce the band are shown below:

σ_X = 0.00127 cm. = 0.0005 in.

σ_R = 0.00508 cm. = 0.002 in.

σ_θ = 0.0085 degrees = 1/2 minute

σ_B = 10.22 dynes/sq.cm. = 0.000015 psi.

σ_ϕ = 7 degrees

The conditioning numbers associated with the microphone locations are also shown for each speed.

In Figures 49-53, the steady-state mode amplitudes with their standard deviation bands are shown together with the narrow window transient mode amplitudes and those derived from the transient record using a wide window. This wide window was adjusted to allow passage of all data. At all speeds, agreement between steady-state and narrow window transient is best at the ($\pm$,0) modes (dominant modes) with poorer agreement at the remaining modes which are lower in level. Agreement is generally seen to be poorest for the low amplitude modes where the estimated standard deviation bands are largest, indicating that part of the differences for these low level modes can be attributed to the sensitivity of the calculations to experimental error. In no case, however, does the mode structure derived from the wide window transient data compare favorably with the other mode structures. This result was anticipated based on the lack of agreement of pressure amplitudes and phases.

The mode structure at the blade passing frequency of 1632 Hz requires further discussion. Although agreement of steady-state and transient data is excellent for this case, it will be recalled that the ($\pm$3,0) modes do not propagate at

this frequency. It was found that the high amplitudes shown for these modes are the result of the choice of the axial coordinate origin, which is the fan face in the current program. Since nonpropagating modes decay exponentially from the source, pressure data due to these modes could be expected to predict much higher mode amplitudes at the source if the source is assumed far away from the microphone array than if the source is assumed to be nearby. This result was confirmed by predicting mode structures at the source for several locations of the source and noting that only the nonpropagating modes changed in level as described.

A repeatability evaluation was made for the mode structures at 3394 rpm (1810 Hz). Mode amplitudes were calculated for each of the two taped records at this frequency and are shown in Figure 54. Also shown for comparison are two separate reductions of the windowed data and the results of a previous test program (See Reference 1). As was seen previously, agreement is excellent at the (±3,0) modes with somewhat larger differences at the other modes. Both the steady-state and transient modes repeat within 2 dB, but larger differences are seen between the two types of data reduction. A possible explanation of the larger differences lies in the fact that the speed variation observed in the steady record is comparable to the amount of variation in the transient record after windowing. If the data is very sensitive to speed variation and the two ranges are not exactly the same, as is likely in the present case, differences in calculated mode structure can occur. Narrower windowing of both types of data with window centers equal may then be required to improve agreement.

A further evaluation of the quality of the measured mode structure is provided by comparing measured pressures at several check microphone locations with values derived from the estimated mode structure. Since data was taken at 11 locations and 7 were used to estimate the mode structure, 4 sets of data were available for the comparison. Steady-state predicted and measured levels and windowed predicted and measured levels are shown in Figure 55 for microphone locations 8 through 11 at the 5 speeds tested. These results, together with corresponding phase angles are also presented in Tables A2-A14 for reference. Agreement between predicted and measured levels is best at 1632 Hz and slightly poorer at 1810, 1904 and 1992 Hz. Agreement is poorest at 1732 Hz which is the frequency where the pressure amplitude was seen to be most sensitive to speed change. To quantify these results, the standard error of the estimate was computed according to the following equation:

$$S.E.E. = \sqrt{\frac{\sum (P_{measured} - P_{estimated})^2}{Samples - 2}}$$

Calculations were performed in decibel units and are shown in Figure 55. Average S.E.E. values were computed for both the steady-state and the transient check mike amplitudes using the 5 test speeds. The S.E.E. was then computed for the wide windowed transient data. The average S.E.E. values for steady and transient data are seen to be approximately equal and much smaller than that obtained from the wide window data (i.e. 12.68 dB). From this it is concluded that the accuracy of the narrow windowed modes is equal to the steady-state, both of which represent a substantial improvement over the wide window data.

5.0 CONCLUSIONS

5.1 Analytical Studies

In each of the sections 3.1, 3.2, and 3.3, dealing respectively with partial circumferential arrays, arrays incorporating fan speed changes, and cutoff ratio arrays, detailed conclusions are given concerning the operation and feasibility of the methods.

Summarizing this material briefly, it is concluded that none of the array methods explored would be feasible to use for their intended purpose.

Underlying all these methods was the constraint that a "reasonable" number of fixed, flush-mounted wall microphones be used. This constraint immediately precludes the possibility of accurately measuring all of the large number of modes propagating in large fan rigs or engines. By establishing, instead, the objective of broadly defining the general structure of the sound field - which circumferential modes were dominant, and how the modes were distributed with respect to cutoff ratio - it was initially believed that acceptable tradeoffs could be found between accuracy of the systems and number of microphones required.

It was found that such tradeoffs could not be achieved. By any criterion, microphone numbers were excessive for even quite modest accuracy requirements. In the case of the cutoff ratio array, for example, a very crude definition of the distribution of modal power was found to require a number of microphones that actually exceeded the number of propagating modes by a large factor.

Documentation of the essential conclusion that none of the array methods are feasible, is given at length in the sections indicated above.

In a brief examination of the possibility of using axial arrays in random, rather than coherent, discrete frequency fields, it was found that, if the modes were uncorrelated most of the problems associated with the discrete frequency field applications were absent. However, this work was not pursued to the point where the feasibility of the application could be determined reliably.

5.2 Experimental Studies

From the information included in Section 4.0, the following conclusions concerning the experimental work were drawn:

1. The speed window, which passes all transient information, did not provide pressure or modal data which compare favorably with the corresponding steady-state data. However, narrow windowing produced pressure amplitudes, phases, and mode structures which compared more favorably with those steady state data, particularly for the dominant modes for which measurement accuracy is best. Furthermore, since the standard errors of the estimate (computed for transient and steady-state check microphones) were similar, it was concluded that the windowing variation technique was effective in removing the undesired effect of speed on acoustic data.

2. Repeatability was good for repeated use of the windowing technique on the same data record and also for equivalent speed records on the same tape. It was only slightly poorer when data from two separate programs, run three years apart, were compared. From this it is concluded that the 10-inch rig was a satisfactory vehicle for demonstrating the effects of speed windowing.

3. The difference between steady-state and transient modes was greater than the scatter in either set of data for the one speed at which this comparison was made. This difference suggests that small speed changes, such as were seen to exist in a typical steady-state record, may produce detectable errors in computed mode structure and require that windowing be applied to apparently steady-state data when a high degree of accuracy is desired.

4. Pressure amplitudes were seen to be sensitive to slight changes of speed near those speeds where any mode transitions from cutoff to cuton. In these regions a higher accuracy in setting the window location and width is therefore required.

6.0 RECOMMENDATIONS

No further efforts are warranted to develop fixed flush-mounted wall microphone arrays for the purposes of defining dominant modes or cutoff ratio distributions in coherent, discrete frequency fan noise fields.

For measuring the distribution of modal power with respect to cutoff ratio in random noise fields having uncorrelated modes, a preliminary examination shows that the requirements are less severe than for coherent, discrete frequency fields. This application cannot yet be ruled unfeasible, and could be reserved for future consideration in more detail.

Since the need to define mode structure in fans cannot be expected to diminish, schemes other than the fixed array systems involving excessive numbers of microphones should be re-examined to determine whether some of their undesirable features can be overcome.

The speed windowing technique should be considered for applications where speed change causes degradation in the accuracy of measured pressure amplitudes and phases and an improved accuracy is desired.

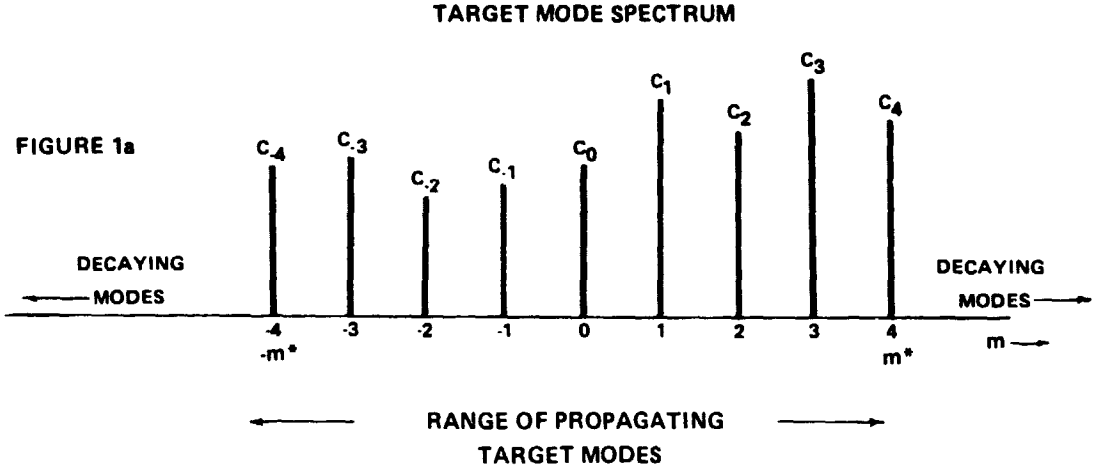

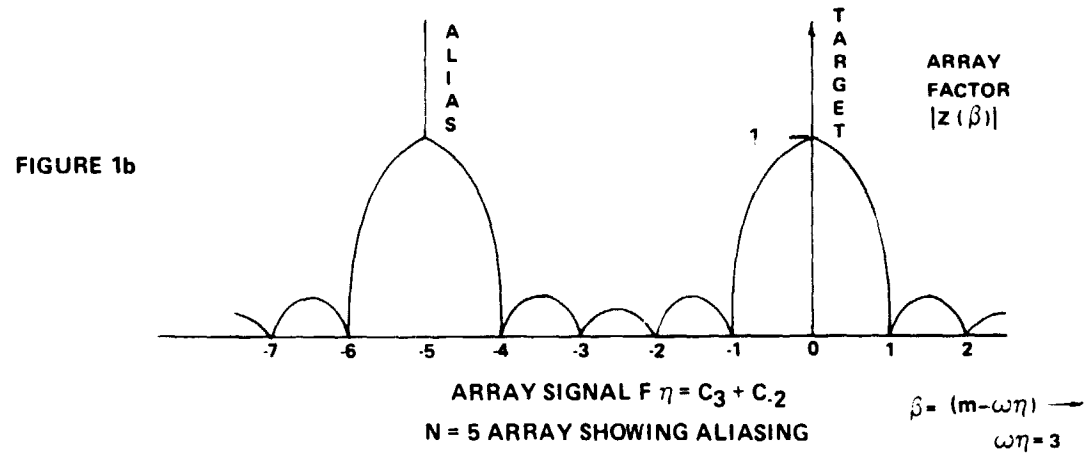

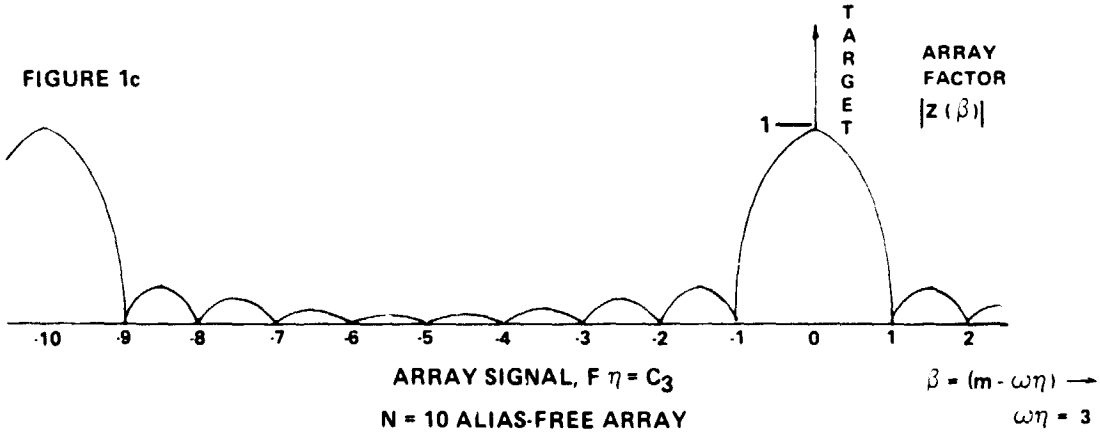

Figure 1 Illustration of Arrays With and Without Aliasing

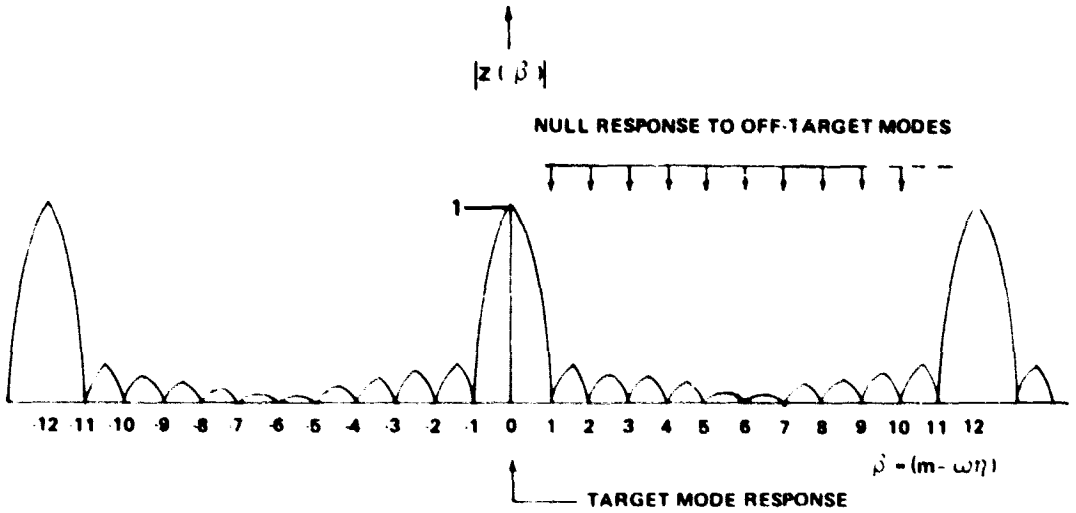

REFERENCE FULL ARRAY N = 12

FIGURE 2a

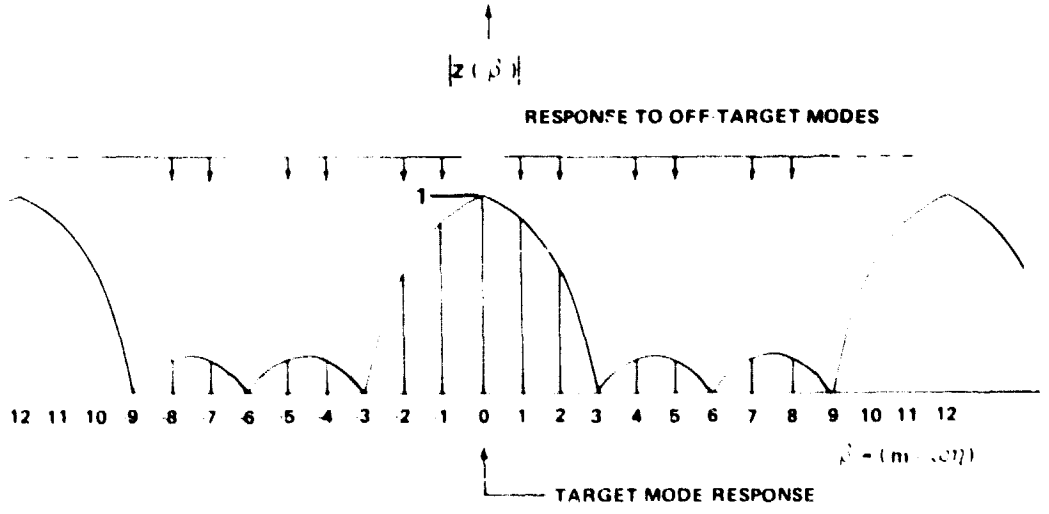

PARTIAL CIRCUMFERENTIAL ARRAY N = 4, F = 3

FIGURE 2b

Figure 2 Array Factors for Full and Partial Circumferential Arrays

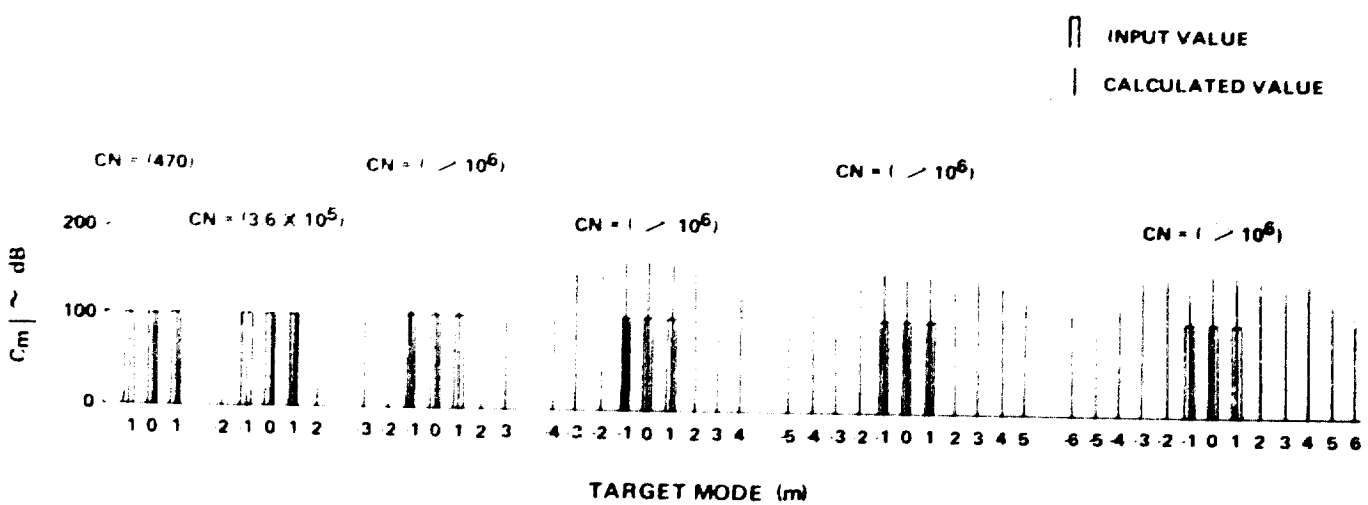

Figure 3 Calculated Modal Amplitudes for Input Modes m = -1, 0, 1. N = 10, P = 4 Array (Microphone Readings Truncated to 0.1 dB)

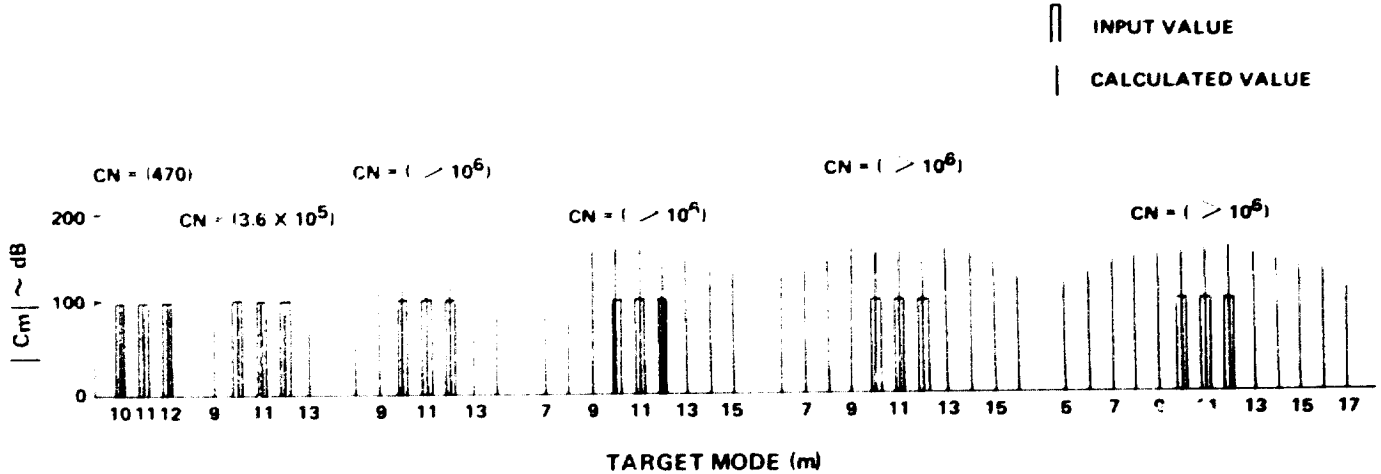

Figure 4 Calculated Modal Amplitudes for Input Modes m = 10, 11, 12. N = 10, P = 4 Array (Microphone Readings Truncated to 0.1 dB)

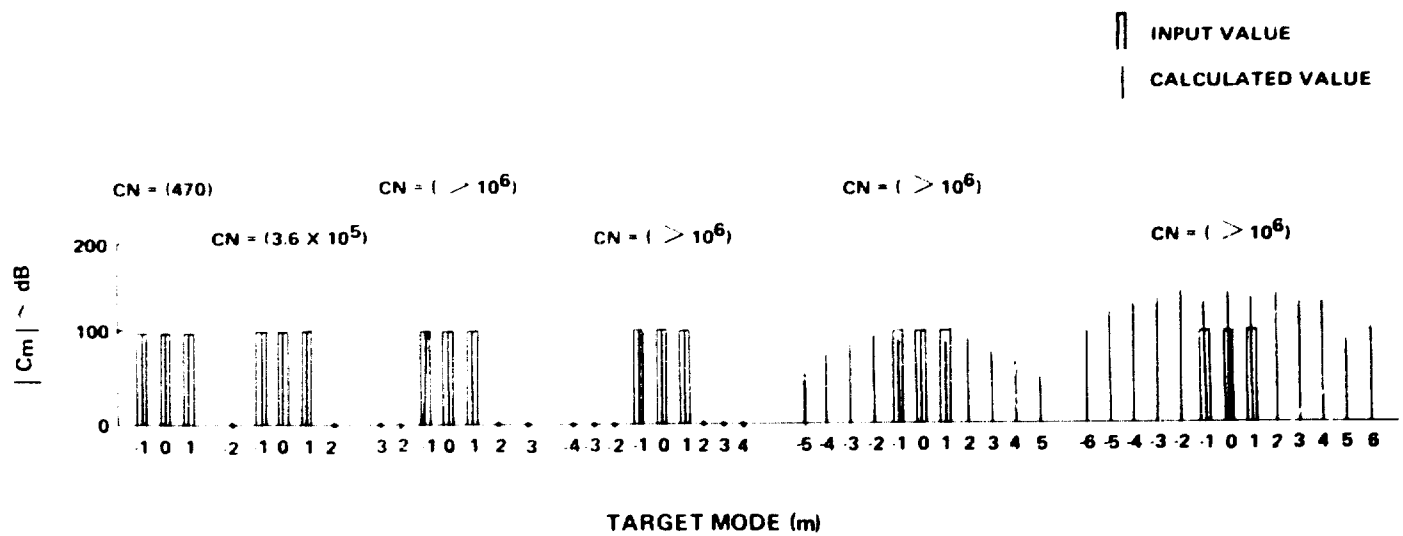

Figure 5 Calculated Modal Amplitudes for Input Modes m = 1, 0, 1. N = 10, F = 4 Array (Microphone Readings Not Truncated)

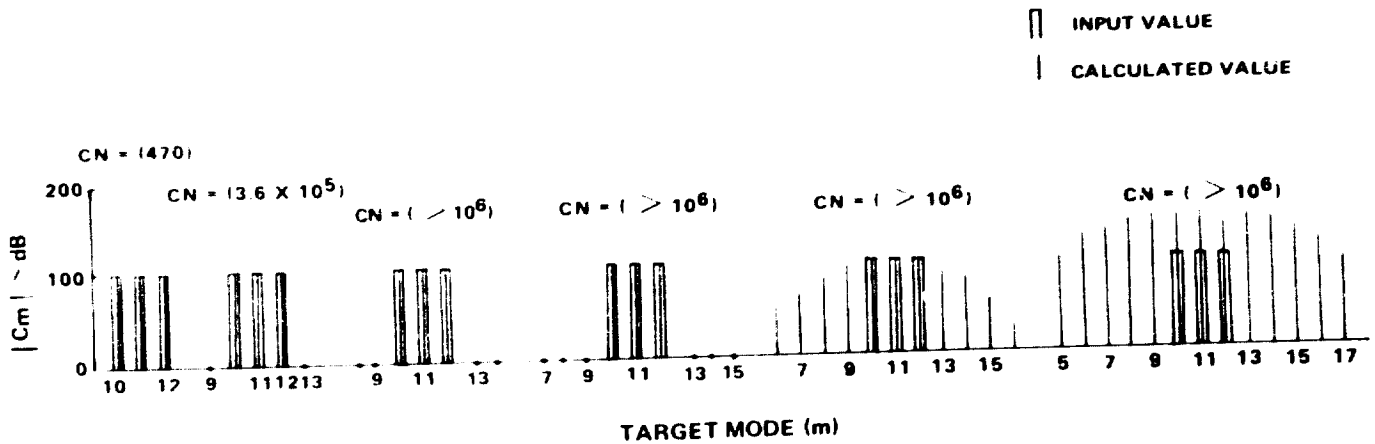

Figure 6 Calculated Modal Amplitudes for Input Modes m = 10, 11, 12, N = 10, P = 4 Array (Microphone Readings Not Truncated)

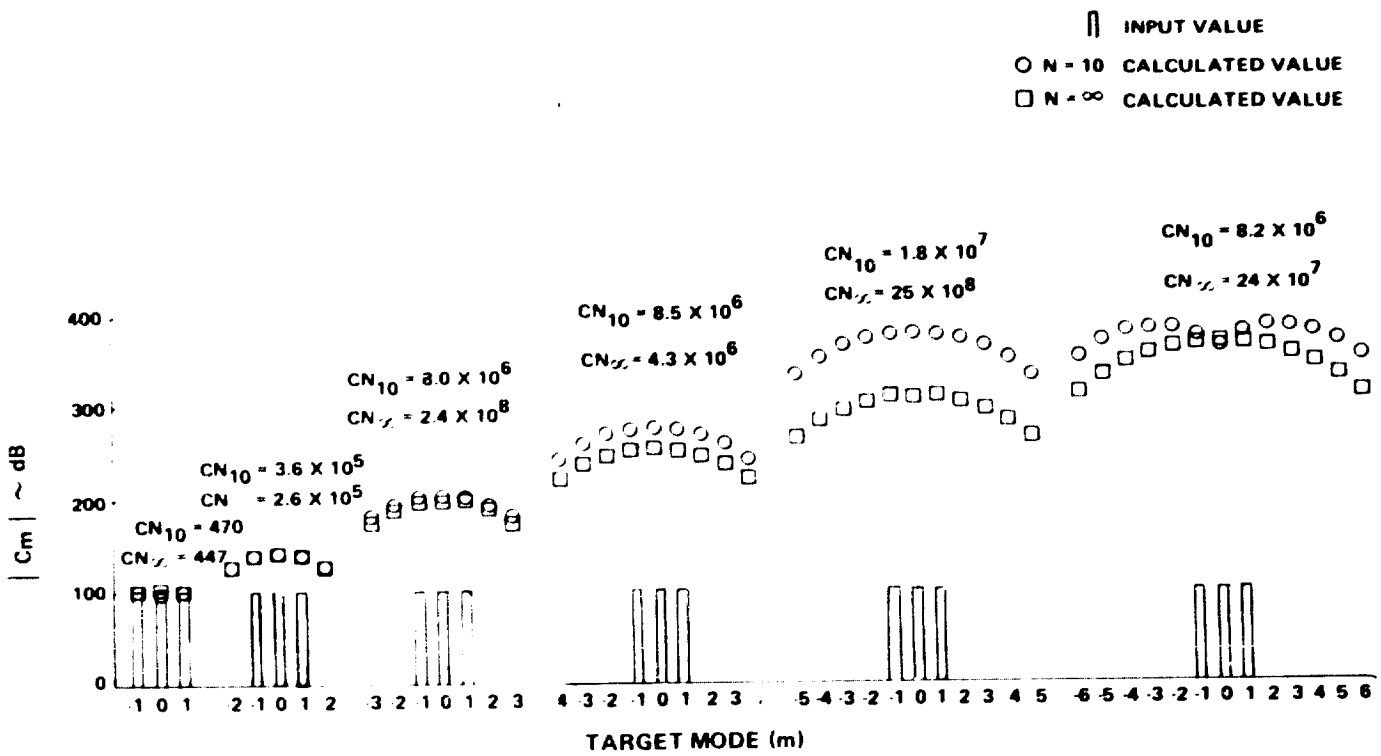

Figure 7 Effect of Microphone Number on Accuracy of P = 4 Partial Circumferential Array, N = 10 and N = ∞, Input Modes -1, 0, 1, (Array Signal Rounded to Nearest dB)

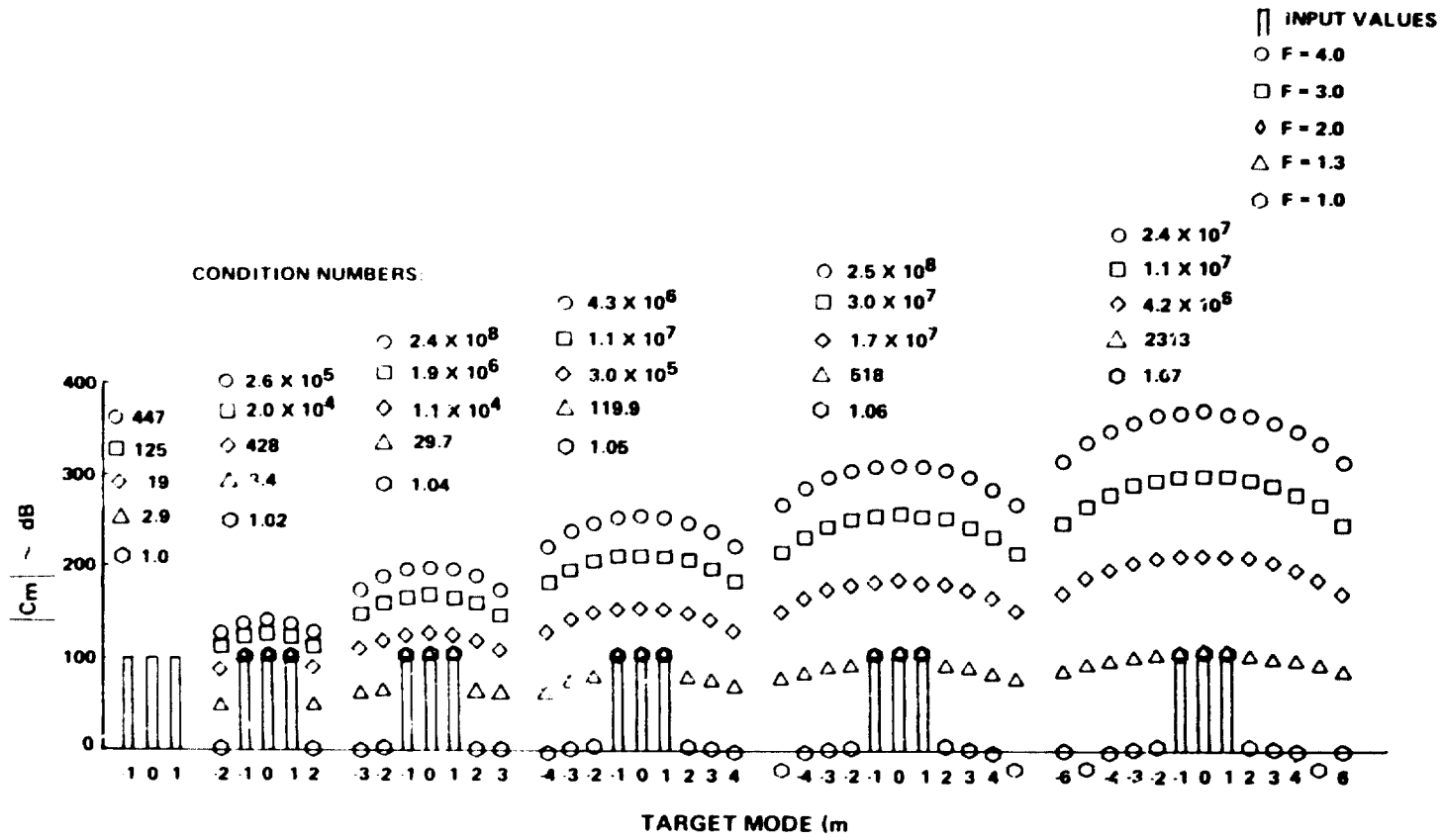

Figure 8 Effect of Circumferential Array Length on Accuracy of N = ∞ Array (Array Signal Rounded to Nearest ~ dB)

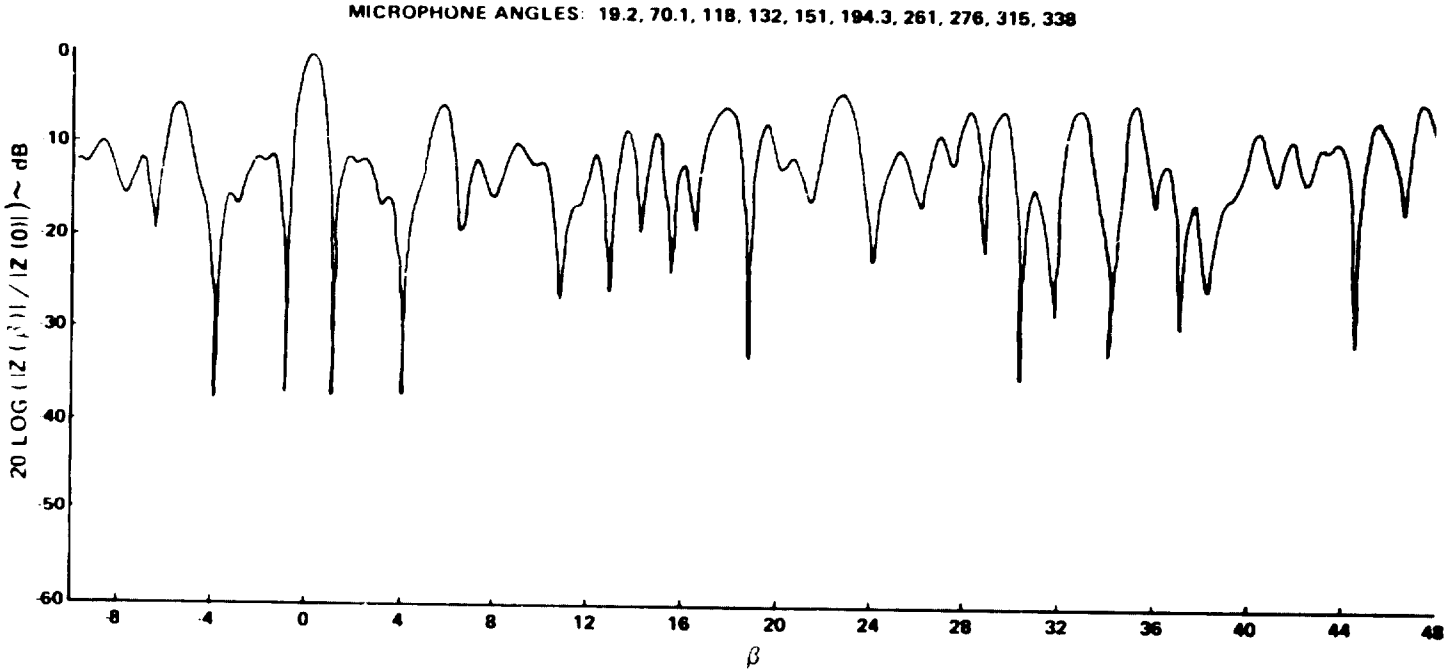

Figure 9 Array Factor for 10 Irregularly Spaced Microphones

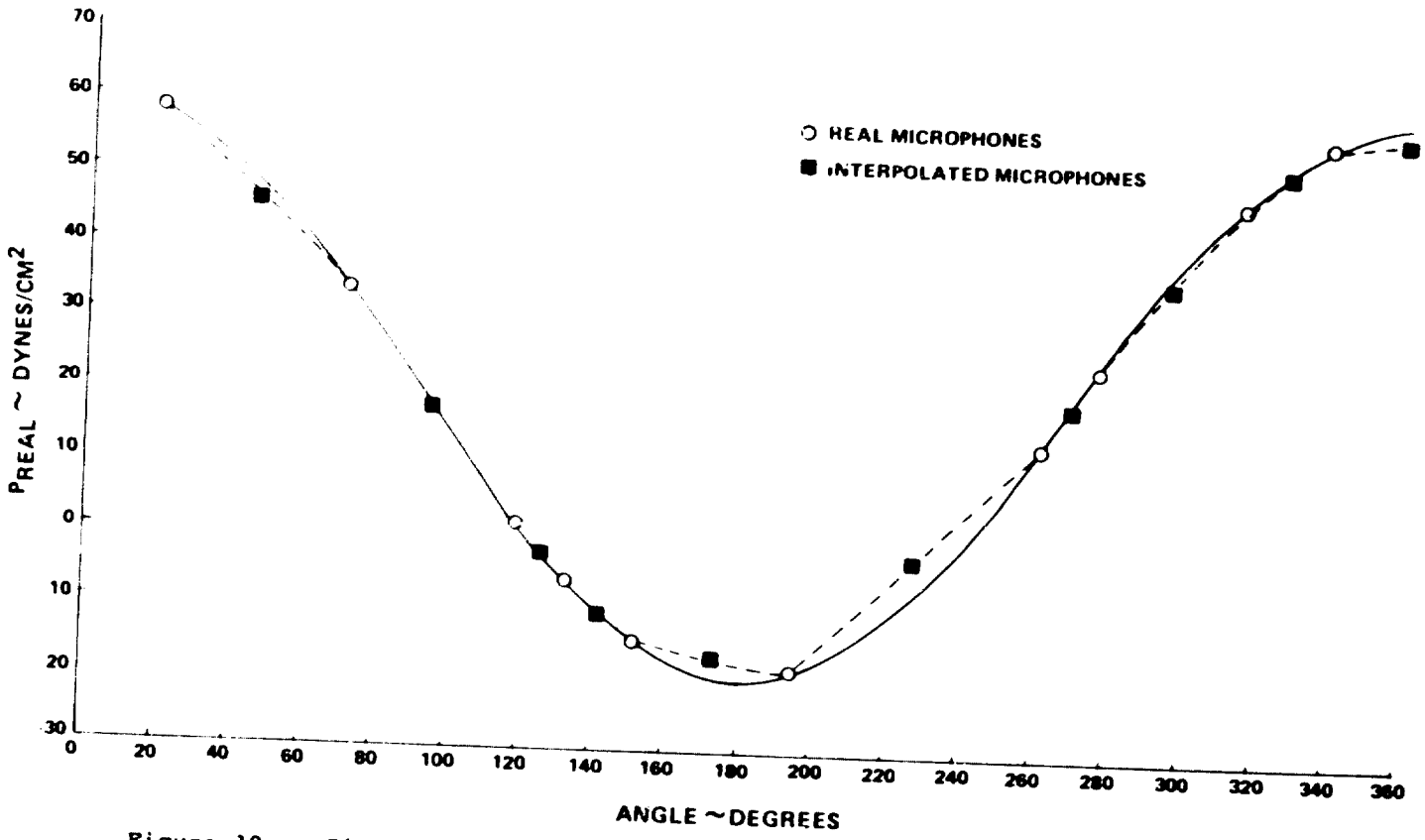

Figure 10 Circumferential Distribution of Pressure and Microphone Readings, Irregularly Spaced Array, Input Modes m = -1, 0, 1

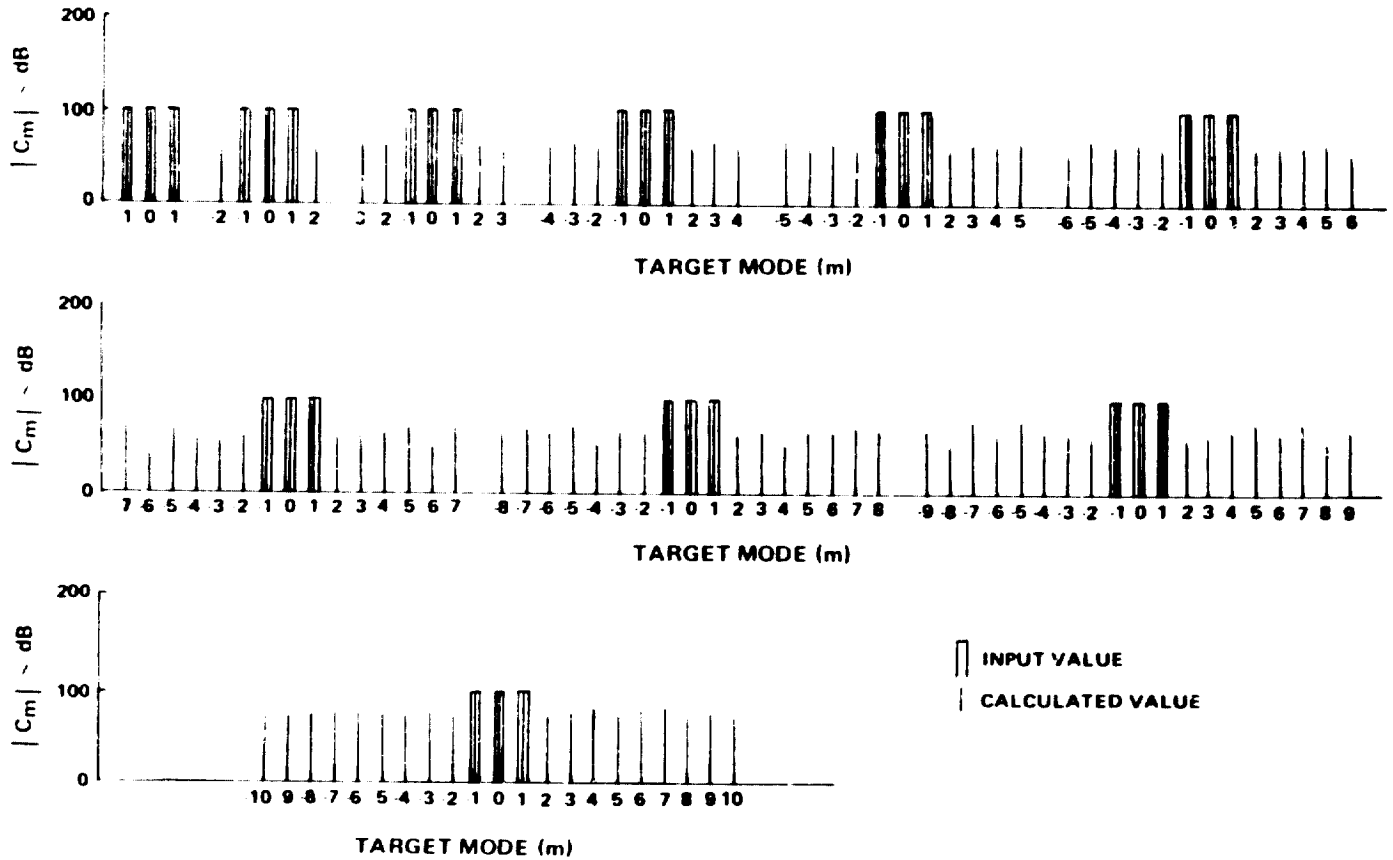

Figure 11 Accuracy of Irregularly Spaced Array, 10 Real Microphones Plus 10 Interpolated Readings, Input Modes m = -1, 0, 1 (Pressures Truncated to 0.1 dB)

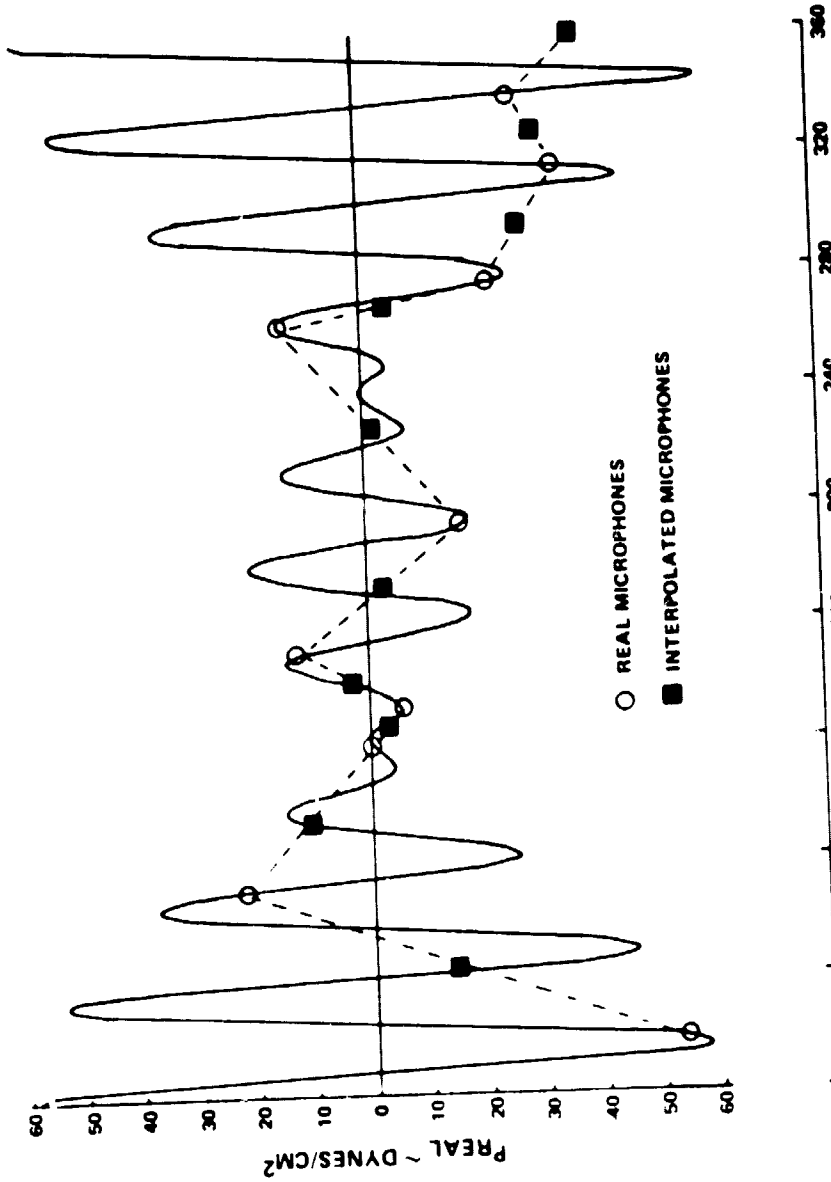

Figure 12 Circumferential Distribution of Pressure (Real Part) and Microphone Readings, Irregularly Spaced Array, Input Modes m = 10, 11, 12

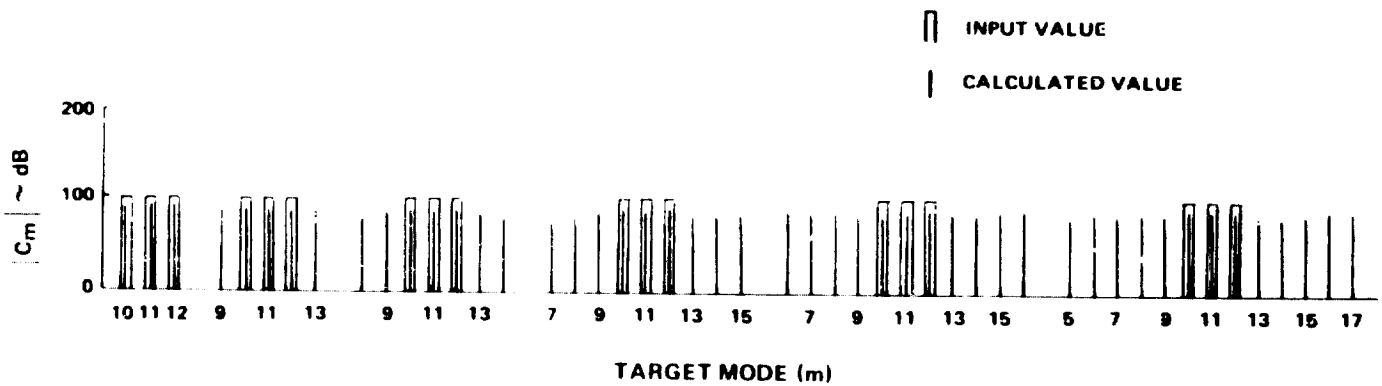

Figure 13 Accuracy of Irregularly Spaced Array, 10 Real Microphones Plus 10 Interpolated Readings, Input modes m = 10, 11, 12

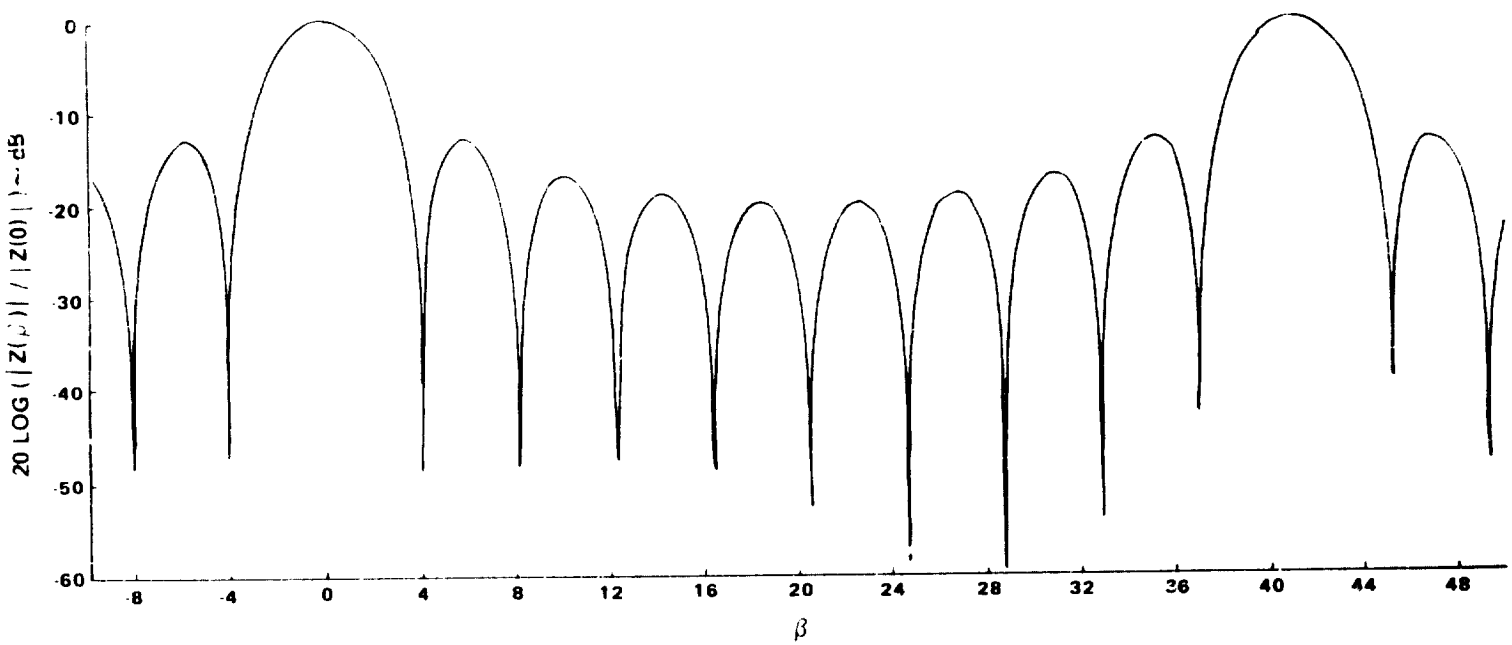

Figure 14 Array Factor for N = 10, F = 4.1 Partial Circumferential Array, Rectangular Window

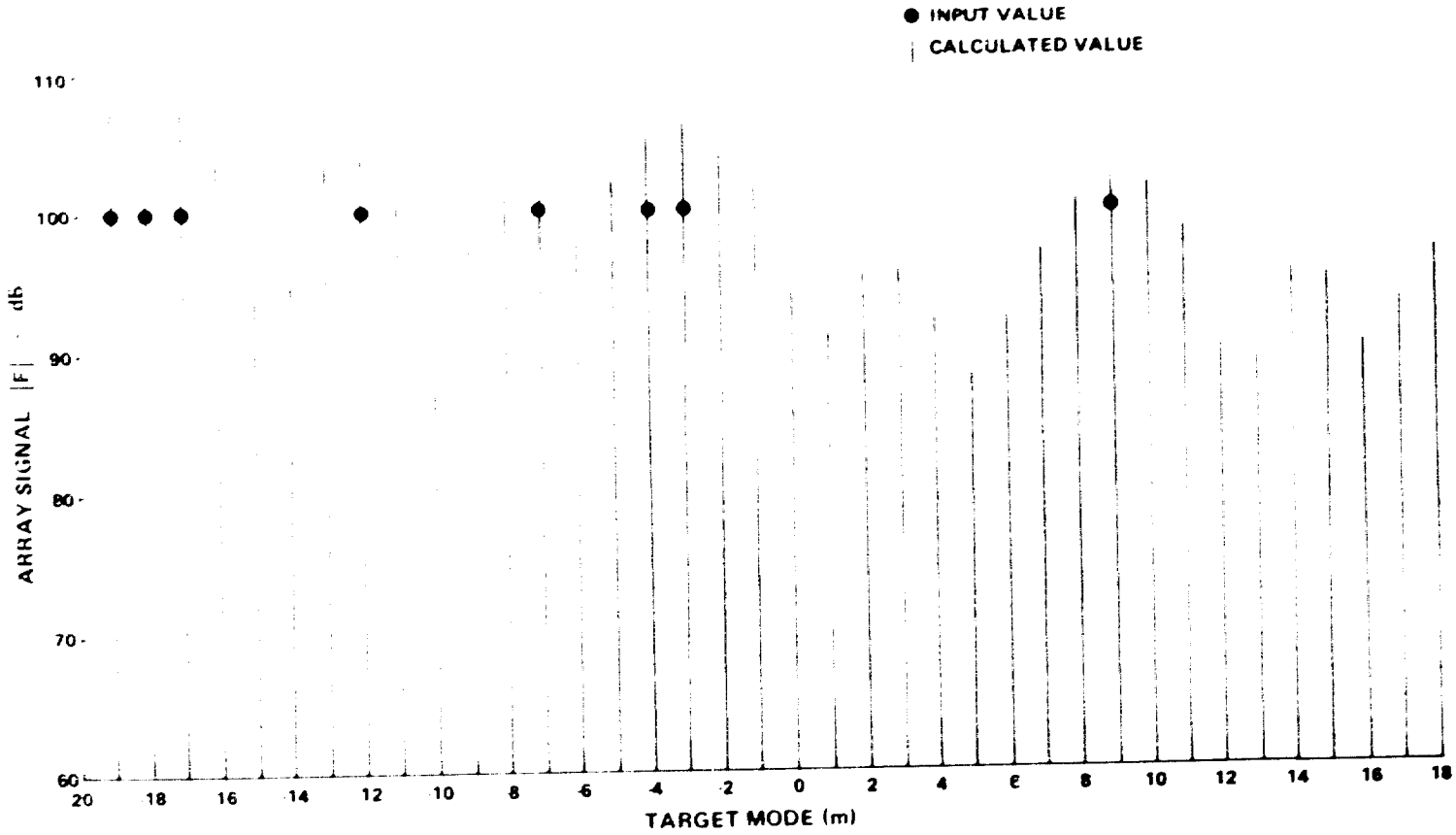

Figure 15 Response of N = 10, P = 4.1 Array to Set of 8 Modes of Equal Amplitude and Phase

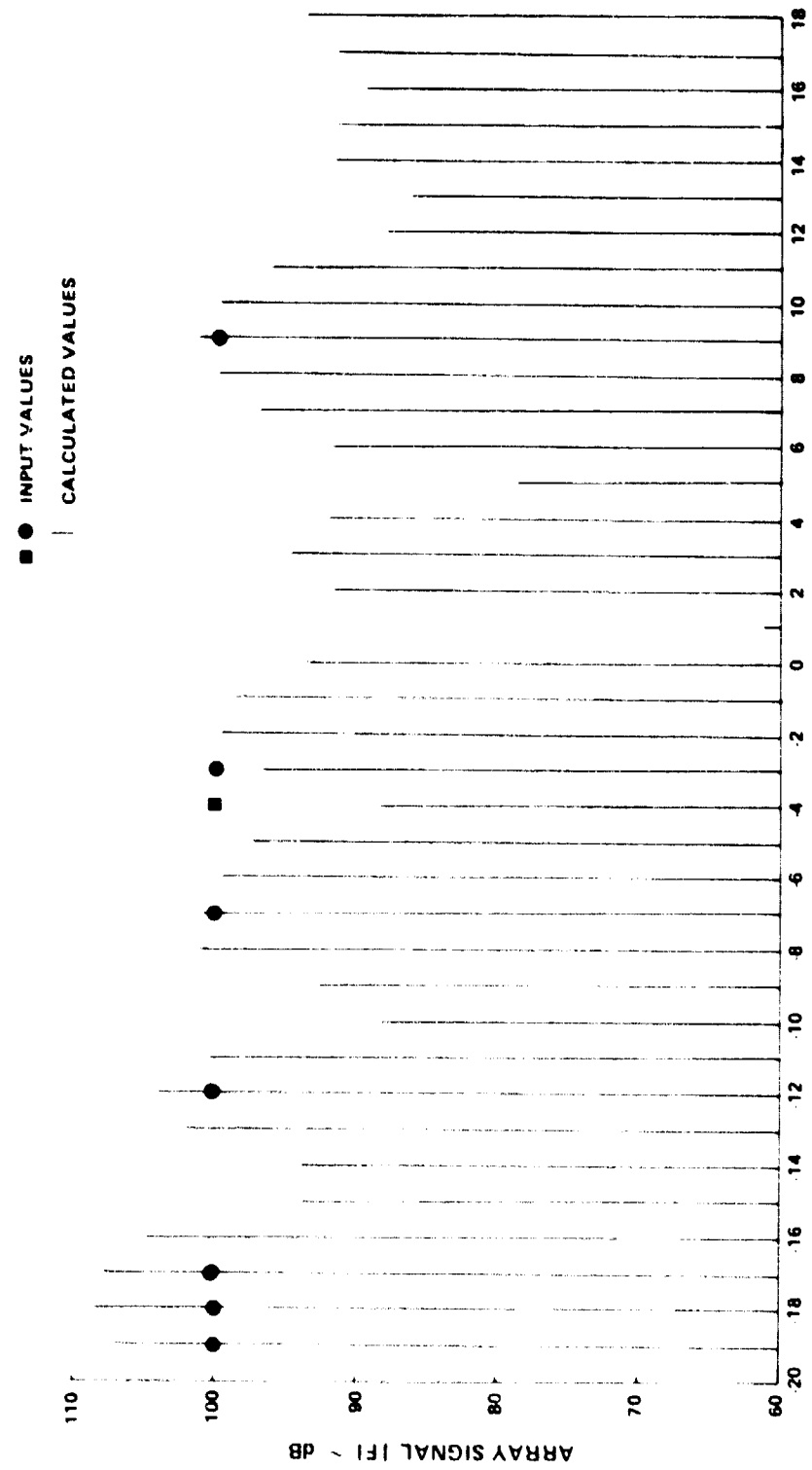

Figure 16 Response of N = 10, P = 4.1 Array, 7 Equal Input Modes Plus 1 Shifted 180°

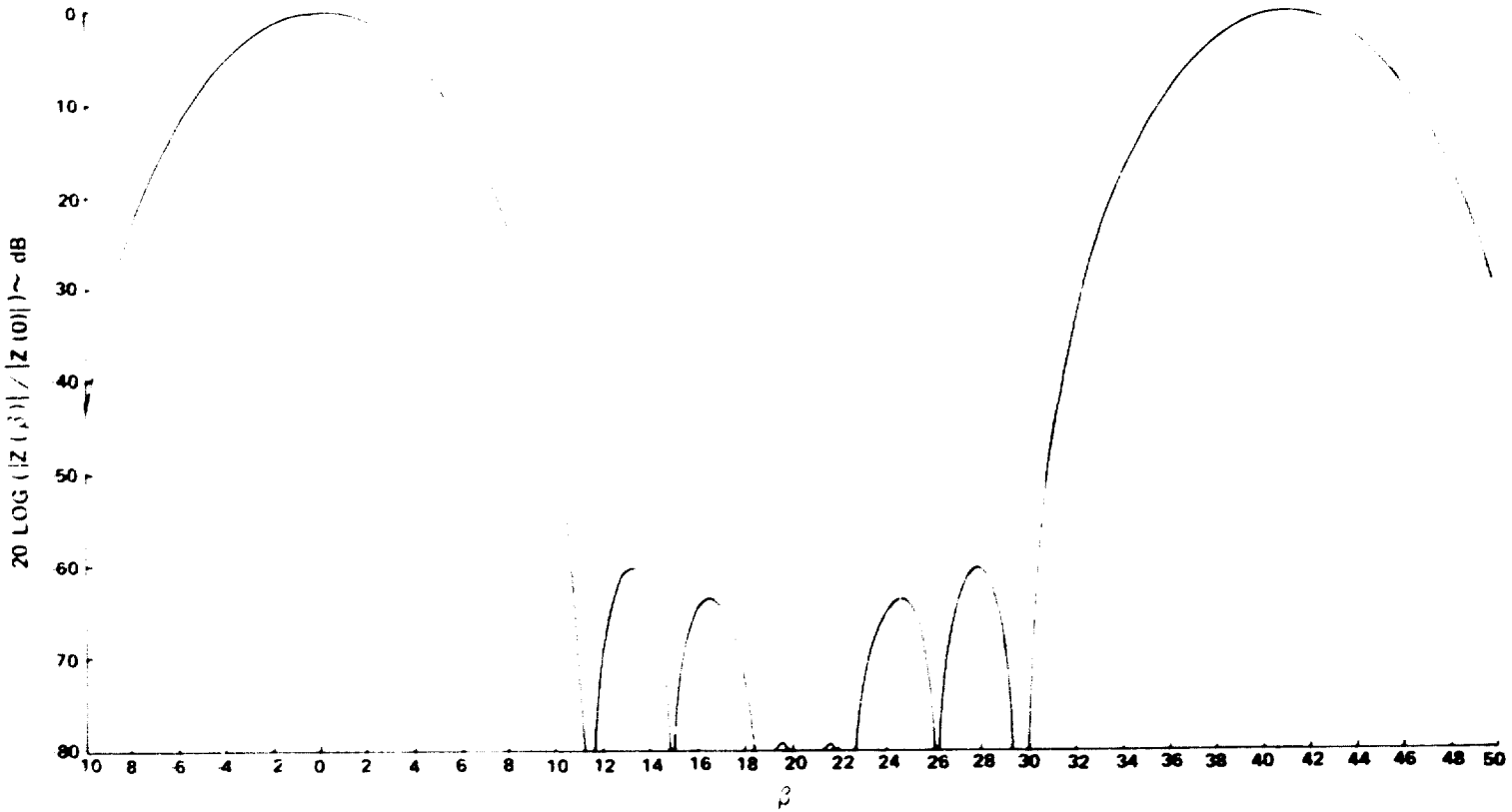

Figure 17 Array Factor for N = 10, P = 4.1 Partial Circumferential Array, Blackman Window

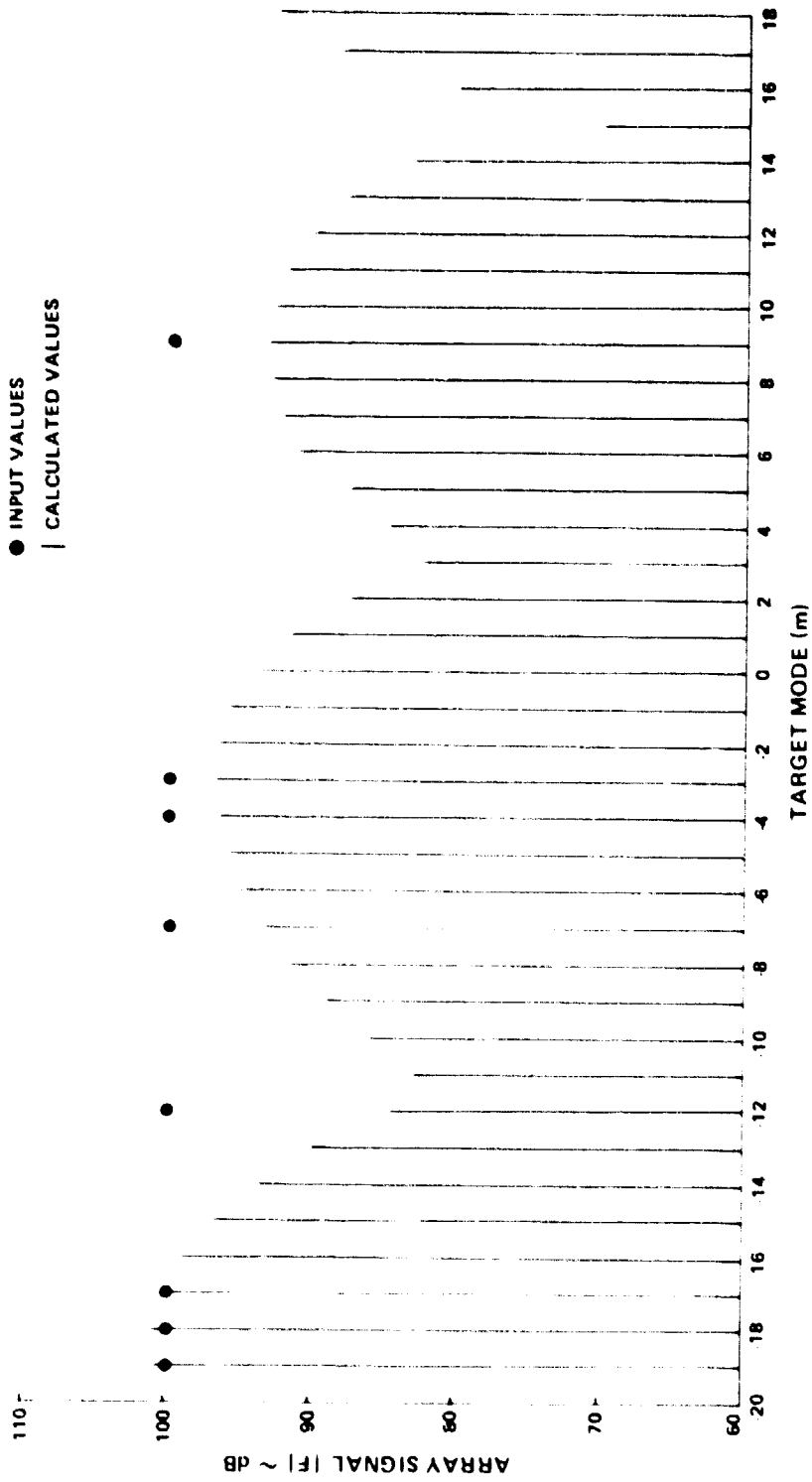

Figure 19 Response of N = 10, P = 4.1 Array with Blackman Window, 8 Equal Input Modes

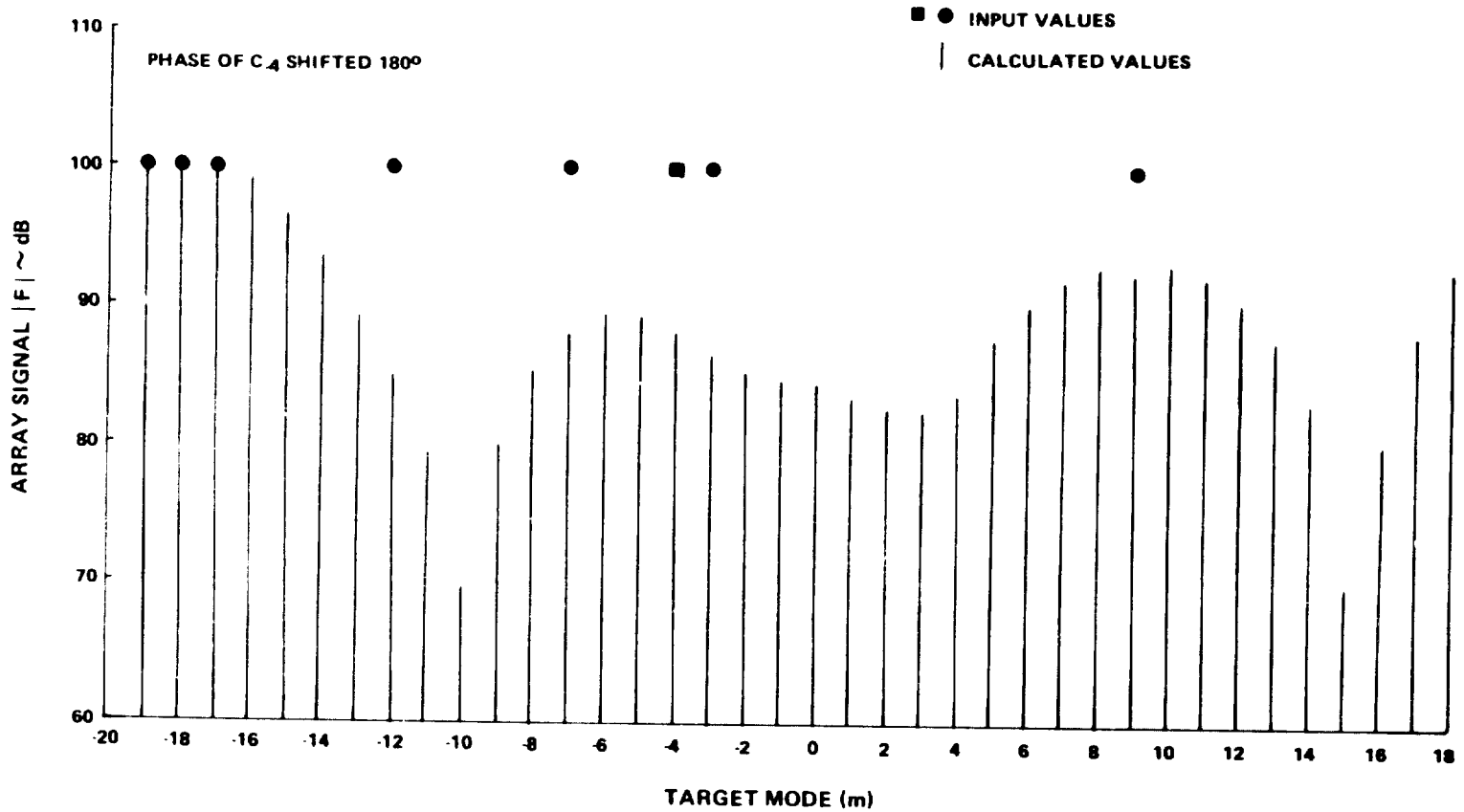

Figure 19 Response of N = 10, F = 4.1 Array with Blackman Window, 7 Equal Modes Plus 1 Shifted 180°

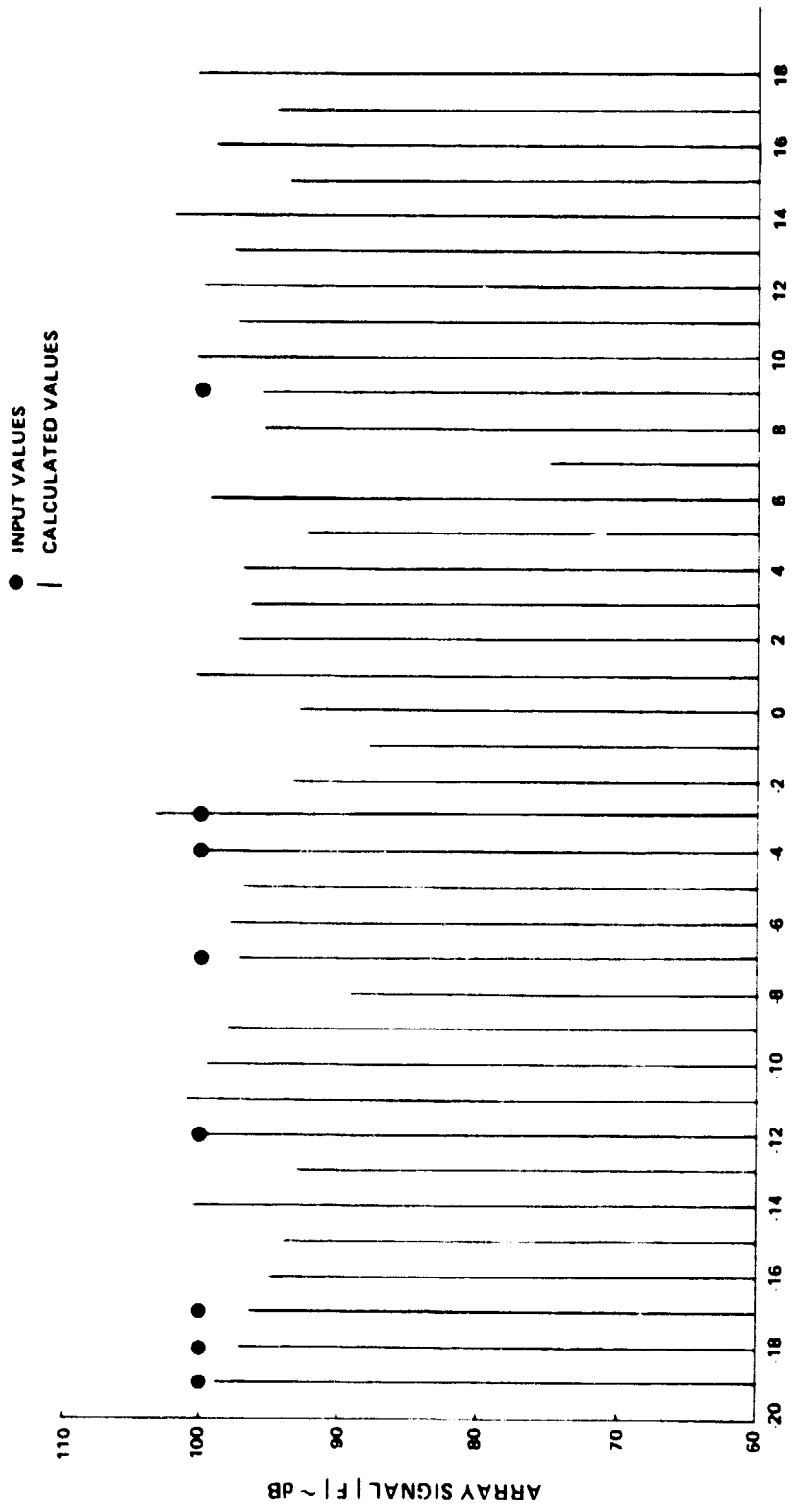

Figure 20 Response of Irregularly Spaced Array (Z (β) in Fig. 9) to Set of 8 Equal Input Modes

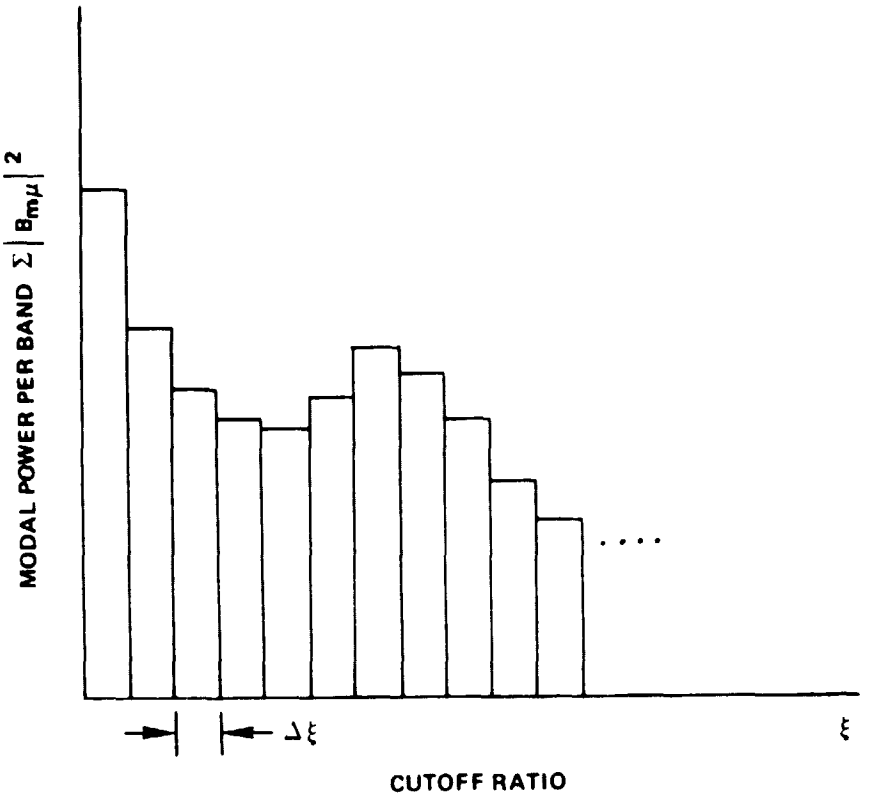

Figure 21 Illustrative Distribution of Modal Power With Respect to Cutoff Ratio

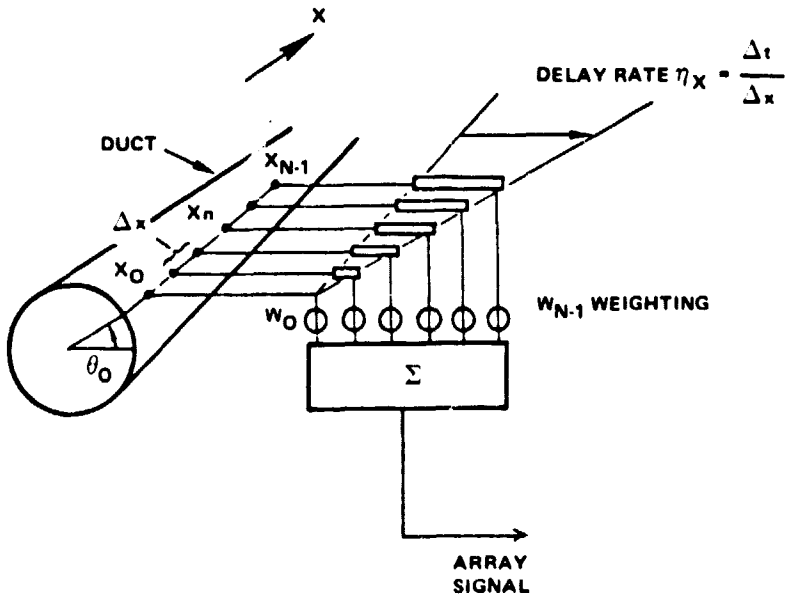

Figure 22 Diagram of Axial Array for Enhancing Modes on a Cutoff Ratio Basis

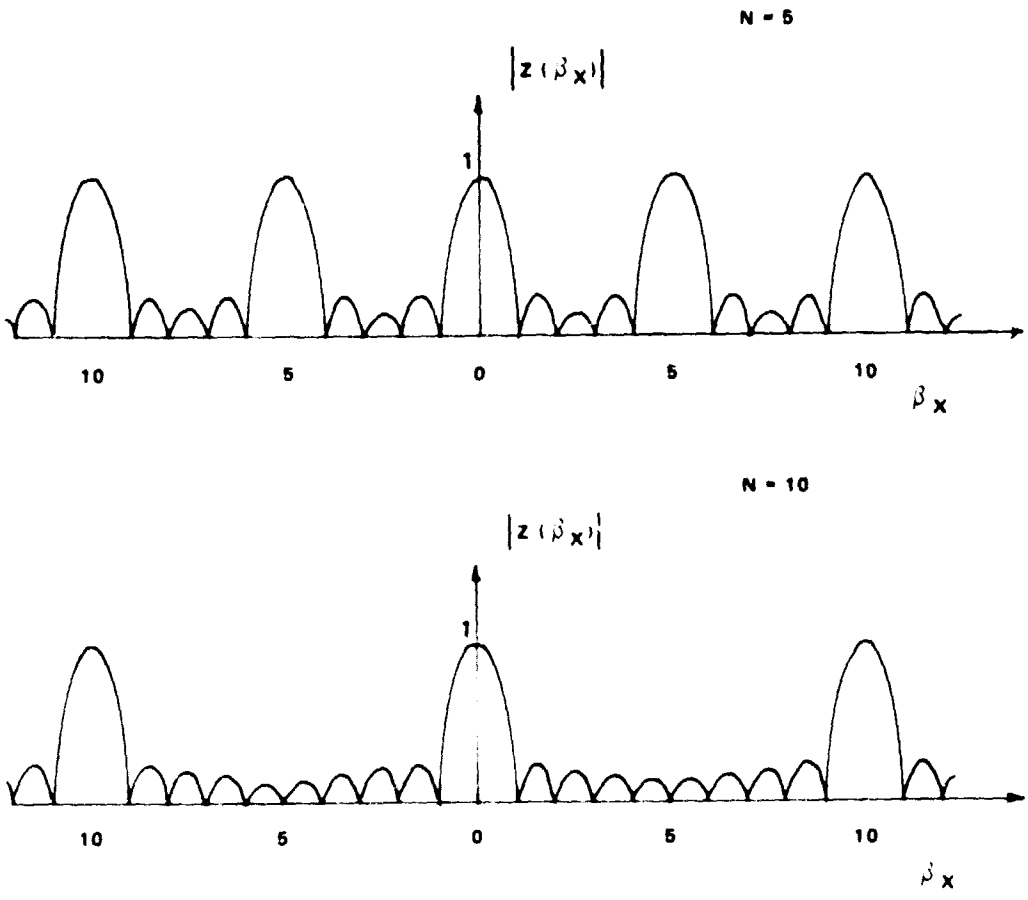

Figure 23 Array Factors for 5 and 10 Microphone Axial Arrays

FIGURE 24a

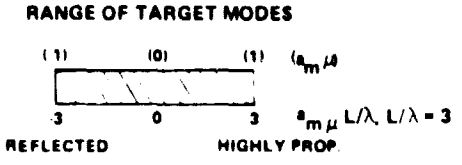

FIGURE 24b

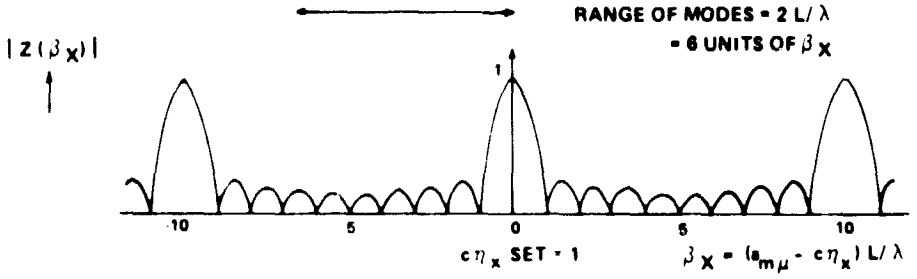

ARRAY TRACKING HIGHLY PROPAGATING MODES ($a_{m\mu}$ 1)

FIGURE 24c

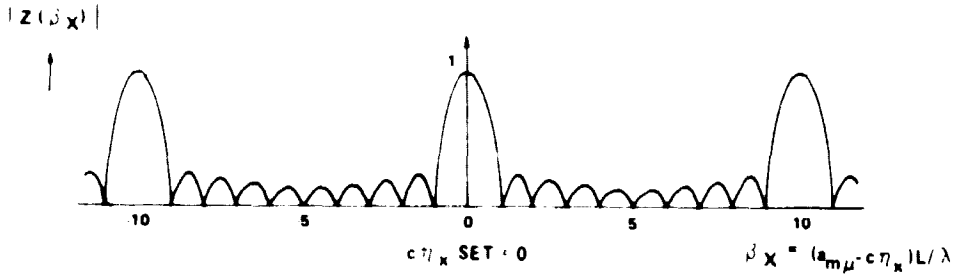

ARRAY TRACKING MODES NEAR CUTOFF ($a_{m\mu}$ = 0)

FIGURE 24d

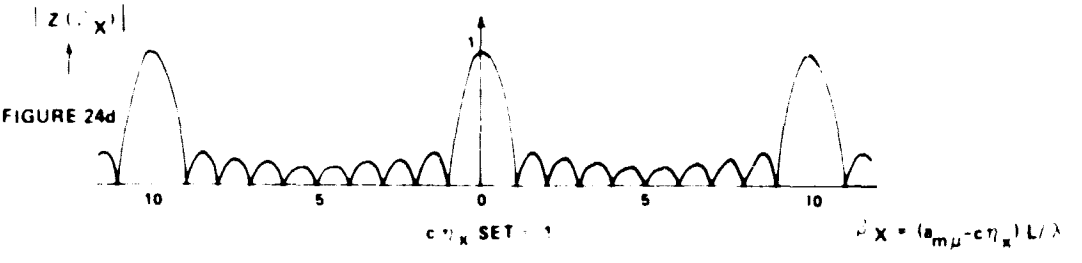

ARRAY TRACKING REFLECTED MODES ($a_{m\mu}$ = -1)

Figure 24 Use of N = 10, L/λ = 3 Axial Array in Tracking Different Target Modes

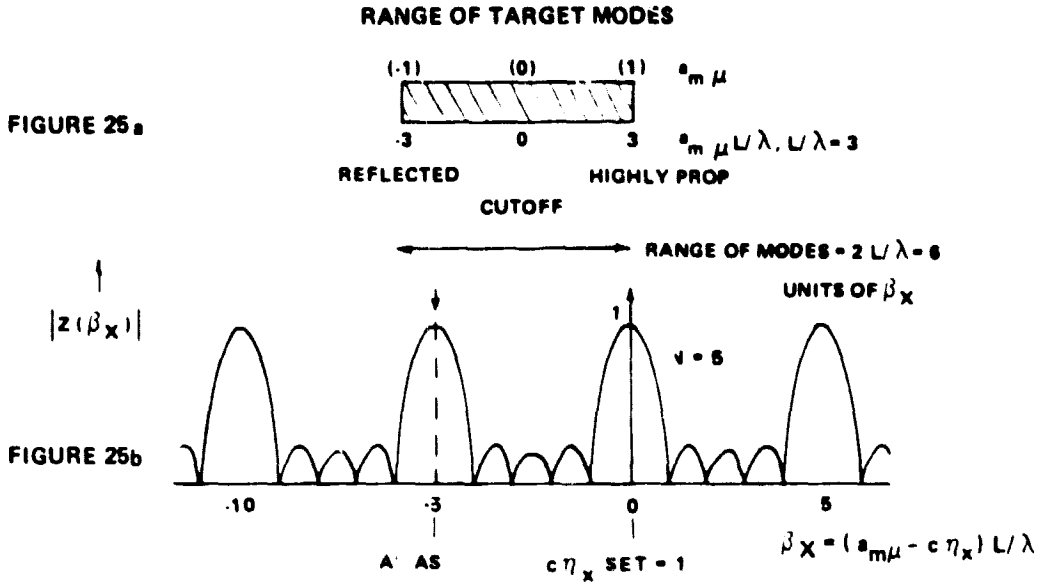

FIGURE 25a

FIGURE 25b

ARRAY TRACKING PROPAGATING MODES SIGNAL ALIASED BY MODES AT $a_{m\mu} = -2/3$

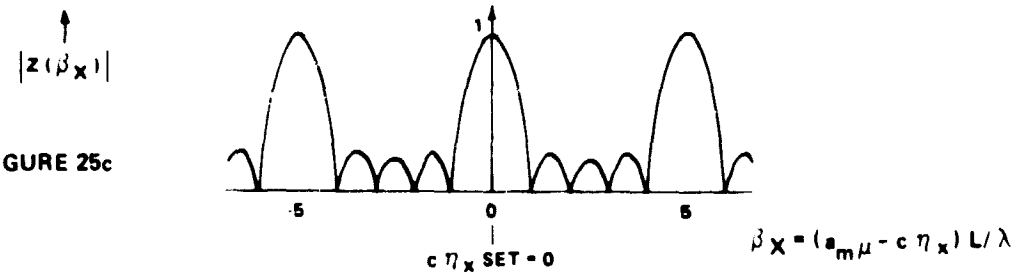

FIGURE 25c

ARRAY TRACKING MODES NEAR CUTOFF, NO ALIASING

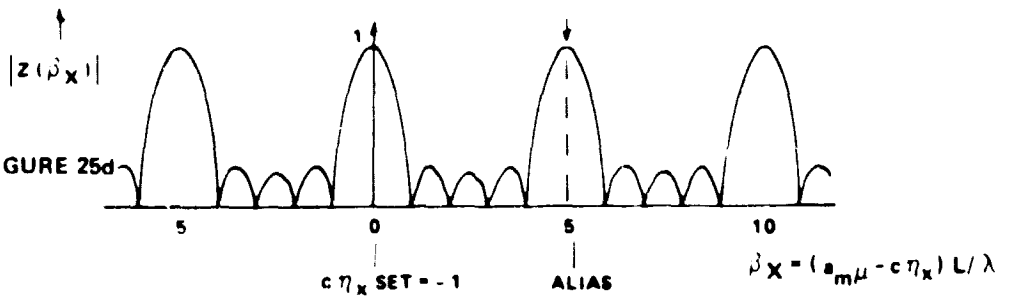

FIGURE 25d

ARRAY TRACKING REFLECTED MODES SIGNAL ALIASED BY MODES AT $a_{m\mu} = 2/3$

Figure 25 Illustration of Aliasing Caused by Insufficient Number of Microphones

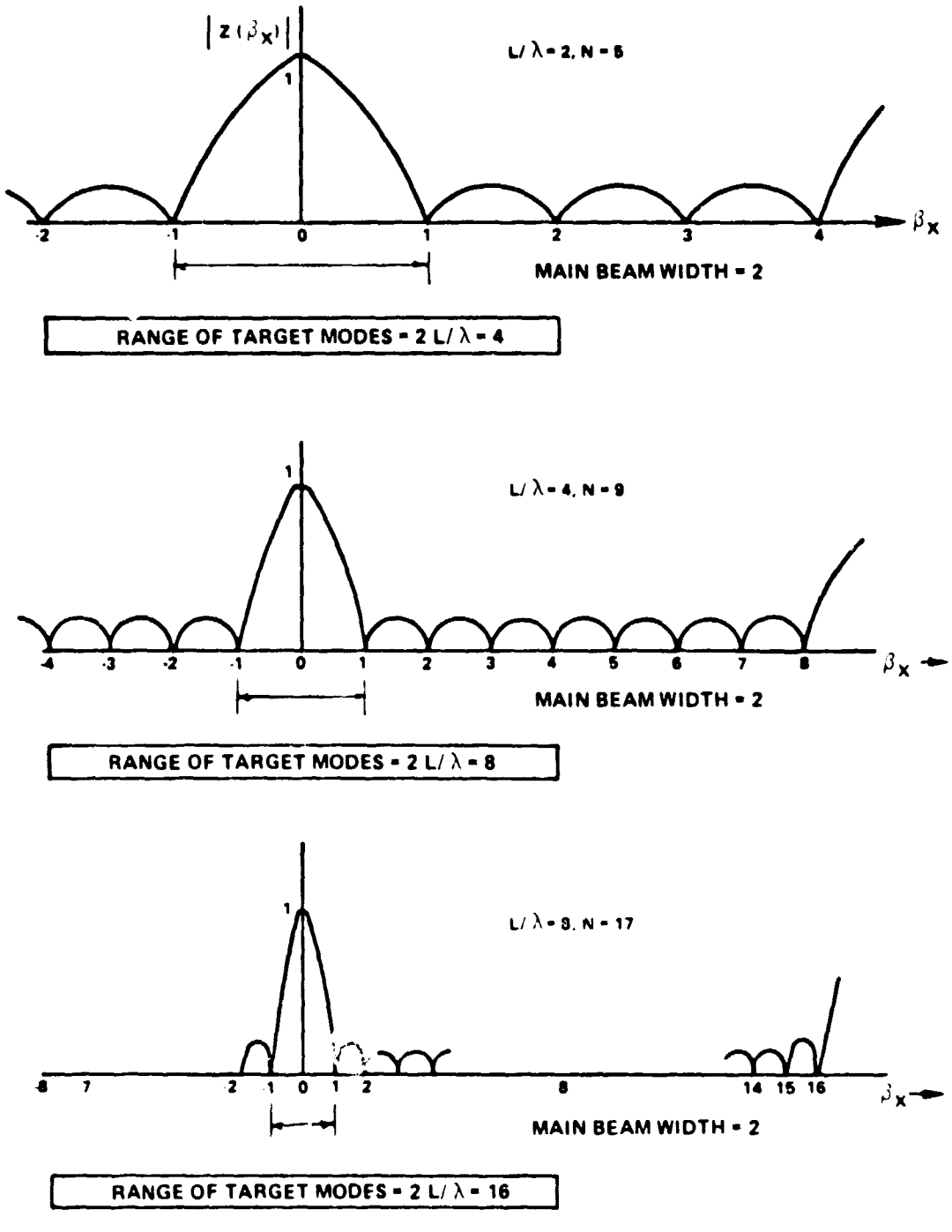

Figure 26 Use of Increased Array Length of Improve Sharpness or Resolution

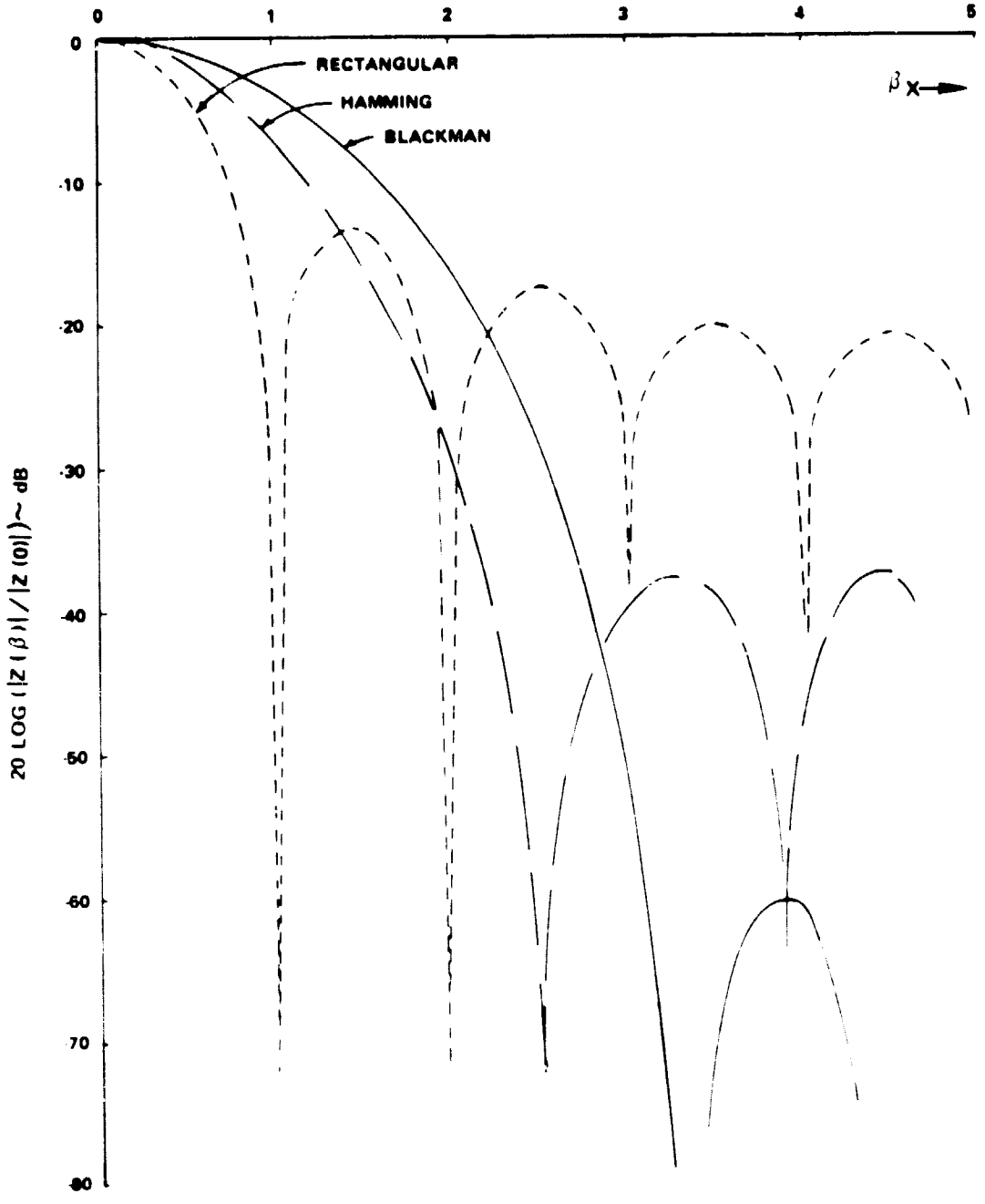

Figure 27 Illustration of Minor Lobe Suppression and Main Lobe Broadening With Use of Weighting Functions, N = 12 Array

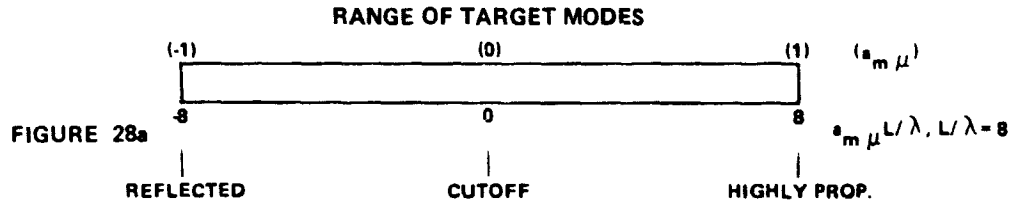

FIGURE 28a

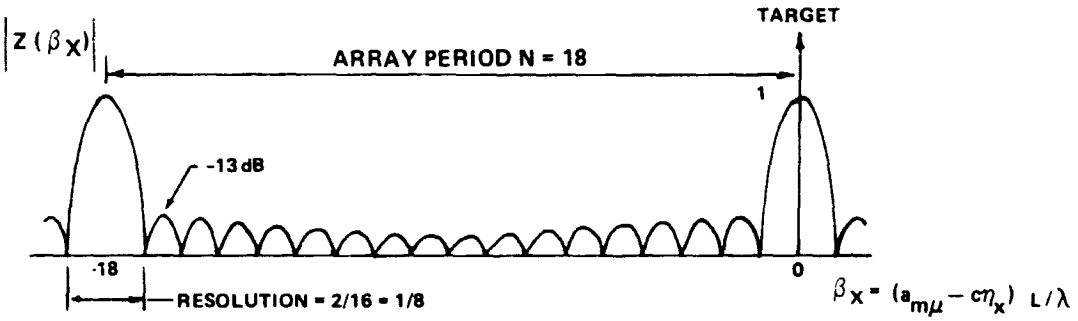

FIGURE 28b

$C\eta_X$ SET = 1

N = 18 RECTANGULAR WEIGHTING

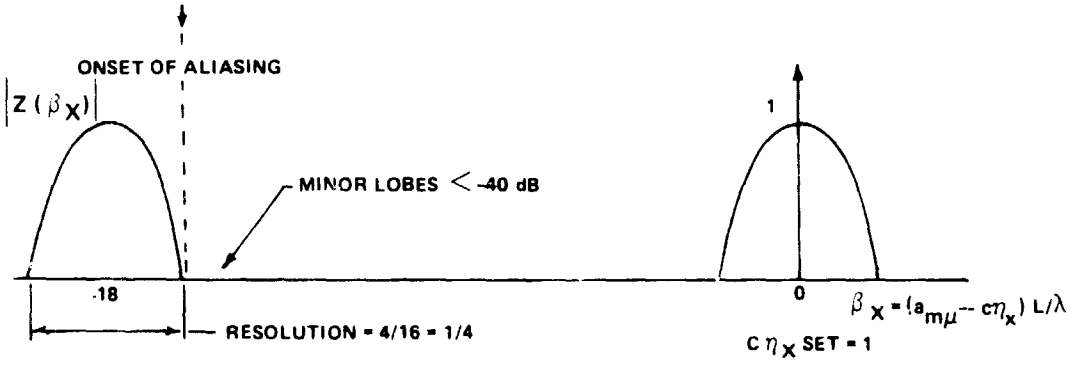

FIGURE 28c N = 18 ARRAY-HAMMING WEIGHTING

Figure 28 Reduction of Resolution and Antialiasing Margin -- Byproducts of Use of Hamming Weighting to Reduce Minor Lobe Response

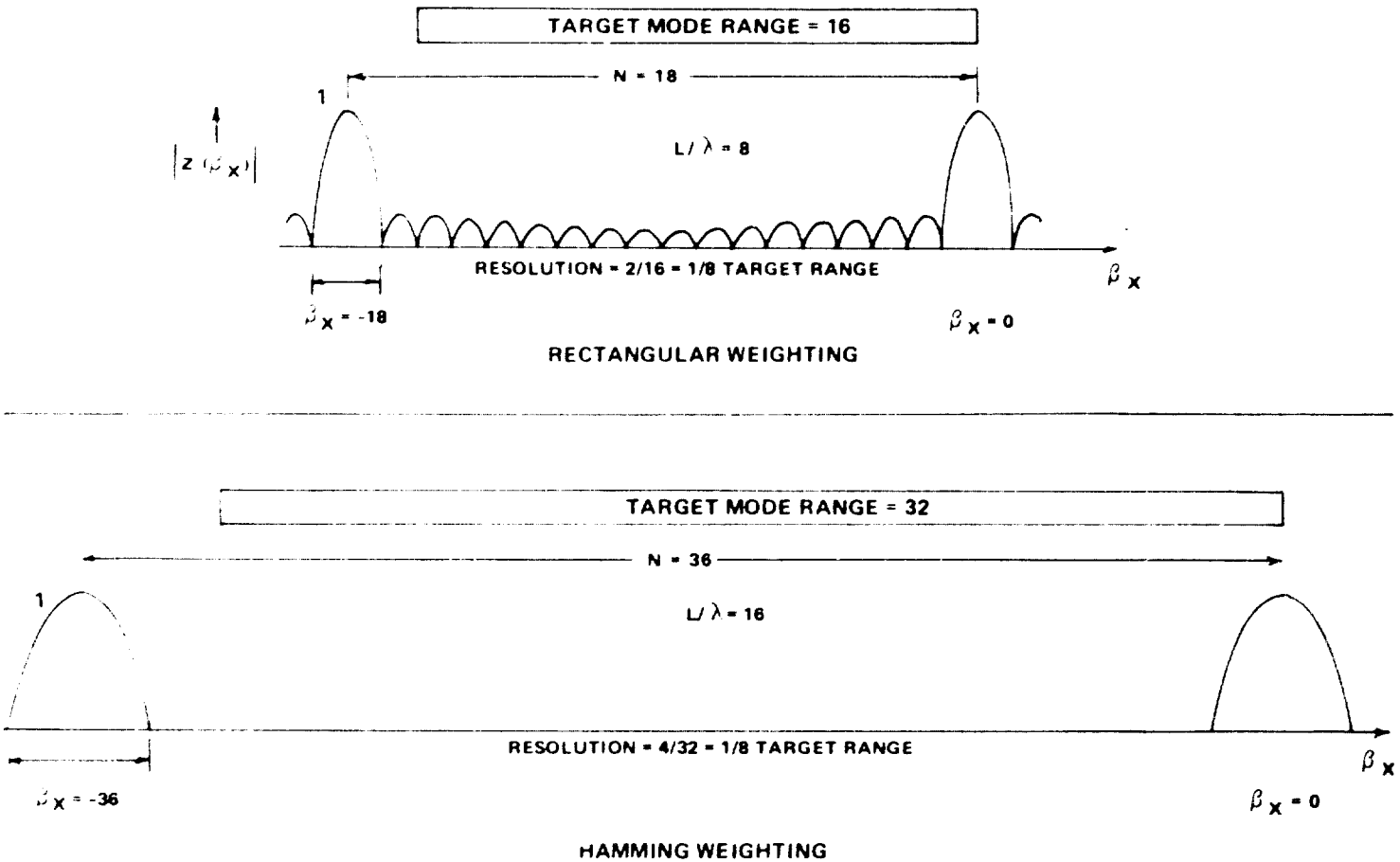

Figure 29 Comparison of Rectangular and Hamming Weighted Arrays Providing Equal Resolution

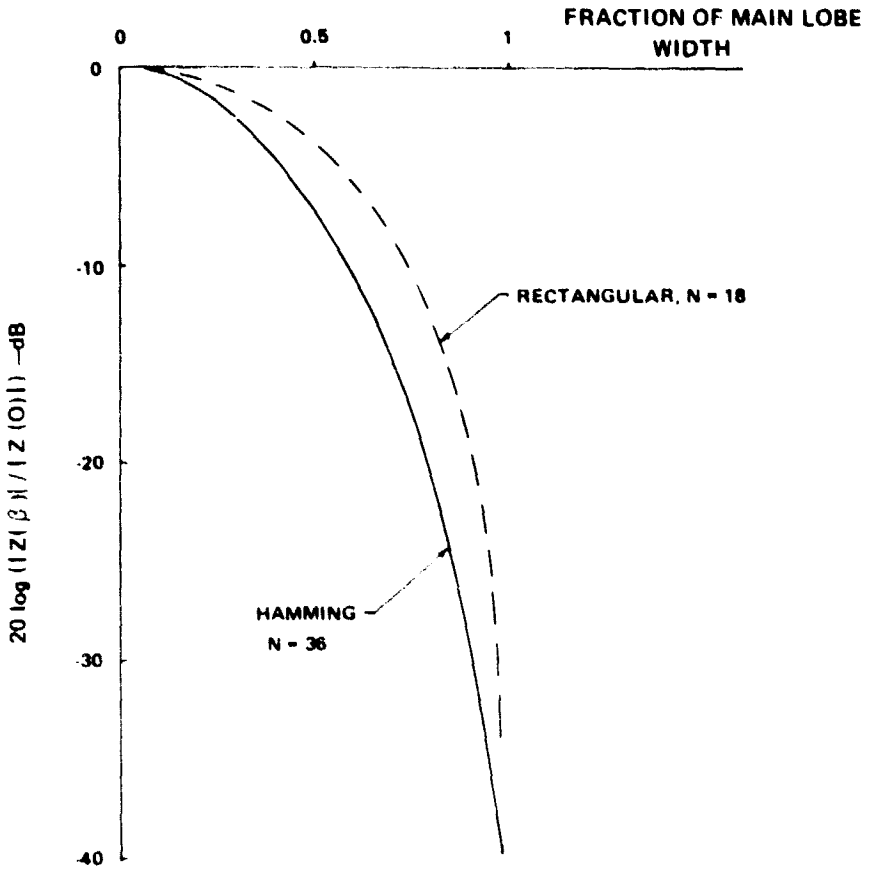

Figure 30 Shape of Main Lobe Response for Rectangular and Hamming Weighted Arrays of Equal Resolution

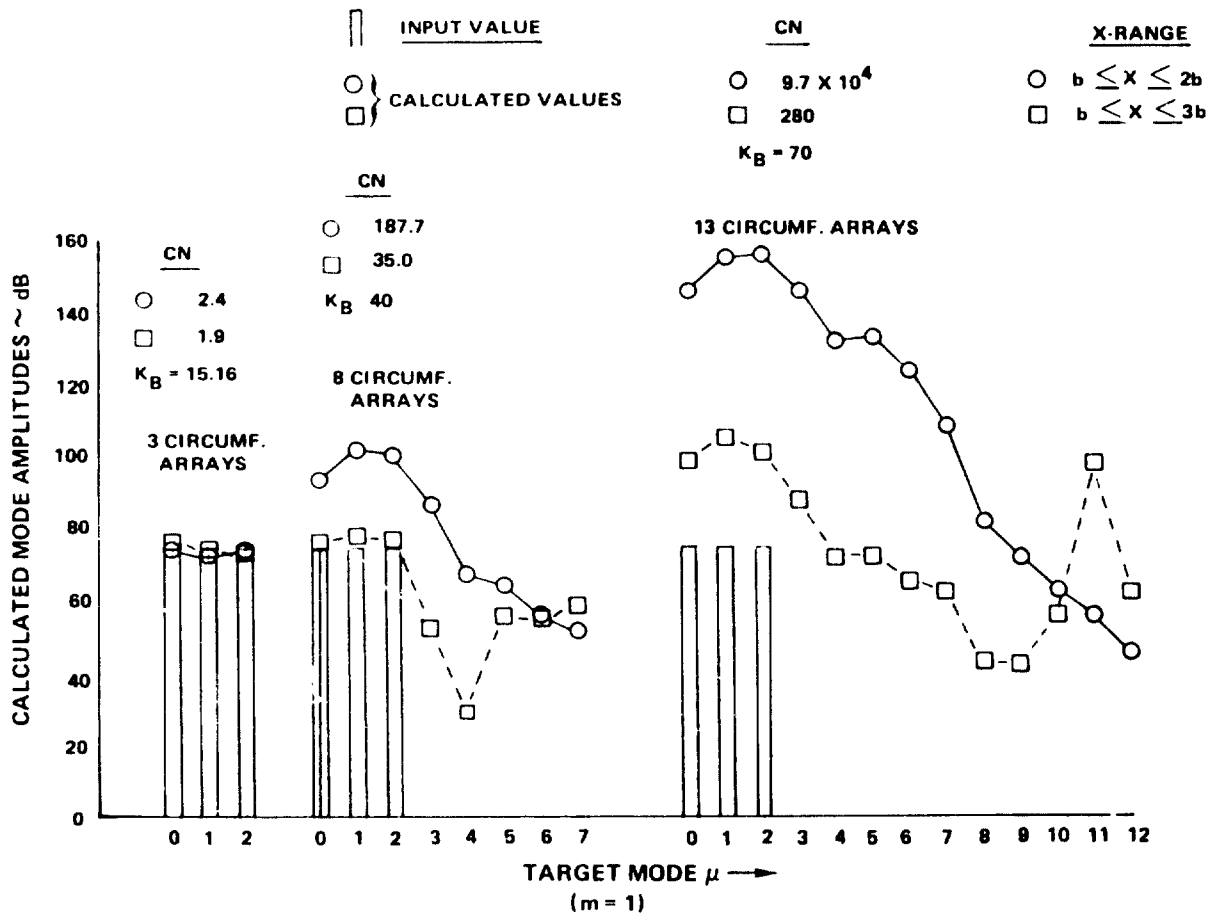

Figure 31 Results of Sensitivity Calculations for Circumferential Axial Arrays Spaced Axially Over 1 Radius (○) and 1 Diameter (□), Input modes (1, 0), (1, 1), and (1, 2) at 74 dB. (Array Signals Rounded to Nearest 1 dB)

Figure 32 Measured Signal Enhancement, JT9D Engine

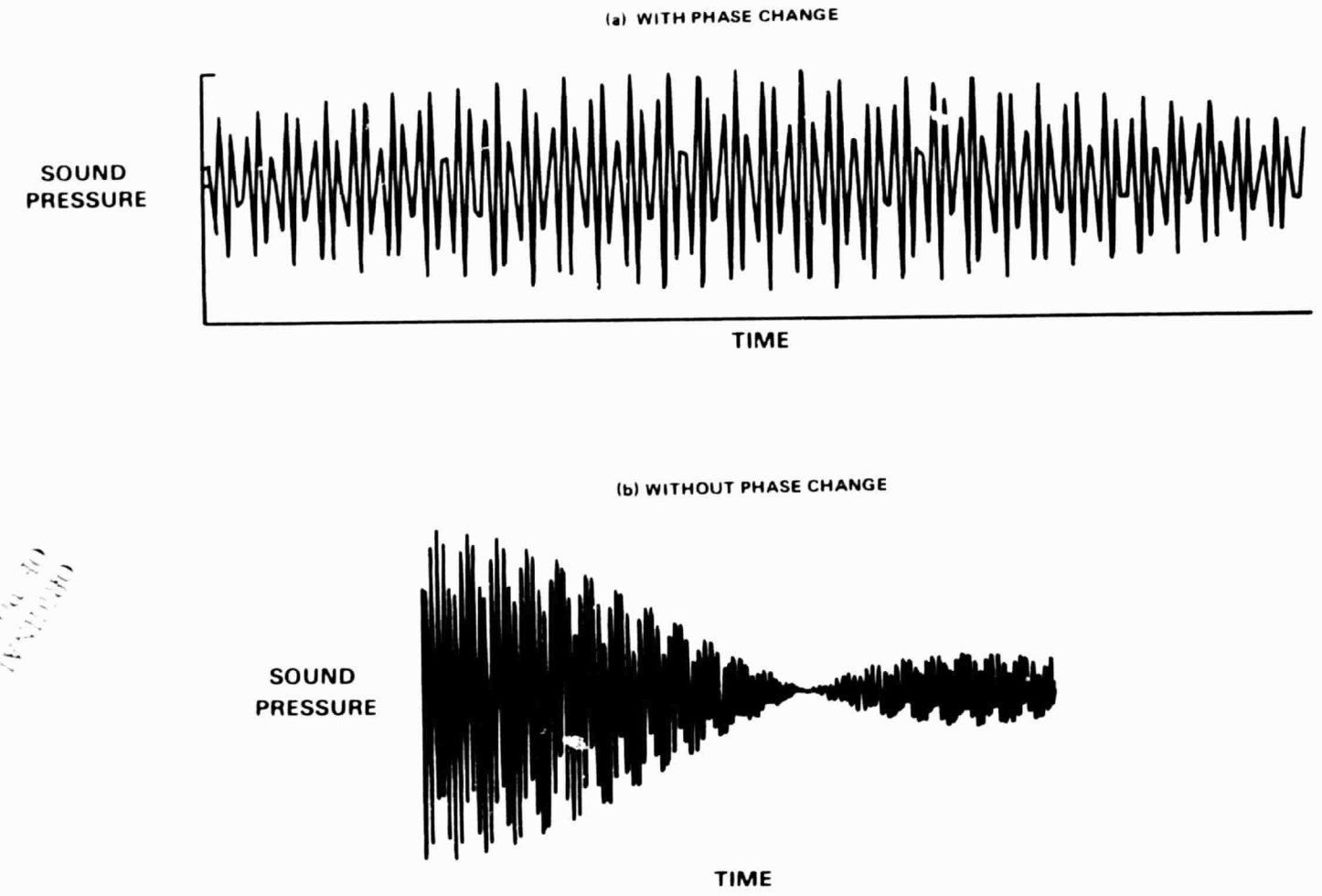

Figure 33 Computer Simulated Signal Enhancement Showing the Effect of Speed Change

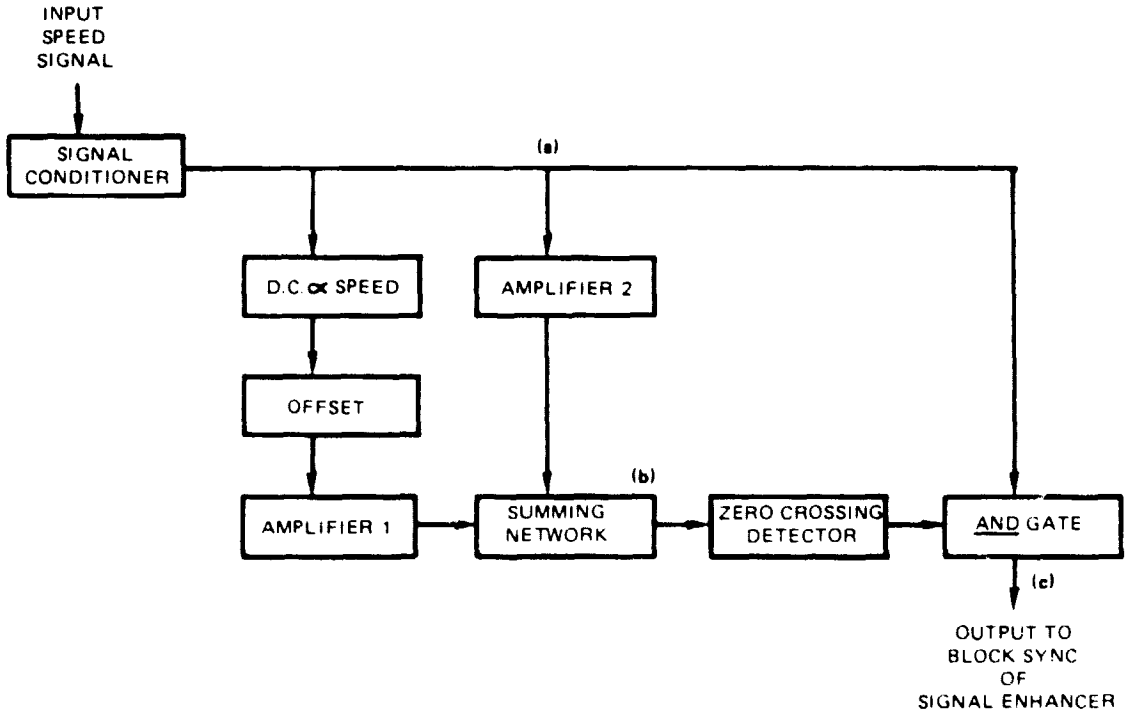

Figure 34 Functional Block Diagram for Speed Windowing System

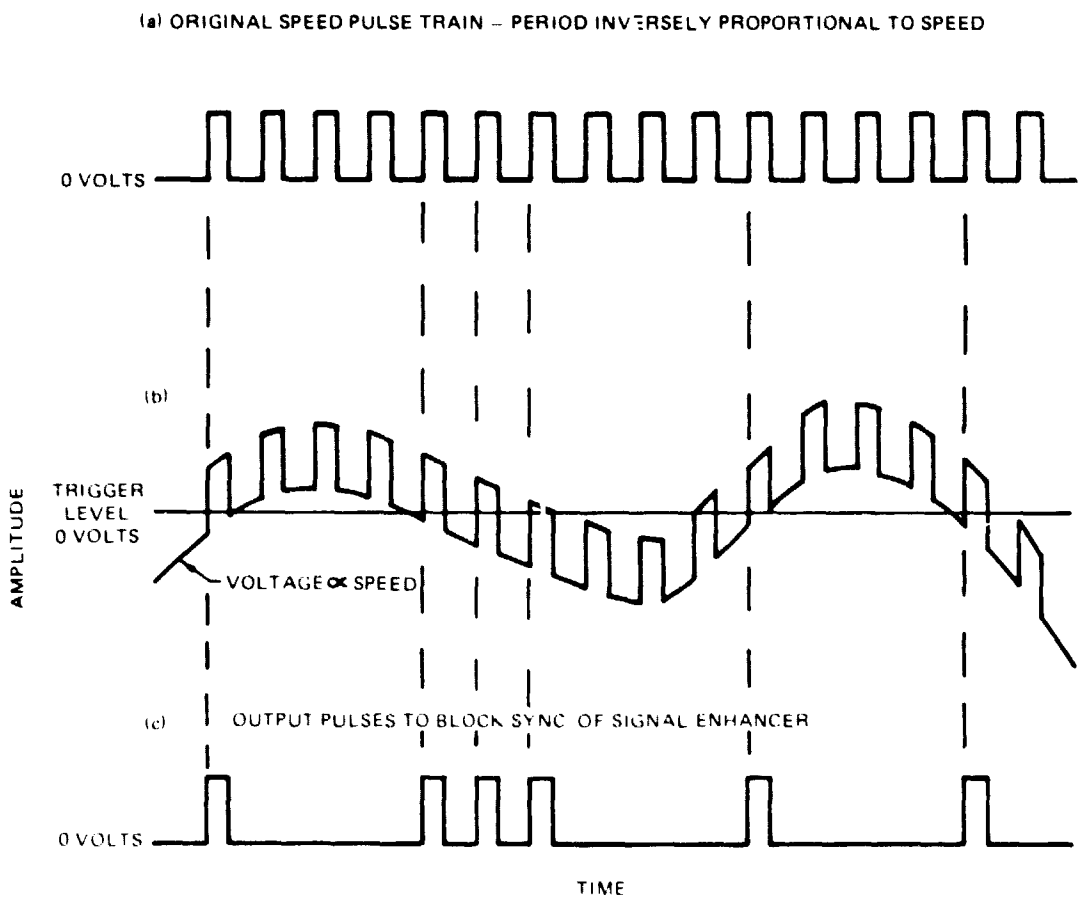

Figure 35 Timing Diagram for Speed Windowing System

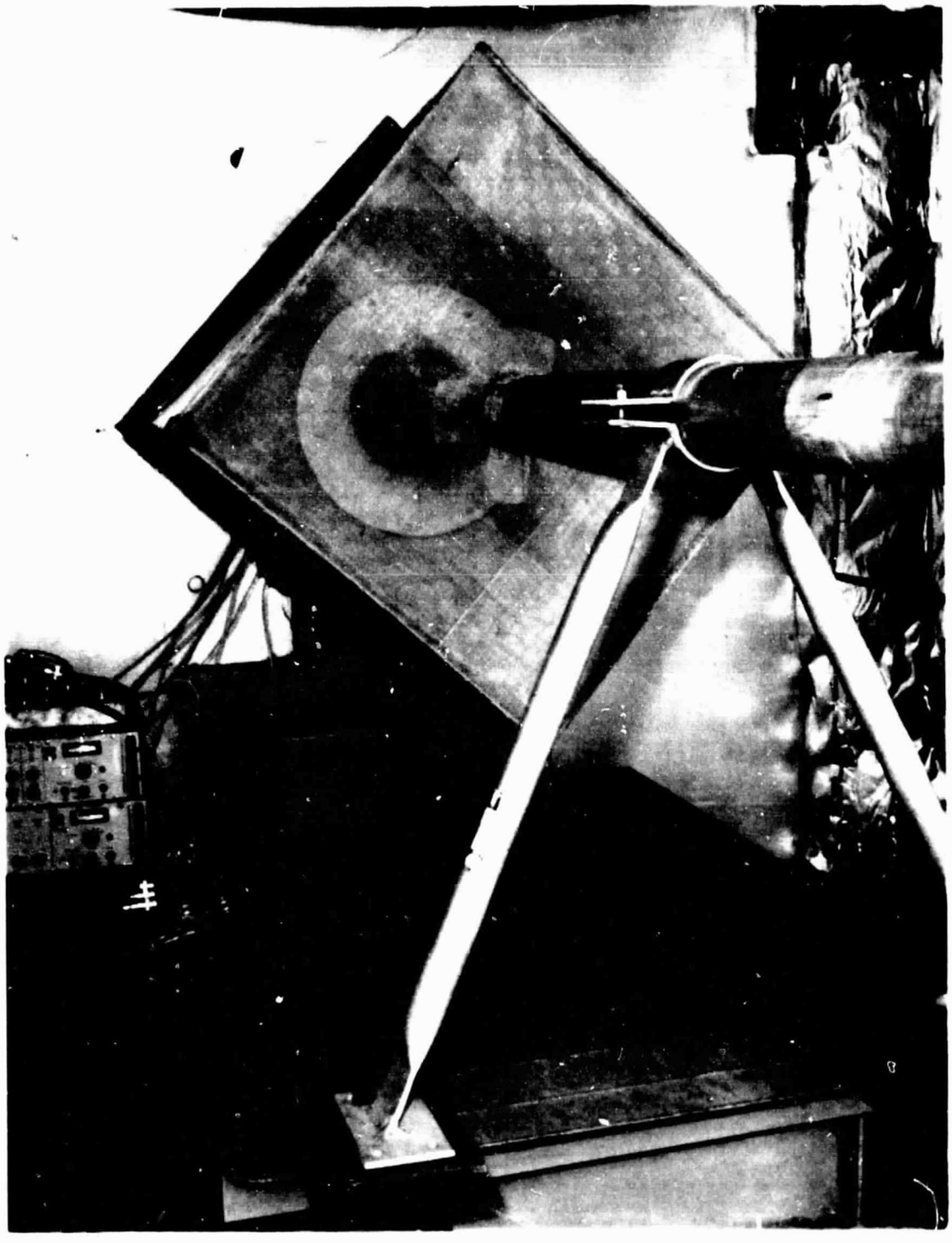

Figure 36 Photograph of 25 cm (10 in.) Acoustic Fan Rig

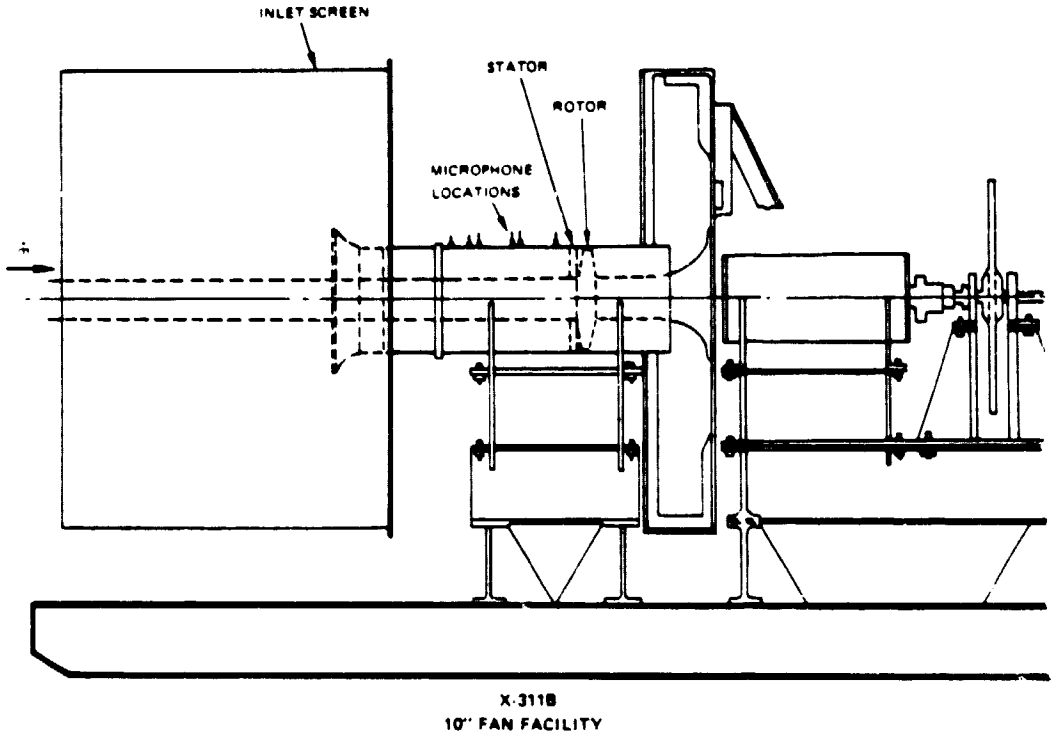

Figure 37 Schematic of 25 cm (10 in.) Acoustic Fan Rig

DUCT OUTER RADIUS 12.786 CM = 5.0338 IN.
HUB RADIUS 5.588 CM = 2.2 INCHES
FLOW MACH NUMBER – 0.07
HUB-TIP RATIO = 0.437
AIR TEMPERATURE 20.5° ± .5°C

SPEED OF SOUND 34,365.0 CM./SEC.
13529.5 IN./SEC.

MIKE	AXIAL COORDINATE (CM)	AXIAL COORDINATE (INCHES)	CIRCUMFERENTIAL COORDINATE (DEGREES)
1	0.000	0.000	247.883
2	13.525	5.325	337.933
3	0.023	0.009	53.867
4	17.414	6.856	108.633
5	30.300	7.992	285.700
6	13.223	5.206	64.700
7	12.675	4.990	23.917
8	2.283	0.899	23.933
9	7.882	3.103	53.867
10	14.933	5.879	53.850
11	0.157	0.062	0.000

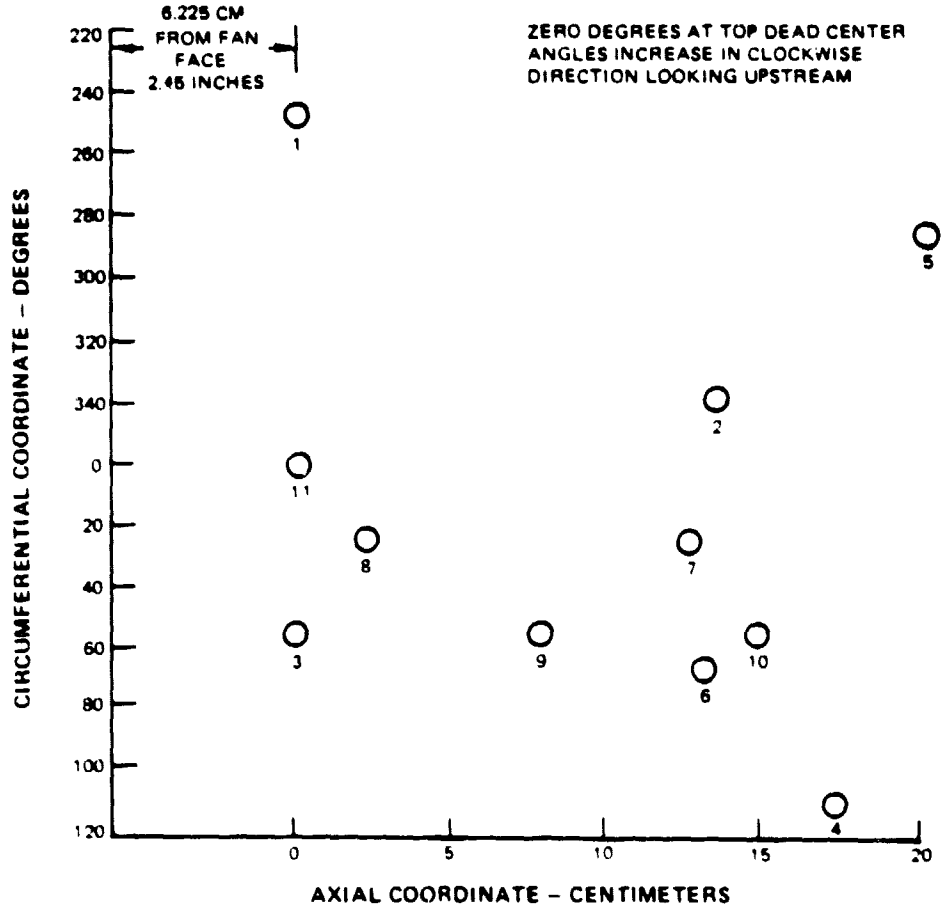

Figure 38 Input Variables for Mode Calculations

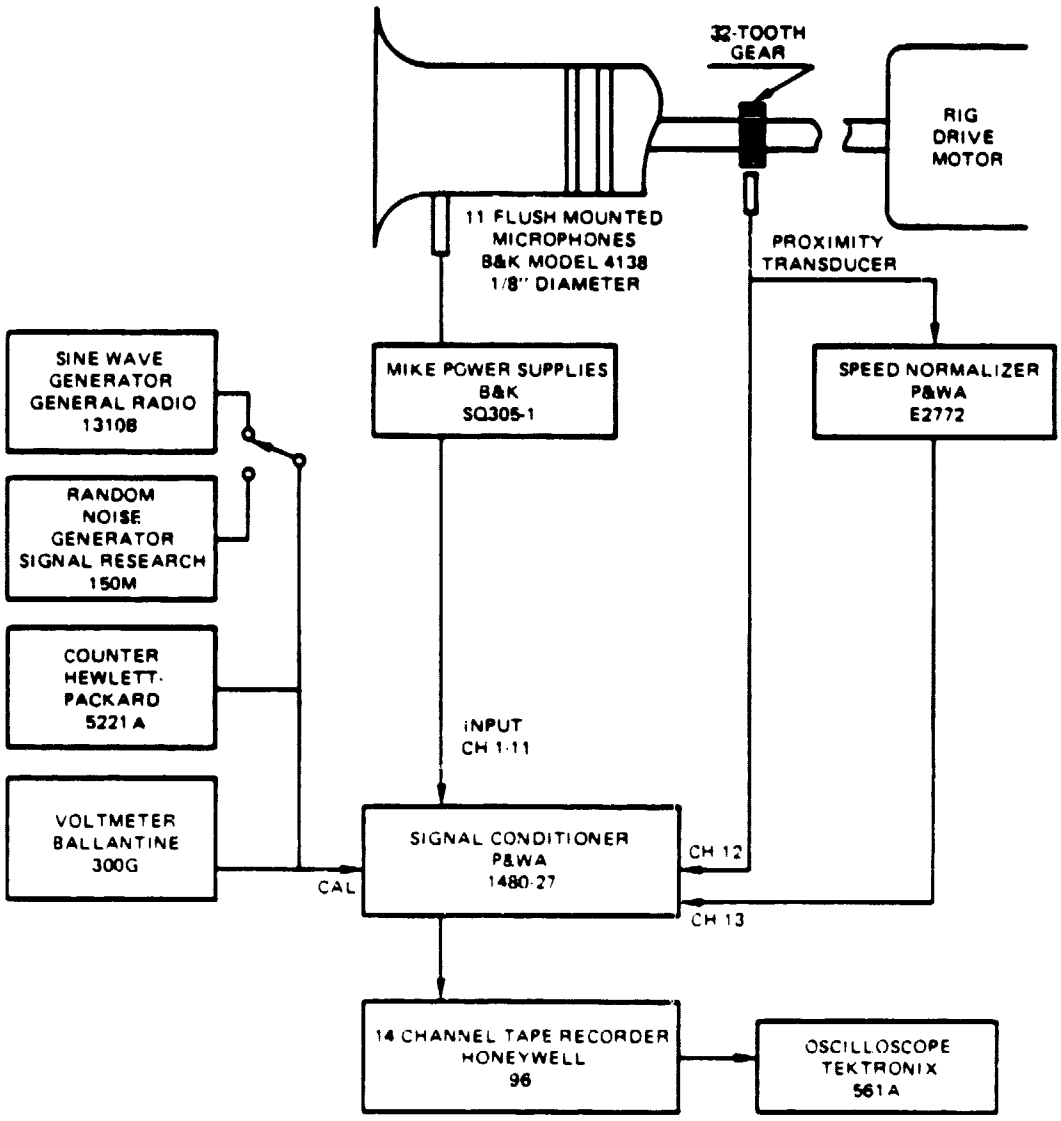

Figure 39 Data Acquisition System

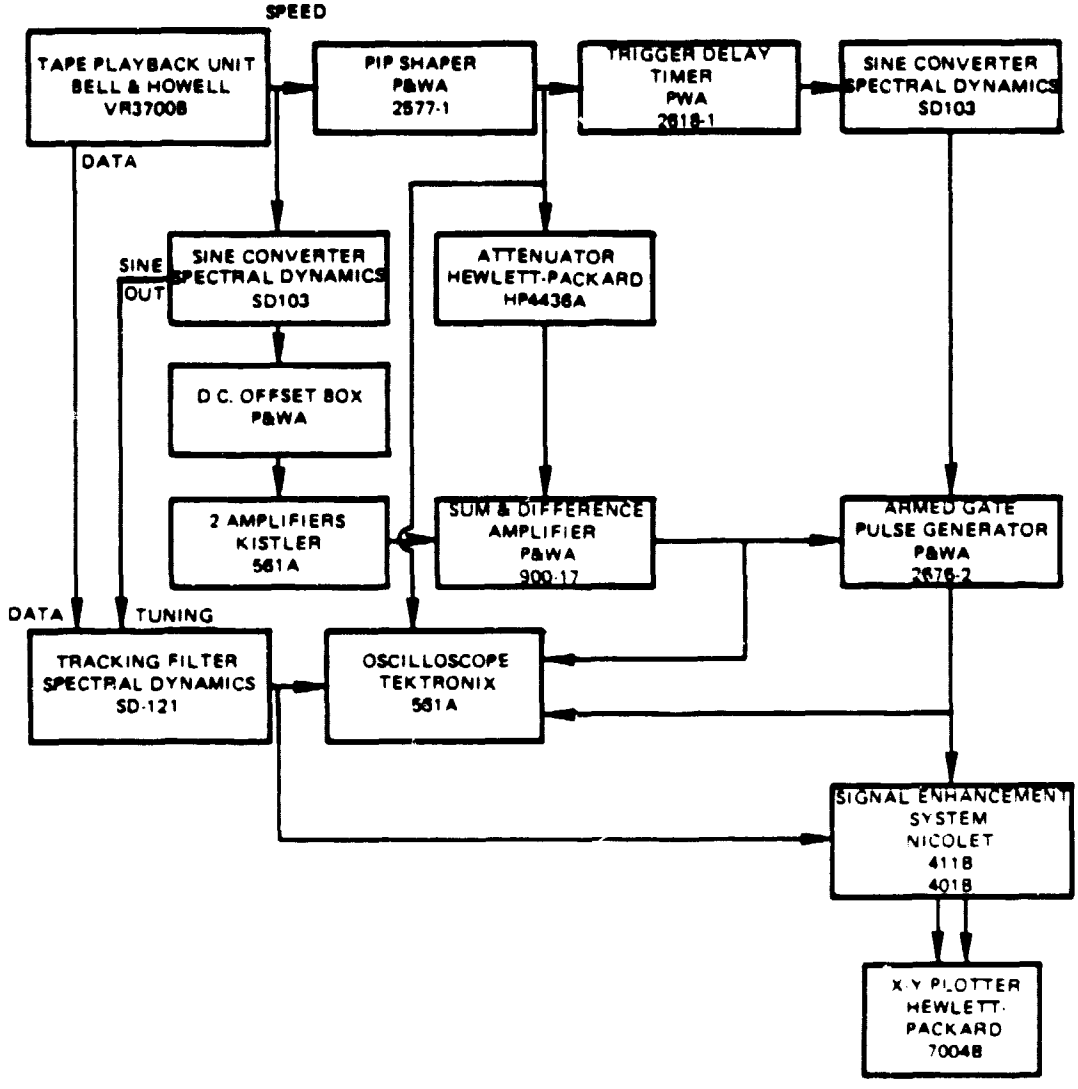

Figure 40 Signal Enhancement System With Speed Window

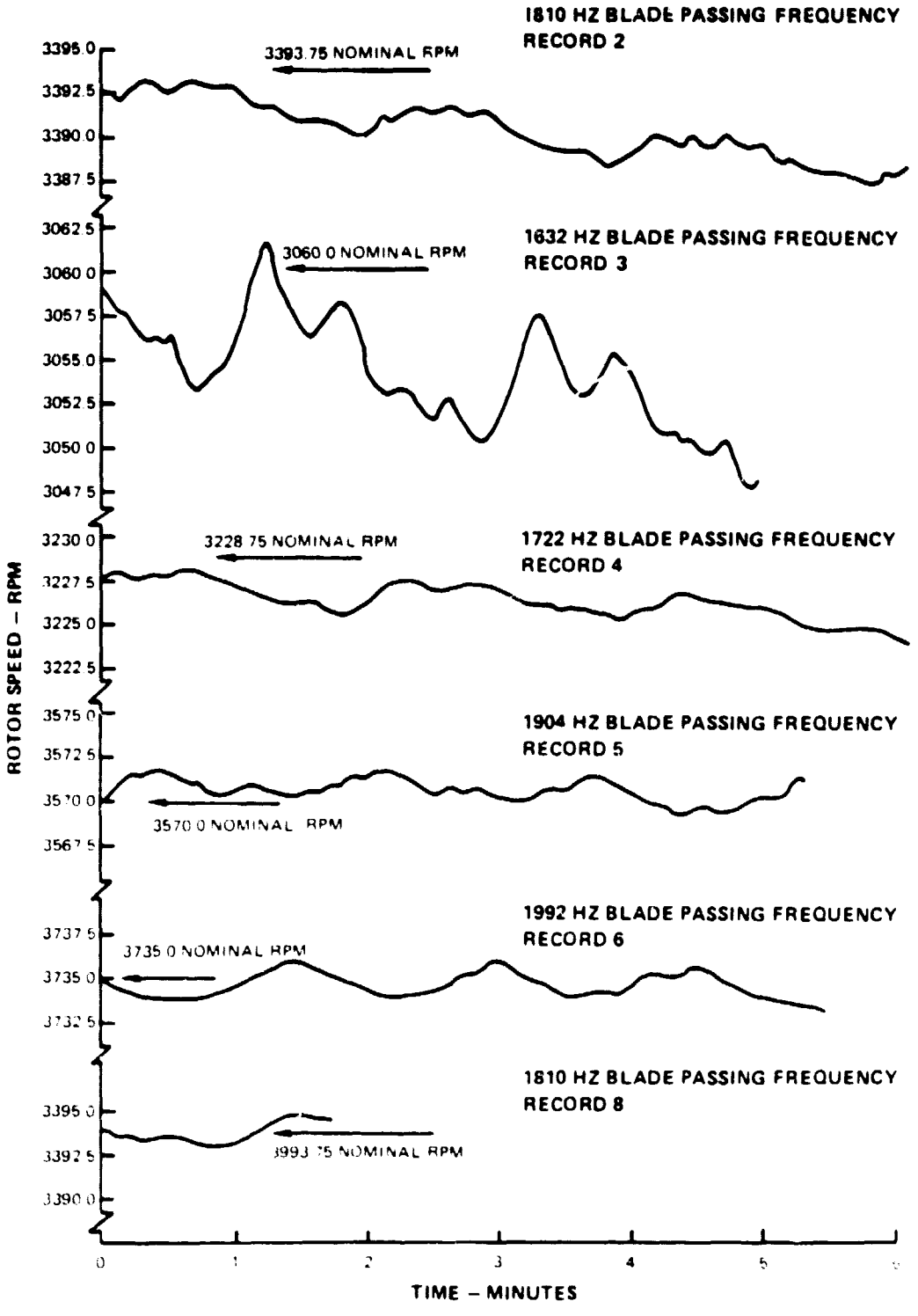

Figure 41 Steady State Speed Histories

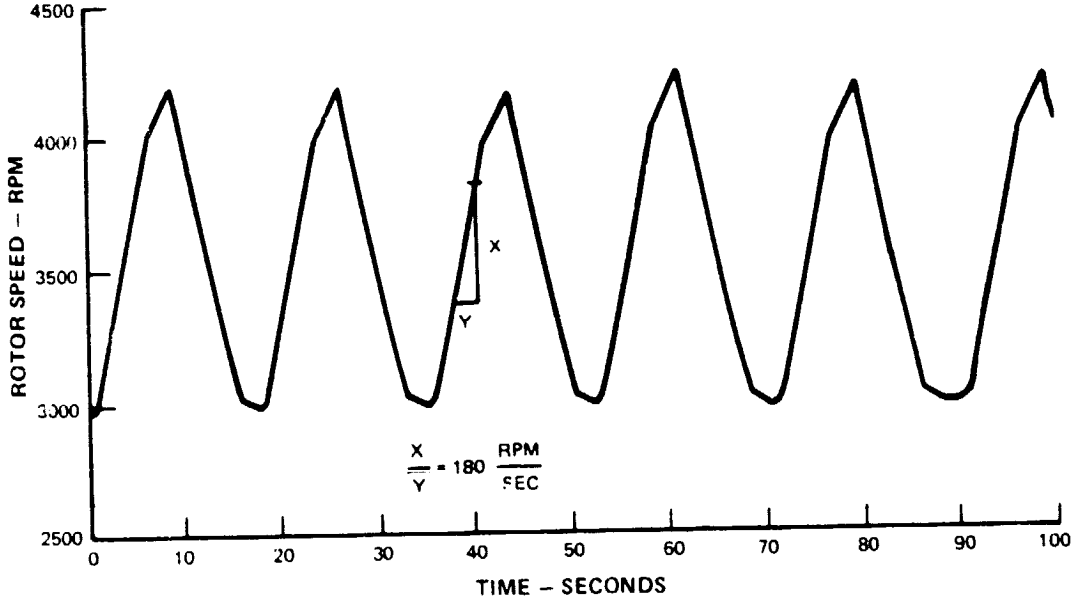

Figure 42 Sample Transient Speed History

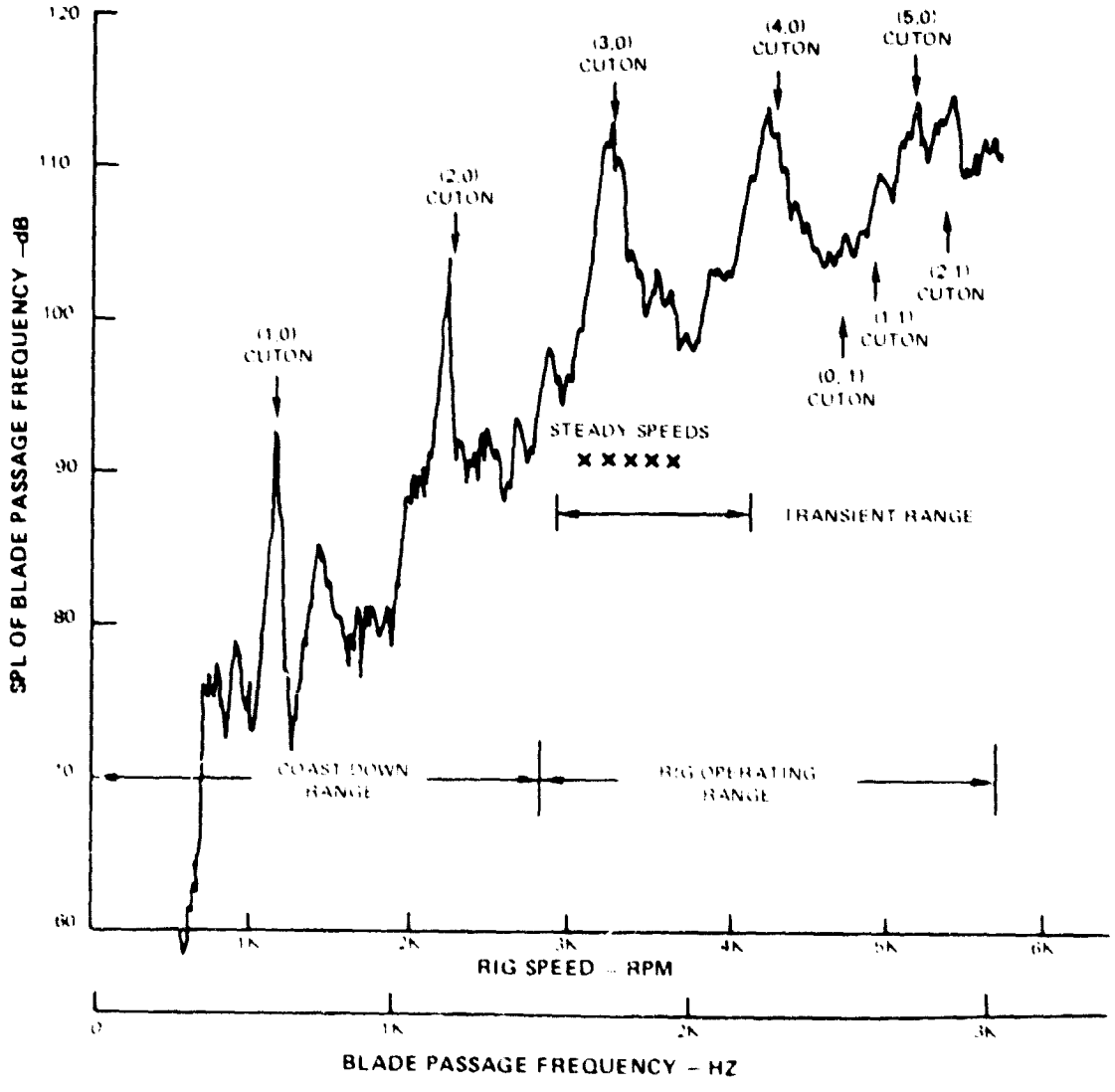

Figure 43 Effect of Rig Speed on Blade Passing Frequency Levels

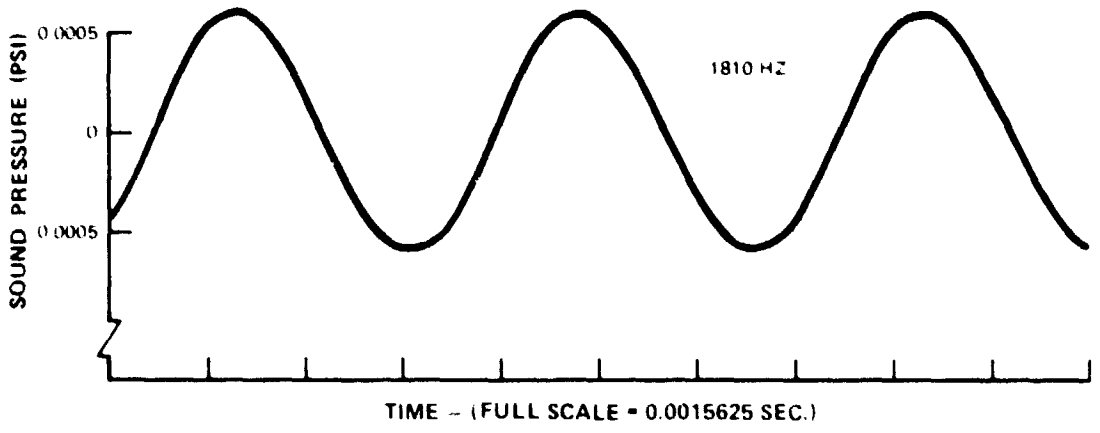

Figure 44 Typical Signal Enhancement of Blade Passing Frequency

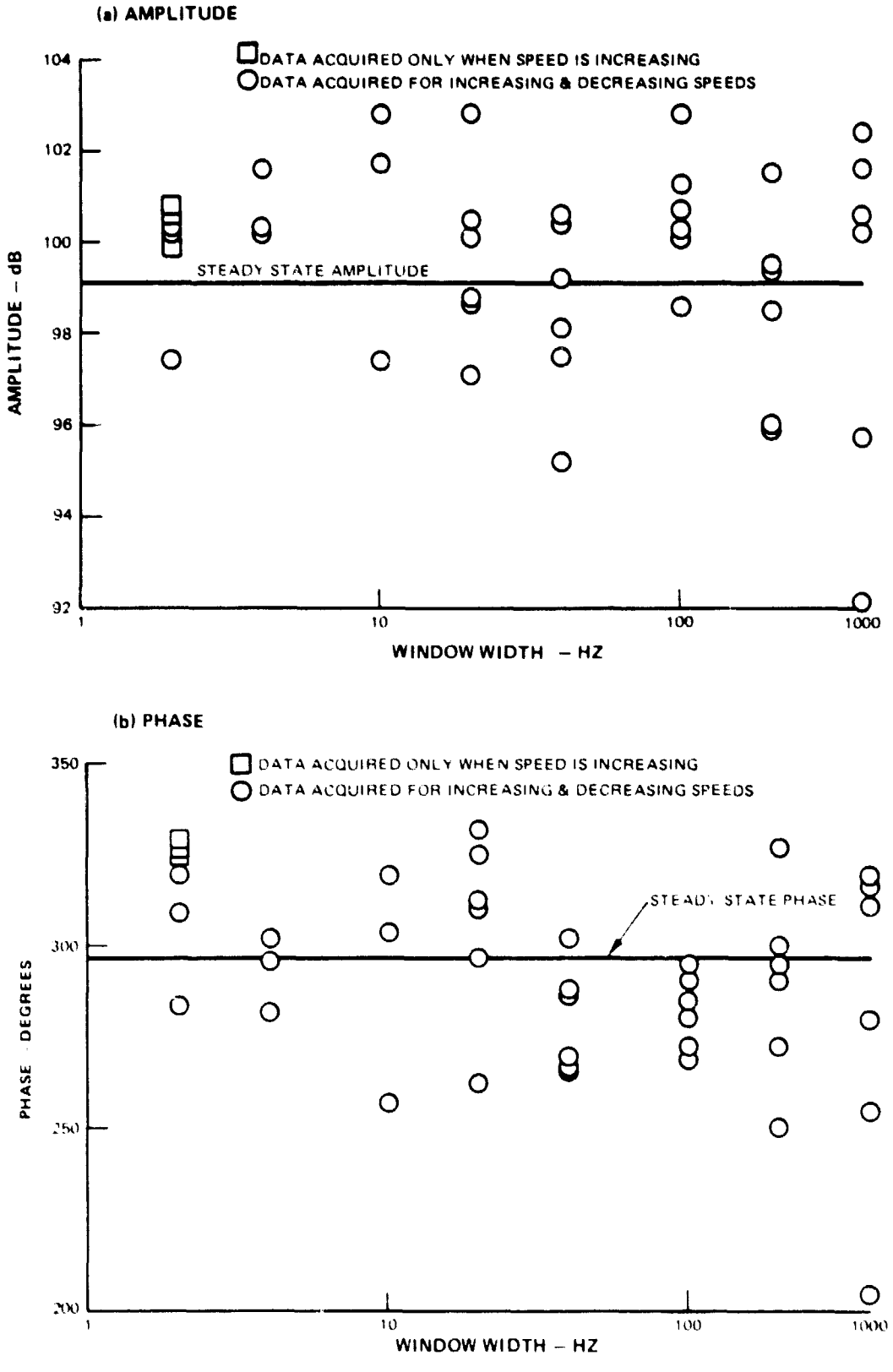

Figure 45 Effect of Window Size on the Amplitudes and Phases of the Signal Enhanced Pressure at 1810 Hz

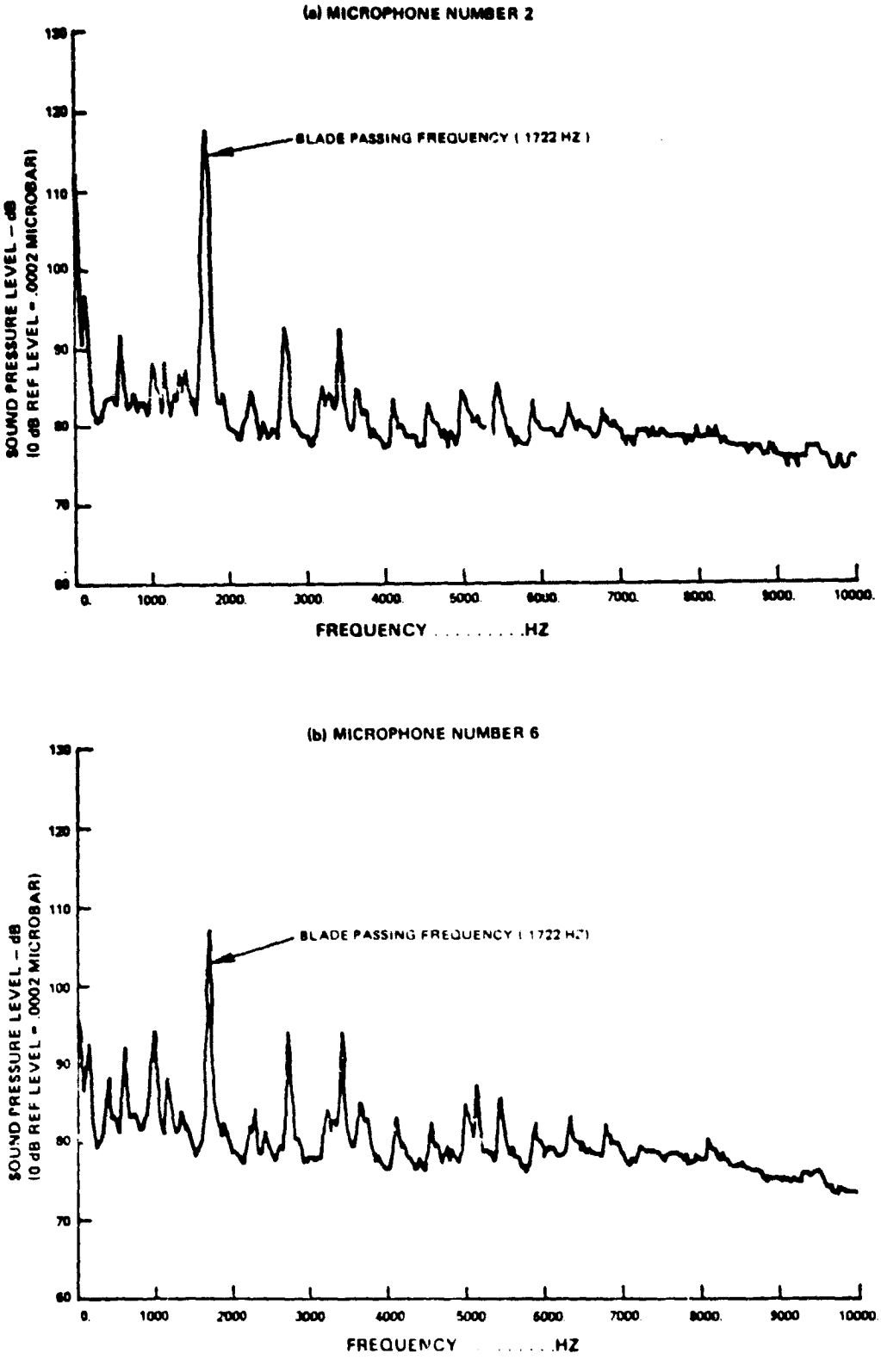

Figure 46 Sound Pressure Spectrum at 3229 RPM (50 Hz Filter Bandwidth)

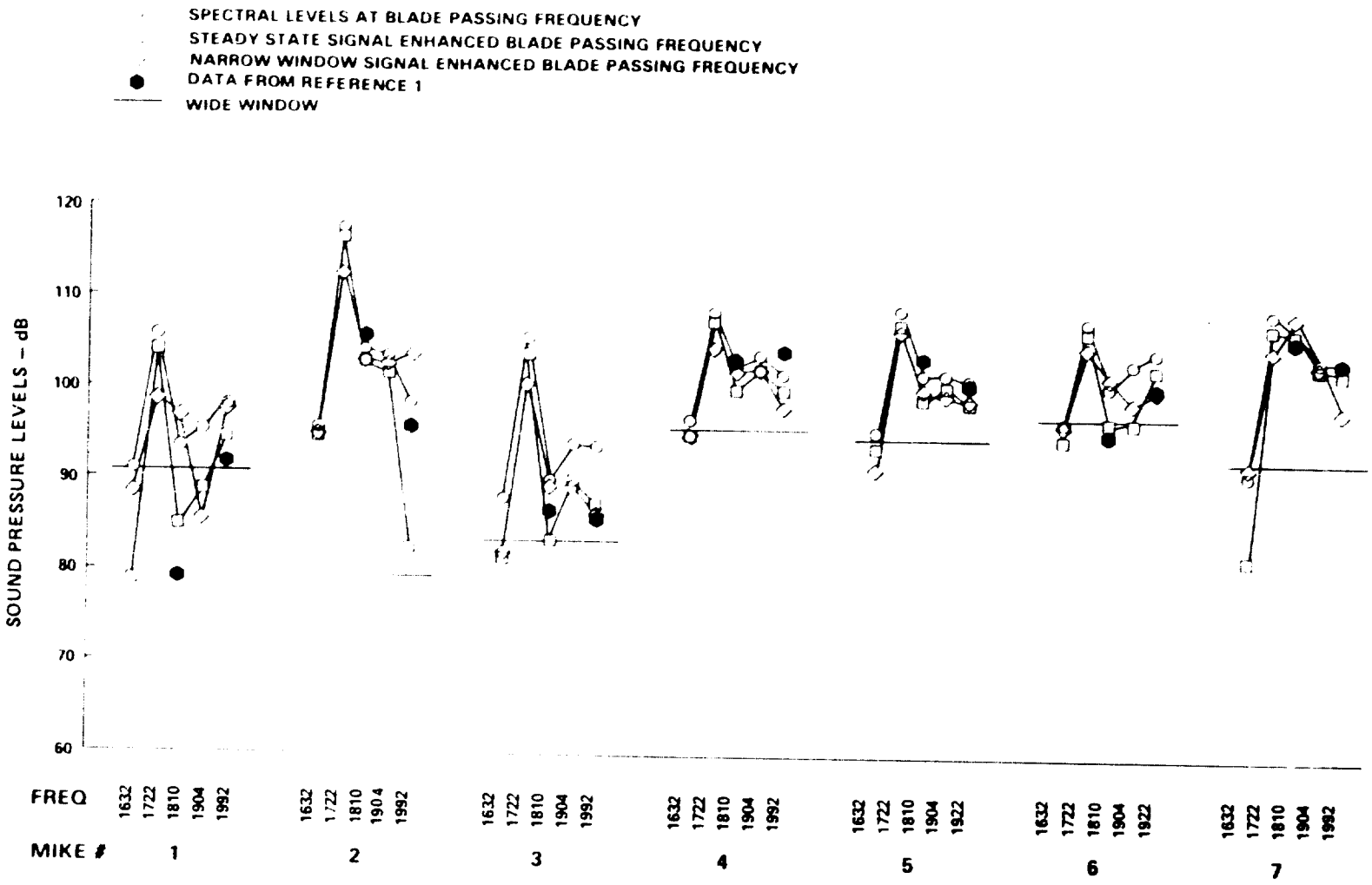

Figure 47 Comparison of Enhanced Blade Passing Frequency Levels With Spectral Levels

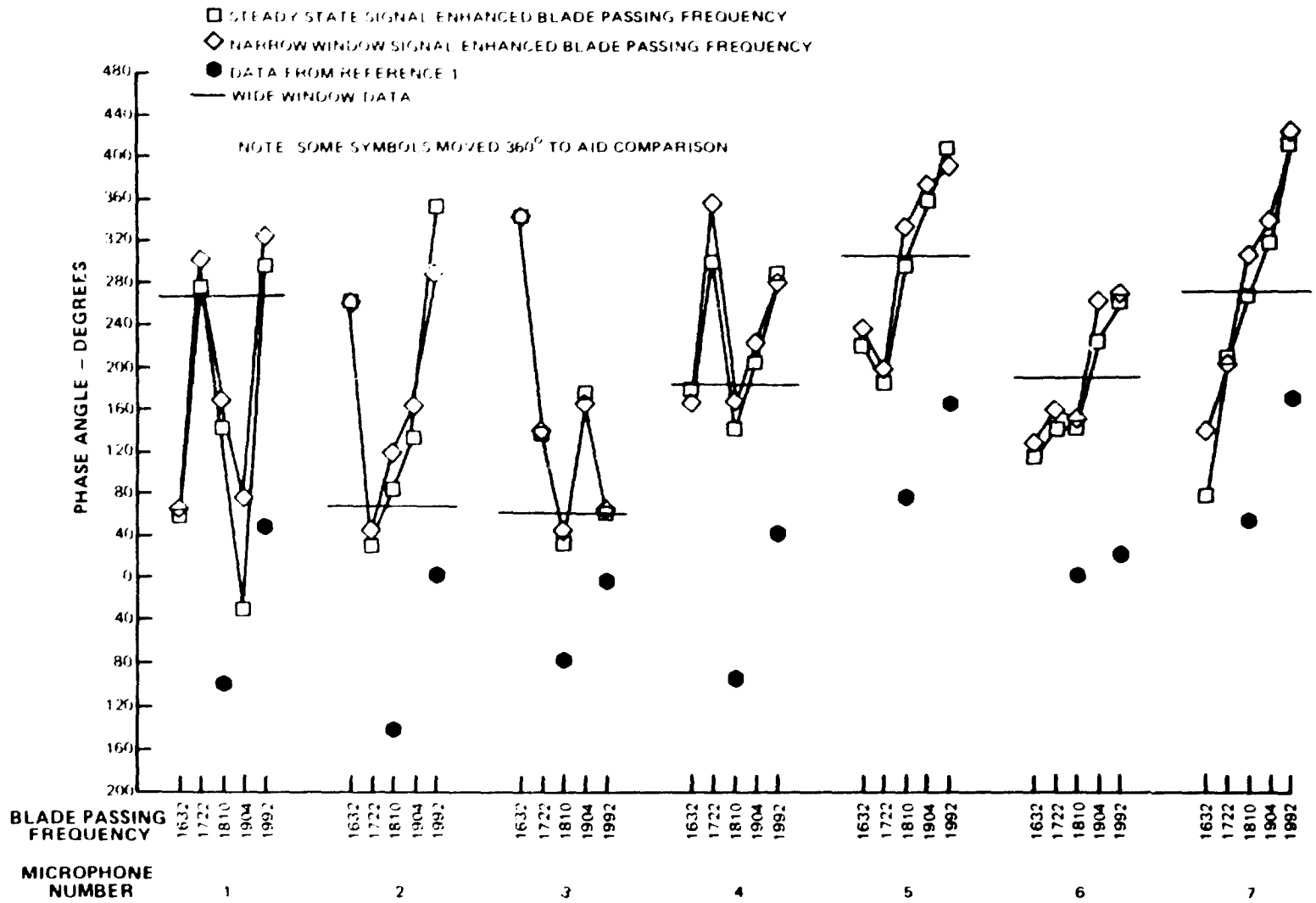

Figure 48 Comparison of Enhanced Phase Angles at Blade Passing Frequency

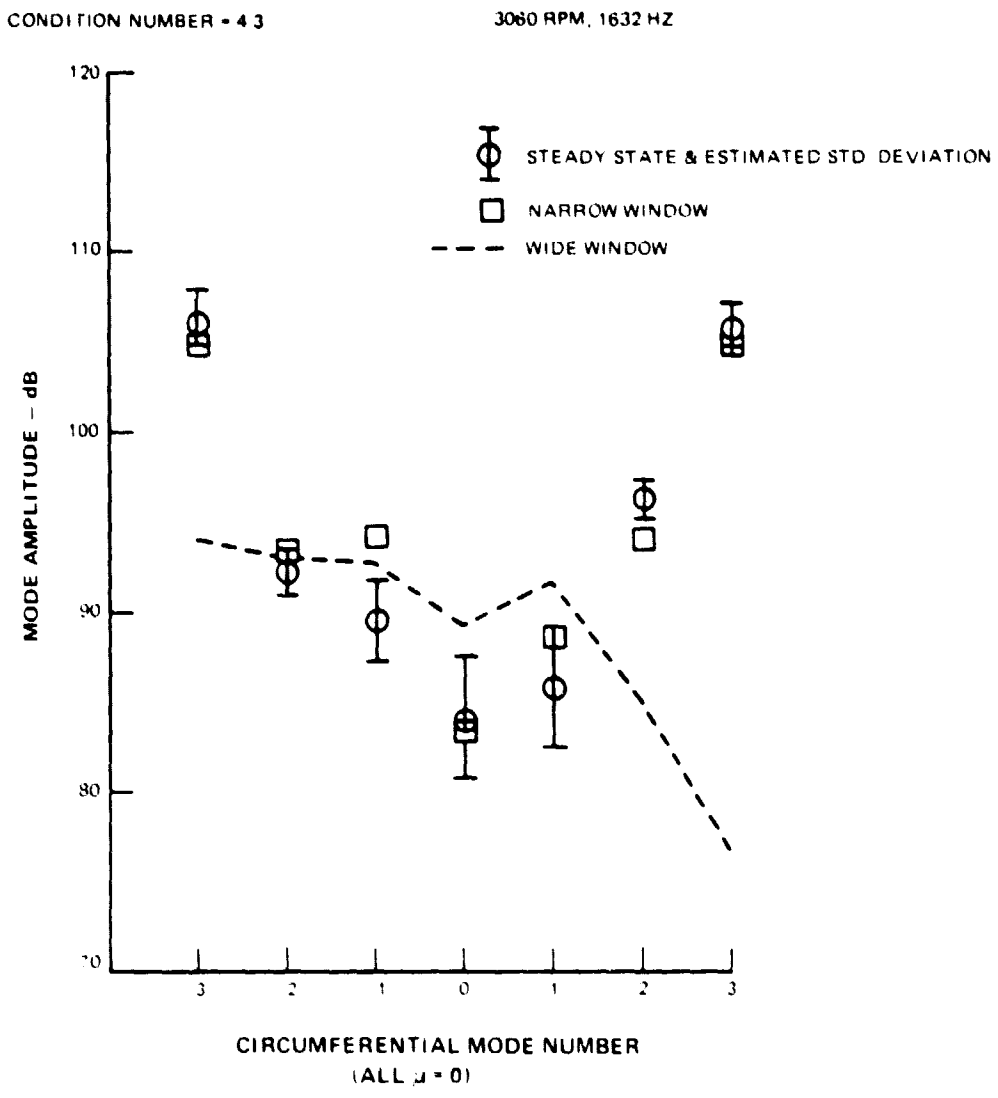

Figure 49 Measured Mode Amplitudes at 3060 RPM, 1632 Hz

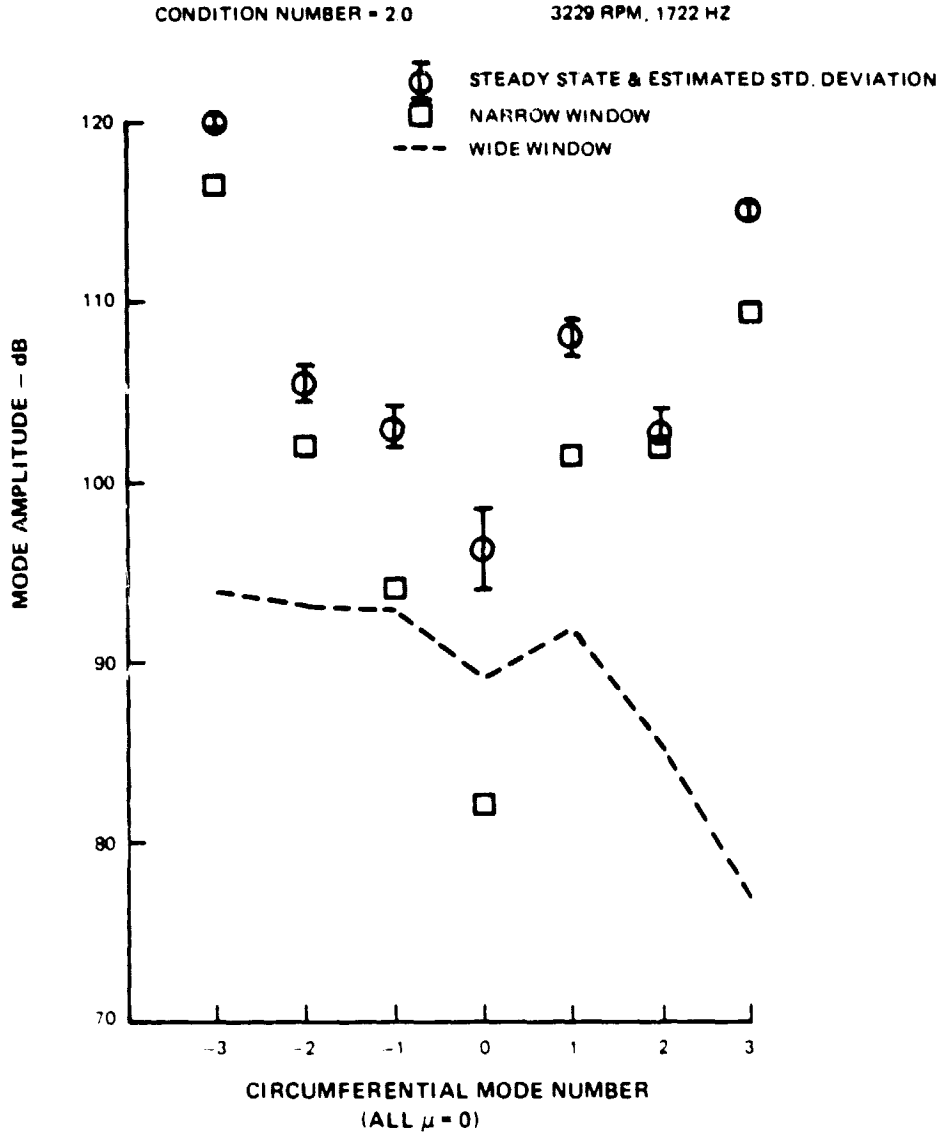

Figure 50 Measured Mode Amplitudes at 3229 RPM, 1722 Hz

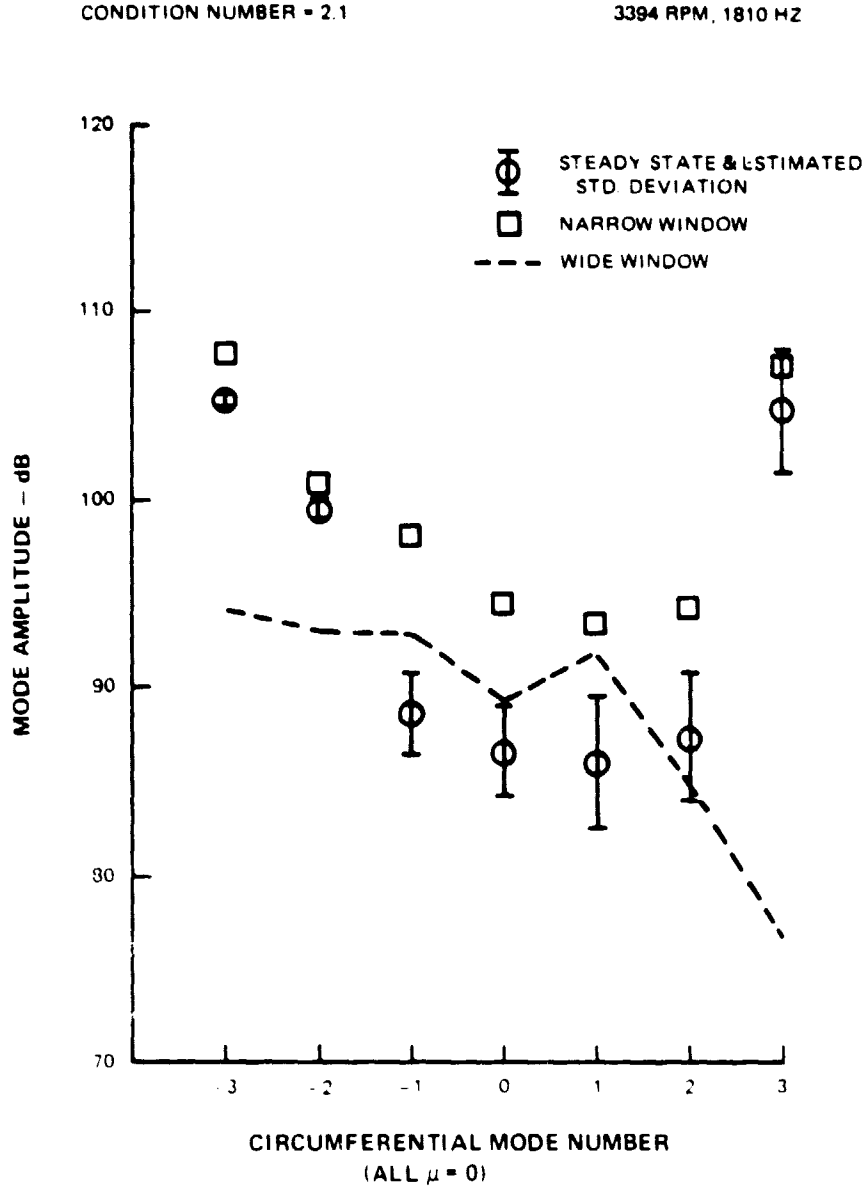

Figure 51 Measured Mode Amplitudes at 3394 RPM, 1810 Hz

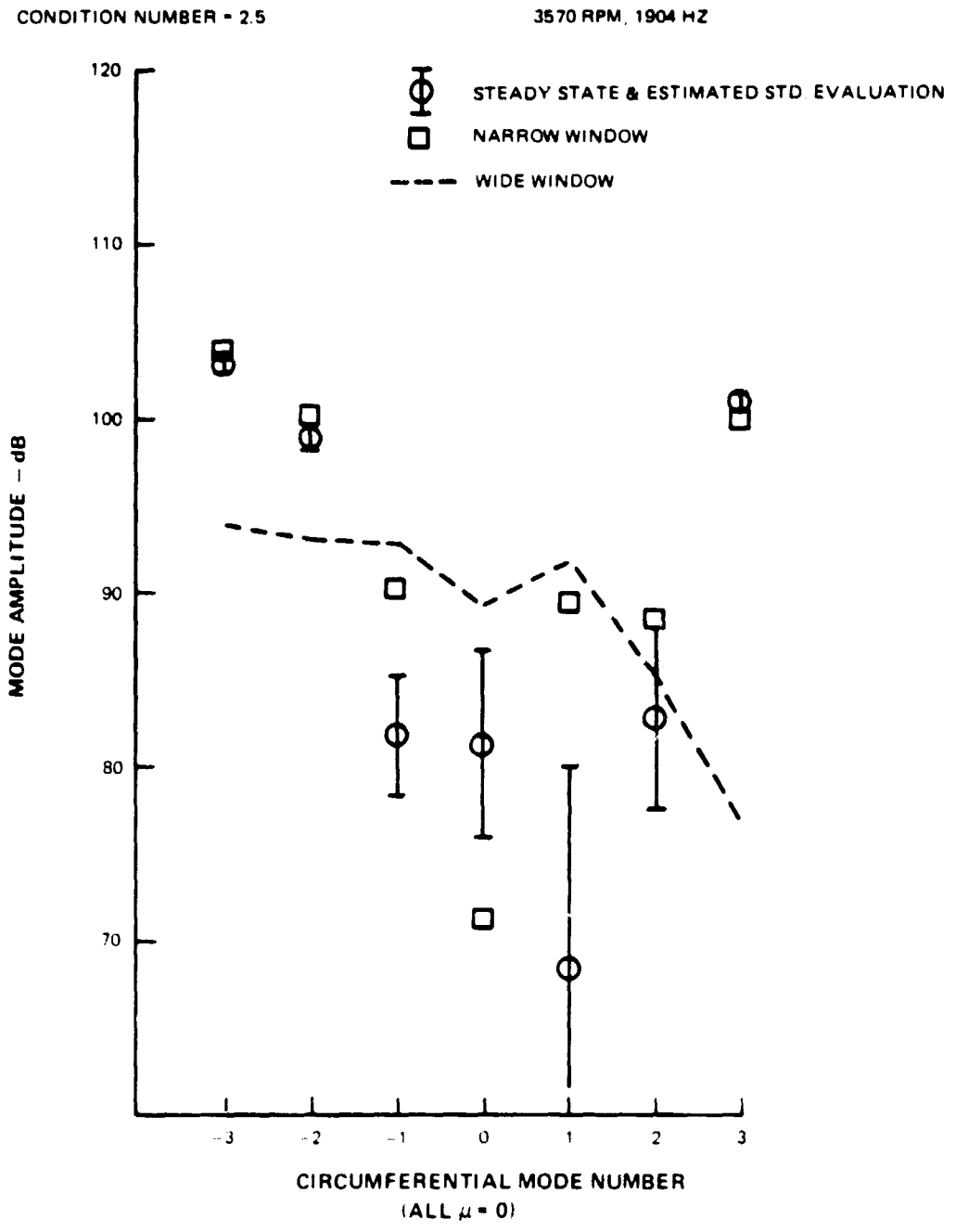

Figure 52 Measured Mode Amplitudes at 3570 RPM, 1904 Hz

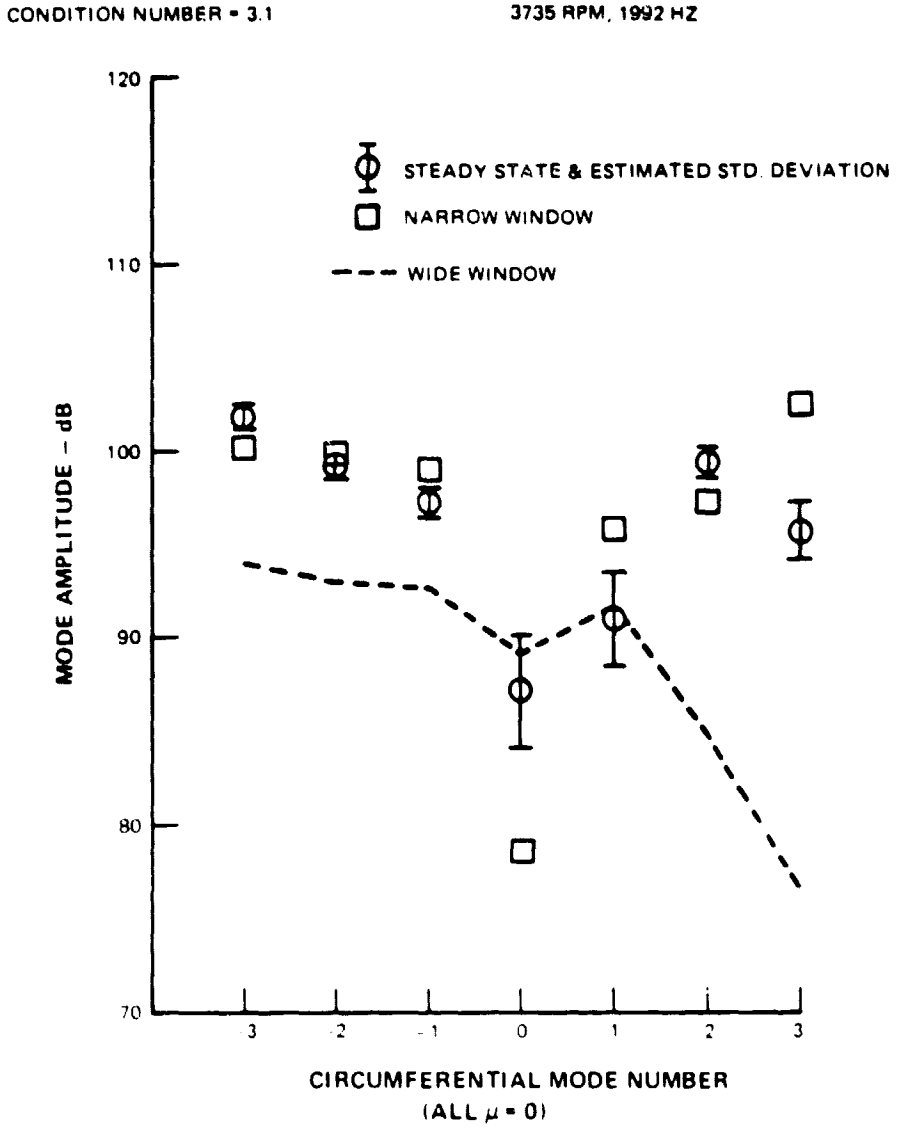

Figure 53 Measured Mode Amplitudes at 3735 RPM, 1992 Hz

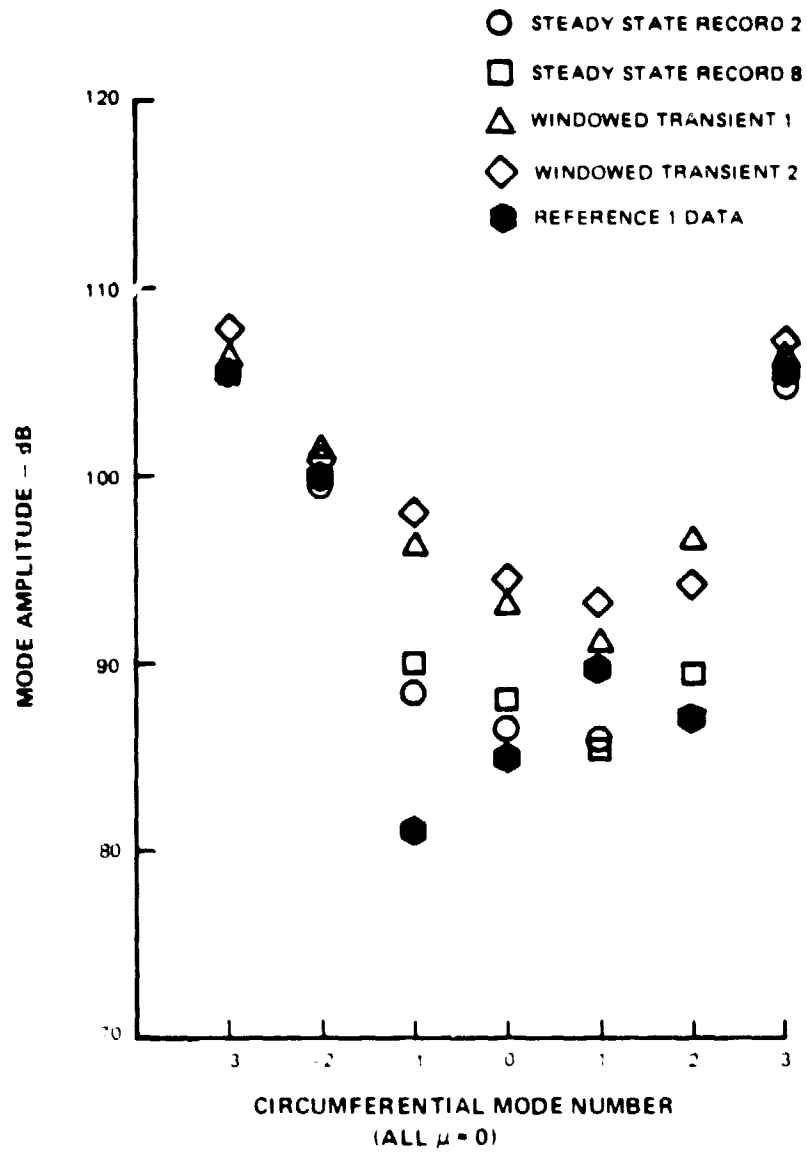

Figure 54 Mode Amplitude Repeatability at 3394 RPM, 1810 Hz

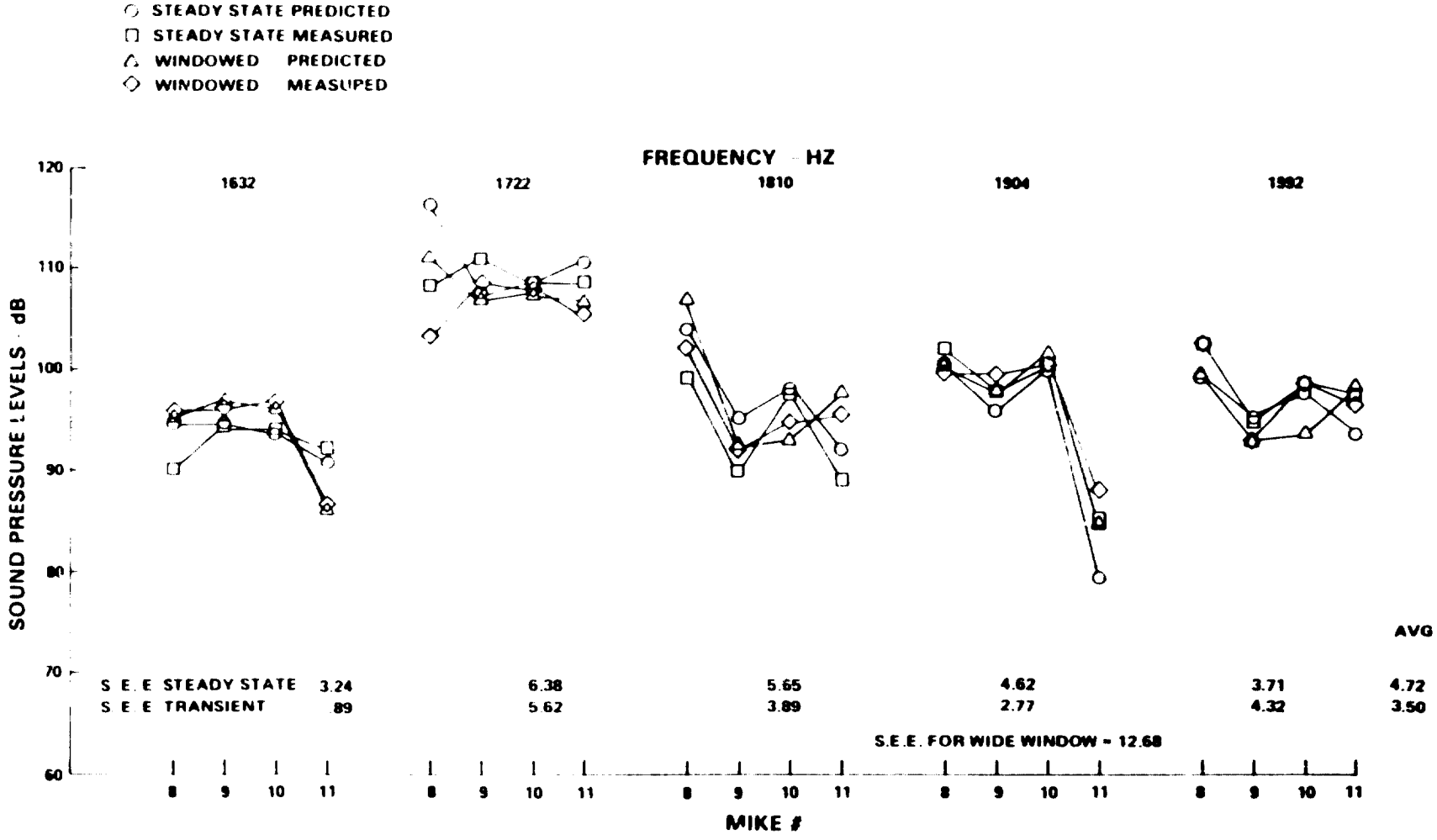

Figure 55 Check Microphone Amplitudes (Predicted vs. Measured)

REFERENCES

1. Pickett, G. F., Sofrin, T. G., Wells, R. A., "Method of Fan Sound Mode Structure Determination - Final Report", NASA-CR-135293, August 1977.

2. Gorton, R. E., "Facilities and Instrumentation for Aircraft Engine Noise Studies", ASME Paper No. 66-GT/N-41, March 1966.

3. Sofrin, T. G. and McCann, J. C., "Pratt & Whitney Aircraft Experience in Compressor Noise Reduction", Acoustical Soc. Amer. 72nd Meeting, Los Angeles, California, November 1966.

4. Mugridge, B. D., "The Measurement of Spinning Acoustic Modes Generated in an Axial Flow Fan", J. Sound and Vibrtion, 10(2), 1969, pp. 227-249.

5. Bolleter, U. and Chanaud, R. C., "Propagation of Fan Noise in Cylindrical Ducts", J. Acoustical Soc. Amer. Vol. 49, No. 3, (Part 1), 1971.

6. Moore, C. J. "In-Duct Investigation of Subsonic Fan 'Rotor Alone' Noise", J. Acoustical Soc. Amer., Vol. 51, No. 5, (Part 1), 1972.

7. Bolleter, U. and Crocker, M., "Theory and Measurement of Modal Spectra in Hardwall Cylindrical Ducts", J. Acoustical Soc. Amer., Vol. 51, No. 5 (Part 1), 1972.

8. Plumblee, H. E., Dean, P. D., Wynne, G. A., and Burrin, R. H., "Sound Propagation in and Radiation from Acoustically Lined Ducts: A Comparison of Experiment and Theory", NASA CR-2306, October 1973.

9. Kraft, R. E. and Posey, J. W., "A Preliminary In-Duct Measurement of Spinning Modes in the Inlet of a Rotating Vehicle", Acoustical Soc. Amer., 91st Meeting, Washington, D. C., April 1976.

10. Resanoff, R. A. and Ginsburg, T. A., "Matrix Error Analysis for Engineers", AFFDL-TR-66-80, p. 889.

11. Wilkinson, J. H., "Rounding Errors in Algebraic Processes", National Physical Laboratory Notes on Applied Science, No. 32, H.M.S.O., London, 1963.

12. Rice, E. J., Heidmann, M. F., and Sofrin, T. G., "Modal Propagation Angles in a Cylindrical Duct with Flow and their Relation to Sound Radiation", AIAA Paper 79-0183, 17th Aerospace Science Meeting, New Orleans, LA, Jan. 1979.

13. Rice, E. J., "Modal Density Function and Number of Propagating Modes in Ducts", NASA TMX 73539, November 1976.

14. Collin, R. E. and Zucker, F. J., "Antenna Theory", McGraw-Hill, New York, 1969.

15. Oppenheim, A. V. and Schafer, R. W., "Digital Signal Processing", Prentice-Hall, Inc., New Jersey, 1975.

16. Blackman, R. B. and Tukey, J. W., "The Measurement of Power Spectra", Dover Publications, New York, 1959.

APPENDIX A

ACOUSTIC DATA FOR SECTION 4

TABLE A1

BLADE PASSING FREQUENCY SPECTRUM LEVELS

Rotor Speed (rpm)	3060	3229	3394	3394	3570	3735
Blade Passing Frequency (Hz)	1632	1722	1810	1810	1904	1992
Tape Record No.	3	4	2	8	5	6
Microphone No.	Levels (dB re. 0.0002 dynes/cm^2)					
1	91.0	105.7	93.5	93.7	95.3	98.0
2	95.5	117.5	104.2	104.2	103.5	98.5
3	88.0	105.5	90.0	90.5	94.0	93.7
4	96.7	108.5	102.5	102.0	103.7	101.7
5	95.5	108.7	101.7	102.0	101.7	101.0
6	96.5	107.5	100.5	100.5	103.0	104.2
7	91.0	108.5	106.5	107.5	103.5	103.2
8	93.7	110.7	100.5	101.5	103.0	104.3
9	95.5	111.5	99.0	99.5	103.2	98.7
10	95.7	109.5	100.5	101.7	102.0	102.0
11	95.5	110.0	95.5	96.0	97.0	101.0

TABLE A2

COHERENT DUCT ACOUSTIC PRESSURE
STEADY STATE DATA
RPM = 3060 BPF = 1632 Hz TAPE RECORD NO. = 3

Measured Data Mike Number	Amplitude (dB)	(dynes/cm^2)	(lbf/in^2)	Phase (degrees)
1	78.8	1.75	0.00002563	56.2
2	94.5	10.58	0.0001552	273.1
3	81.5	2.38	0.00003491	343.6
4	95.1	11.39	0.0001672	178.2
5	93.8	9.76	0.0001432	221.0
6	94.8	11.06	0.0001623	115.8
7	81.8	2.47	0.00003623	77.3
Measured Check Mike Number				
8	90.0	6.36	0.00009332	12.5
9	94.2	10.20	0.0001497	50.7
10	93.9	9.94	0.0001458	140.2
11	92.0	8.00	0.0001175	231.5
Calculated Check Mike Number				
8	94.4	10.50	0.0001540	101.7
9	94.5	10.62	0.0001558	46.7
10	93.6	9.57	0.0001405	133.6
11	90.8	6.93	0.0001018	164.5

TABLE A3

COHERENT DUCT ACOUSTIC PRESSURE
STEADY STATE DATA
RPM = 3229 BPF = 1722 Hz TAPE RECORD NO. = 4

Measured Data Mike Number	Amplitude (dB)	(dynes/cm^2)	(lbf/in^2)	Phase (degrees)
1	103.9	31.49	0.0004622	275.2
2	116.5	133.99	0.001966	30.4
3	103.8	31.07	0.0004560	137.4
4	107.4	46.97	0.0006893	299.6
5	107.3	46.37	0.0006804	186.0
6	106.4	41.91	0.0006151	142.4
7	107.0	44.68	0.0006557	208.6
Measured Check Mike Number				
8	108.2	51.19	0.0007512	177.0
9	110.8	69.62	0.001022	148.1
10	108.6	54.20	0.0007954	167.1
11	108.5	52.99	0.0007777	291.4
Calculated Check Mike Number				
8	116.3	130.63	0.001917	202.4
9	107.5	47.43	0.0006960	129.2
10	108.6	53.83	0.0007900	186.8
11	110.7	68.55	0.001006	204.3

TABLE A4

COHERENT DUCT ACOUSTIC PRESSURE
STEADY STATE DATA
RPM = 3394 BPF = 1810 Hz TAPE RECORD NO. = 2

Measured Data Mike Number	Amplitude (dB)	(dynes/cm^2)	(lbf/in^2)	Phase (degrees)
1	84.8	3.47	0.00005083	143.0
2	102.8	27.58	0.0004048	83.5
3	83.7	3.05	0.00004475	32.6
4	100.2	20.43	0.0002998	141.6
5	99.1	18.07	0.0002651	296.8
6	96.5	13.37	0.0001962	142.8
7	106.6	42.83	0.0006285	268.9
Measured Check Mike Number				
8	99.0	17.95	0.0002634	198.8
9	89.8	6.22	0.00009120	185.8
10	97.1	14.33	0.0002103	285.1
11	89.0	5.61	0.00008237	161.5
Calculated Check Mike Number				
8	104.0	31.70	0.0004652	183.6
9	95.2	11.51	0.0001689	168.4
10	98.0	15.89	0.0002331	262.0
11	92.0	7.96	0.0001168	149.0

TABLE A5

COHERENT DUCT ACOUSTIC PRESSURE
STEADY STATE DATA
RPM = 3394 BPF = 1810 Hz TAPE RECORD NO. = 8

Measured Data Mike Number	Amplitude (dB)	(dynes/cm^2)	(lbf/in^2)	Phase (degrees)
1	85.0	3.56	0.00005219	147.8
2	103.2	28.91	0.0004242	88.9
3	83.8	3.10	0.00004546	45.8
4	100.3	20.70	0.0003038	148.7
5	101.0	22.44	0.0003293	306.8
6	95.6	12.05	0.0001768	134.6
7	106.9	44.26	0.0006495	280.3
Measured Check Mike Number				
8	99.8	19.54	0.0002868	203.6
9	92.2	8.15	0.0001196	196.8
10	98.3	16.44	0.0002413	303.3
11	89.7	6.11	0.00008966	160.7
Calculated Check Mike Number				
8	105.4	37.24	0.0005465	189.7
9	94.0	10.02	0.0001471	189.8
10	96.4	13.21	0.0001939	281.0
11	96.2	12.91	0.0001895	152.7

TABLE A6

COHERENT DUCT ACOUSTIC PRESSURE
STEADY STATE DATA
RPM = 3570 BPF = 1904 Hz TAPE RECORD NO. = 5

Measured Data Mike Number	Amplitude (dB)	(dynes/cm^2)	(lbf/in^2)	Phase (degrees)
1	88.6	5.42	0.00007954	327.8
2	101.6	24.09	0.0003535	132.8
3	89.9	6.26	0.00009191	174.5
4	102.4	26.32	0.0003862	205.3
5	100.5	21.14	0.0003102	358.1
6	96.8	13.85	0.0002033	225.2
7	102.7	27.40	0.0004021	316.1
Measured Check Mike Number				
8	102.1	25.59	0.0003756	237.2
9	97.8	15.54	0.0002280	230.2
10	100.2	20.36	0.0002987	302.6
11	85.3	3.70	0.00005426	214.9
Calculated Check Mike Number				
8	100.6	21.43	0.0003145	204.1
9	95.7	12.19	0.0001789	220.2
10	100.0	20.00	0.0002935	305.3
11	79.3	1.85	0.00002708	121.2

TABLE A7

COHERENT DUCT ACOUSTIC PRESSURE
STEADY STATE DATA
RPM = 3735 BPF = 1992 Hz TAPE RECORD NO. = 6

Measured Data Mike Number	Amplitude (dB)	(dynes/cm^2)	(lbf/in^2)	Phase (degrees)
1	94.2	10.24	0.0001502	296.2
2	82.4	2.65	0.00003889	352.3
3	87.4	4.70	0.00006893	61.5
4	100.1	20.17	0.00002961	287.6
5	98.5	16.86	0.0002475	48.3
6	102.6	26.89	0.0003946	260.7
7	101.9	24.84	0.0003645	51.0
Measured Check Mike Number				
8	102.5	26.74	0.0003924	279.9
9	94.8	10.99	0.0001613	187.3
10	98.6	17.04	0.0002501	305.1
11	97.5	15.06	0.0002209	249.1
Calculated Check Mike Number				
8	99.3	18.45	0.0002708	279.0
9	95.3	11.64	0.0001708	193.6
10	97.6	15.17	0.0002226	308.5
11	93.5	9.46	0.0001389	245.5

TABLE A8

COHERENT DUCT ACOUSTIC PRESSURE
NARROW WINDOWED TRANSIENT DATA
RPM = 3060 BPF = 1632 Hz TAPE RECORD NO. = 7

Measured Data Mike Number	Amplitude (dB)	(dynes/cm^2)	(lbf/in^2)	Phase (degrees)
1	88.6	5.39	0.00007910	65.7
2	94.7	10.84	0.0001591	261.2
3	82.0	2.52	0.00003703	343.6
4	95.1	11.44	0.0001679	167.1
5	91.4	7.47	0.0001096	236.3
6	96.3	13.07	0.0001918	128.0
7	91.7	7.68	0.0001127	141.2
Measured Check Mike Number				
8	95.9	12.53	0.0001838	31.6
9	95.9	12.47	0.0001829	71.0
10	96.8	13.91	0.0002041	169.4
11	86.5	4.25	0.00006239	277.2
Calculated Check Mike Number				
8	95.5	11.91	0.0001748	88.9
9	96.7	13.68	0.0002007	62.2
10	96.0	12.62	0.0001852	154.2
11	86.1	4.04	0.00005924	232.4

TABLE A9

COHERENT DUCT ACOUSTIC PRESSURE
NARROW WINDOWED TRANSIENT DATA
RPM = 3229 BPF = 1722 Hz TAPE RECORD NO. = 7

Measured Data Mike Number	Amplitude (dB)	(dynes/cm^2)	(lbf/in^2)	Phase (degrees)
1	98.5	16.92	0.0002483	302.3
2	112.7	86.24	0.001266	41.8
3	100.4	21.00	0.0003083	138.4
4	104.6	33.96	0.0004984	355.7
5	106.4	41.87	0.0006144	196.9
6	104.9	35.03	0.0005140	160.9
7	104.6	33.97	0.0004984	205.8
Measured Check Mike Number				
8	103.3	29.24	0.0004291	166.9
9	108.5	53.12	0.0007795	160.4
10	108.1	50.95	0.0007476	179.9
11	105.4	37.04	0.0005435	301.8
Calculated Check Mike Number				
8	111.0	70.96	0.001041	219.6
9	106.9	44.26	0.0006495	140.7
10	107.5	47.43	0.0006960	195.3
11	106.4	41.79	0.0006132	239.2

TABLE A10

COHERENT DUCT ACOUSTIC PRESSURE
NARROW WINDOWED TRANSIENT DATA
RPM = 3394 BPF = 1810 Hz TAPE RECORD NO. = 7

Measured Data Mike Number	Amplitude (dB)	(dynes/cm^2)	(lbf/in^2)	Phase (degrees)
1	96.7	13.73	0.0002015	167.3
2	103.0	28.30	0.0004154	118.2
3	89.4	5.90	0.00008661	43.2
4	102.0	25.17	0.0003694	167.0
5	100.1	20.23	0.0002969	333.0
6	101.4	23.49	0.0003447	151.7
7	108.3	52.21	0.0007662	307.2
Measured Check Mike Number				
8	102.1	25.47	0.0003738	185.2
9	92.1	8.01	0.0001175	175.7
10	94.7	10.90	0.0001600	273.0
11	95.4	11.77	0.0001728	181.8
Calculated Check Mike Number				
8	106.8	43.76	0.0006421	224.4
9	92.4	8.34	0.0001223	178.1
10	92.9	8.83	0.0001296	274.2
11	97.6	15.17	0.0002226	201.4

TABLE A11

COHERENT DUCT ACOUSTIC PRESSURE
NARROW WINDOWED TRANSIENT DATA

RPM = 3394 BPF = 1810 Hz (REPEAT) TAPE RECORD NO. = 7

Measured Data Mike Number	Amplitude (dB)	(dynes/cm^2)	(lbf/in^2)	Phase (degrees)
1	96.1	12.77	0.0001874	155.7
2	102.5	26.56	0.0003897	94.3
3	89.0	5.66	0.00008307	24.9
4	101.5	23.70	0.0003478	170.4
5	101.0	22.40	0.0003288	314.8
6	100.7	21.68	0.0003182	133.4
7	107.1	45.38	0.0006660	299.2
Measured Check Mike Number				
8	102.4	26.45	0.0003881	176.7
9	94.9	11.15	0.0001637	137.9
10	93.6	9.59	0.0001406	256.3
11	96.1	12.79	0.0001877	176.4
Calculated Check Mike Number				
8	106.9	44.26	0.0006495	207.5
9	86.7	4.33	0.00006347	161.4
10	87.8	4.91	0.00007204	259.6
11	100.8	21.93	0.0003218	175.2

TABLE A12

COHERENT DUCT ACOUSTIC PRESSURE
NARROW WINDOWED TRANSIENT DATA
RPM = 3570 BPF = 1904 Hz TAPE RECORD NO. = 7

Measured Data Mike Number	Amplitude (dB)	(dynes/cm^2)	(lbf/in^2)	Phase (degrees)
1	85.5	3.78	0.00005550	75.1
2	102.5	26.56	0.0003897	163.0
3	89.2	5.79	0.00008502	166.4
4	102.2	25.75	0.0003778	233.1
5	99.5	18.85	0.0002766	12.5
6	98.8	17.46	0.0002563	253.4
7	103.2	29.00	0.0004255	339.4
Measured Check Mike Number				
8	99.5	18.88	0.0002771	233.5
9	99.5	18.79	0.0002757	251.2
10	100.4	20.93	0.0003071	324.8
11	87.9	4.98	0.00007317	374.0
Calculated Check Mike Number				
8	100.3	20.70	0.0003038	233.2
9	97.6	15.17	0.0002226	232.5
10	101.3	23.23	0.0003409	326.2
11	84.7	3.44	0.00005042	292.8

TABLE A13

COHERENT DUCT ACOUSTIC PRESSURE
NARROW WINDOWED TRANSIENT DATA
RPM = 3735 BPF = 1992 Hz TAPE RECORD NO. = 7

Measured Data Mike Number	Amplitude (dB)	(dynes/cm^2)	(lbf/in^2)	Phase (degrees)
1	97.6	15.08	0.0002214	324.0
2	83.7	3.07	0.0004507	287.8
3	86.2	4.09	0.00006010	63.3
4	98.1	16.14	0.0002368	279.3
5	98.7	17.16	0.0002519	31.3
6	100.4	20.84	0.0003058	269.1
7	98.0	15.96	0.0002342	64.1
Measured Check Mike Number				
8	102.4	26.50	0.0003889	295.9
9	92.9	8.79	0.0001290	188.8
10	98.6	17.01	0.0002496	303.2
11	96.3	13.10	0.0001922	288.2
Calculated Check Mike Number				
8	99.5	18.88	0.0002771	336.1
9	93.0	8.93	0.0001311	184.2
10	93.5	9.46	0.0001389	310.2
11	98.0	15.89	0.0002331	313.3

TABLE A14

COHERENT DUCT ACOUSTIC PRESSURE
WIDE WINDOWED TRANSIENT DATA
TAPE RECORD NO. 7

Measured Data Mike Number	Amplitude (dB)	(dynes/cm^2)	(lbf/in^2)	Phase (degrees)
1	90.8	6.91	0.0001015	276.0
2	79.4	1.87	0.00002743	68.3
3	83.7	3.06	0.00004489	62.8
4	95.9	12.40	0.0001821	184.3
5	94.8	10.96	0.0001608	305.8
6	97.0	14.21	0.0002086	191.5
7	91.9	7.90	0.0001159	271.8
Measured Check Mike Number				
8	96.6	13.51	0.0001983	173.3
9	94.1	10.09	0.0001481	134.5
10	96.1	12.86	0.0001888	243.8
11	92.3	8.23	0.0001209	228.1
Calculated Check Mike Number				
8	78.9	1.76	0.00002586	287.9
9	93.8	9.79	0.0001437	141.0
10	96.6	13.52	0.0001984	234.6
11	89.5	5.97	0.00008762	293.8

TABLE A15

CALCULATED MODE STRUCTURE AND DEVIATION
STEADY STATE DATA
RPM = 3060 BPF = 1632 Hz TAPE RECORD NO. = 3

Mode	Amplitude (dB)	Deviation (dB)	Phase (degrees)	Deviation (degrees)
(-3, 0)	106.1	1.6	169.0	12.0
(-2, 0)	92.3	1.3	51.9	8.4
(-1, 0)	89.6	2.3	218.7	19.9
(0, 0)	84.1	3.4	64.9	20.7
(1, 0)	85.8	3.4	35.2	26.9
(2, 0)	96.3	1.0	60.2	8.4
(3, 0)	105.8	1.3	158.8	9.4

TABLE A16

CALCULATED MODE STRUCTURE AND DEVIATION
STEADY STATE DATA
RPM = 3229 BPF = 1722 Hz TAPE RECORD NO. = 4

Mode	Amplitude (dB)	Deviation (dB)	Phase (degrees)	Deviation (degrees)
(-3, 0)	120.1	0.3	271.4	3.9
(-2, 0)	105.4	1.0	58.9	5.5
(-1, 0)	103.1	1.1	17.2	14.4
(0, 0)	96.3	2.2	166.1	14.0
(1, 0)	108.0	1.1	231.3	6.5
(2, 0)	102.8	1.3	162.2	20.2
(3, 0)	115.0	0.4	279.7	8.9

TABLE A17

CALCULATED MODE STRUCTURE AND DEVIATION
STEADY STATE DATA
RPM = 3394 BPF = 1810 Hz TAPE RECORD NO. = 2

Mode	Amplitude (dB)	Deviation (dB)	Phase (degrees)	Deviation (degrees)
(-3, 0)	105.4	0.4	223.9	5.4
(-2, 0)	99.5	0.6	31.1	4.1
(-1, 0)	88.6	2.2	155.5	19.2
(0, 0)	86.6	2.4	252.5	29.6
(1, 0)	86.0	3.5	277.3	26.7
(2, 0)	87.3	3.4	310.9	40.8
(3, 0)	104.7	0.3	240.0	5.3

TABLE A18

CALCULATED MODE STRUCTURE AND DEVIATION
STEADY STATE DATA
RPM = 3394 BPF = 1810 Hz TAPE RECORD NO. = 8

Mode	Amplitude (dB)	Deviation (dB)	Phase (degrees)	Deviation (degrees)
(-3, 0)	105.4	0.4	227.8	5.5
(-2, 0)	100.2	0.7	42.4	4.0
(-1, 0)	90.0	2.2	143.4	14.7
(0, 0)	88.1	2.5	273.9	23.5
(1, 0)	85.3	4.5	307.7	22.3
(2, 0)	89.5	3.2	0.8	31.2
(3, 0)	105.6	0.3	245.5	4.9

TABLE A19

CALCULATED MODE STRUCTURE AND DEVIATION
STEADY STATE DATA
RPM = 3570 BPF = 1904 Hz TAPE RECORD NO. = 5

Mode	Amplitude (dB)	Deviation (dB)	Phase (degrees)	Deviation (degrees)
(-3, 0)	103.1	0.6	238.1	5.0
(-2, 0)	99.0	0.8	43.5	5.4
(-1, 0)	81.8	3.5	212.5	48.1
(0, 0)	81.3	5.4	136.6	29.3
(1, 0)	68.4	11.7	276.6	272.5
(2, 0)	82.8	5.2	344.8	58.6
(3, 0)	101.0	0.6	211.3	6.4

TABLE A20

CALCULATED MODE STRUCTURE AND DEVIATION
STEADY STATE DATA
RPM = 3735 BPF = 1992 Hz TAPE RECORD NO. = 6

Mode	Amplitude (dB)	Deviation (dB)	Phase (degrees)	Deviation (degrees)
(-3, 0)	101.9	0.7	258.7	7.4
(-2, 0)	99.3	0.6	89.3	5.1
(-1, 0)	97.2	0.8	250.9	6.8
(0, 0)	87.2	3.0	45.7	14.5
(1, 0)	91.1	2.5	69.3	16.4
(2, 0)	99.4	0.8	73.5	8.1
(3, 0)	95.8	1.5	327.5	7.4

TABLE A21

CALCULATED MODE STRUCTURE AND DEVIATION
NARROW WINDOWED TRANSIENT DATA
RPM = 3060 BPF = 1632 Hz TAPE RECORD NO. = 7

Mode	Amplitude (dB)	Deviation (dB)	Phase (degrees)	Deviation (degrees)
(-3, 0)	107.4	1.7	181.5	10.4
(-2, 0)	93.3	1.3	52.4	7.9
(-1, 0)	94.2	1.5	211.2	13.5
(0, 0)	83.5	3.7	80.8	26.7
(1, 0)	88.5	2.9	40.1	20.1
(2, 0)	94.1	1.3	68.6	11.9
(3, 0)	107.4	1.2	170.4	9.0

TABLE A22

CALCULATED MODE STRUCTURE AND DEVIATION
NARROW WINDOWED TRANSIENT DATA
RPM = 3229 BPF = 1722 Hz TAPE RECORD NO. = 7

Mode	Amplitude (dB)	Deviation (dB)	Phase (degrees)	Deviation (degrees)
(-3, 0)	116.6	0.4	286.8	4.0
(-2, 0)	102.1	0.9	54.2	7.6
(-1, 0)	94.2	2.5	60.8	27.4
(0, 0)	82.0	6.1	2.8	58.5
(1, 0)	101.4	1.8	280.8	8.1
(2, 0)	101.9	1.2	160.2	15.8
(3, 0)	109.5	0.8	278.8	10.7

TABLE A23

CALCULATED MODE STRUCTURE AND DEVIATION
NARROW WINDOWED TRANSIENT DATA
RPM = 3394 BPF = 1810 Hz TAPE RECORD NO. = 7

Mode	Amplitude (dB)	Deviation (dB)	Phase (degrees)	Deviation (degrees)
(-3, 0)	107.7	0.4	249.9	5.1
(-2, 0)	100.7	0.7	71.0	4.1
(-1, 0)	98.1	0.9	195.3	8.7
(0, 0)	94.5	2.0	330.8	8.0
(1, 0)	93.3	2.4	358.3	8.3
(2, 0)	94.3	2.5	44.9	17.4
(3, 0)	107.1	0.3	281.6	4.6

TABLE A24

CALCULATED MODE STRUCTURE AND DEVIATION
NARROW WINDOWED TRANSIENT DATA
RPM = 3394 BPF = 1810 Hz (REPEAT) TAPE RECORD NO. = 7

Mode	Amplitude (dB)	Deviation (dB)	Phase (degrees)	Deviation (degrees)
(-3, 0)	105.9	0.4	233.1	5.6
(-2, 0)	101.5	0.6	62.7	4.0
(-1, 0)	96.2	1.0	187.1	10.5
(0, 0)	93.1	2.2	337.2	6.7
(1, 0)	91.1	2.6	3.1	13.8
(2, 0)	96.5	1.9	49.8	11.7
(3, 0)	106.3	0.4	266.8	4.5

TABLE A25

CALCULATED MODE STRUCTURE AND DEVIATION
NARROW WINDOWED TRANSIENT DATA
RPM = 3570 BPF = 1904 Hz TAPE RECORD NO. = 7

Mode	Amplitude (dB)	Deviation (dB)	Phase (degrees)	Deviation (degrees)
(-3, 0)	104.0	0.5	260.7	5.0
(-2, 0)	100.3	0.6	73.7	4.4
(-1, 0)	90.3	2.0	210.0	15.8
(0, 0)	73.2	8.9	312.6	107.3
(1, 0)	89.6	2.8	342.4	16.8
(2, 0)	88.4	3.4	340.0	28.7
(3, 0)	100.0	0.7	241.3	7.7

TABLE A26

CALCULATED MODE STRUCTURE AND DEVIATION
NARROW WINDOWED TRANSIENT DATA
RPM = 3735 BPF = 1992 Hz TAPE RECORD NO. = 7

Mode	Amplitude (dB)	Deviation (dB)	Phase (degrees)	Deviation (degrees)
(-3, 0)	100.2	0.9	293.7	6.1
(-2, 0)	99.7	0.6	89.2	4.5
(-1, 0)	99.0	0.7	198.3	6.9
(0, 0)	78.6	5.4	215.2	45.1
(1, 0)	95.7	1.3	53.1	9.0
(2, 0)	97.3	1.4	13.1	8.7
(3, 0)	102.4	0.6	352.0	5.5

TABLE A27

CALCULATED MODE STRUCTURE AND DEVIATION
WIDE WINDOWED TRANSIENT DATA
TAPE RECORD NO. 7

Mode	Amplitude (dB)	Deviation (dB)	Phase (degrees)	Deviation (degrees)
(-3, 0)	94.0	1.0	254.4	9.4
(-2, 0)	93.0	0.9	57.2	6.8
(-1, 0)	92.8	1.0	237.2	8.7
(0, 0)	89.3	1.1	93.2	8.2
(1, 0)	91.7	1.2	87.7	8.2
(2, 0)	84.9	2.7	127.4	20.0
(3, 0)	76.8	0.5	35.8	42.8

APPENDIX B NOTATION FOR SECTION 3.0

English Symbols

$A^{\Pi}_{m\mu}$	power-effective modal area
$a_{m\mu}$	direction cosine parameter, $= \sqrt{1-1/\xi^2_{m\mu}}$
$a'_{m\mu}$	$\sqrt{1-1/\xi^2}$ for $\xi < 1$
B	number of rotor blades
$B_{m\mu}$	complex (m, μ) mode coefficient at duct wall
$\lvert B_{m\mu} \rvert^2$	modal power
b	radius of duct
$C_{m\mu}$	complex (m, μ) mode coefficient
C_m	complex coefficient of mth mode at wall in plane of circumferential array resulting from associated μ-modes
c	speed of sound
D_a	normalized modal density with respect to parameter a
D_ξ	normalized modal density with respect to cutoff ratio
$E_{m\mu}$	eigenfunction for (m, μ) mode
F	1/F is fraction of circumference spanned by array
F_η	complex array signal for delay rate, η
F_M	complex array signal for target mode m = M
f_η	array signal for delay rate η
i	$\sqrt{-1}$
K	condition number of matrix
k	free-space wavenumber, ω/c
$k_{m\mu}$	eigenvalue for (m, μ) mode
$k_{xm\mu}$	axial wavenumber of (m, μ) mode

L	- axial array length = $N\Delta x$ - also linear operator
ℓ	linear operator
M	wavenumber of target circumferential mode
$M^*_{m\mu}$	tangential wall Mach number of (m, μ) mode at cutoff
m	wave number of circumferential mode
m^*	largest circumferential wave number
N	number of microphones in array - also number of axial arrays in Section 3.3.4.2 - also number of circumferential arrays in Section 3.3.6
n	- specific microphone in array - also, harmonic of blade passage frequency
P	- complex pressure - also number of target circumferential modes
P_n	complex pressure at nth microphone
p	acoustic pressure
P_n	pressure at nth microphone
p_n'	delayed pressure at nth microphone
Re	- real part of
r	- radial duct coordinate
r	- also resolving ratio of axial array = λ/L
S_1, S_2 etc.	sums involved in array signal power
S	distance between microphone and source of mode
t	time
U, V	expi S_A, expi S_B
W	power of array signal
W_n	weighting factor for nth microphone
X	axial integration length
x	axial duct coordinate

Z	array factor
$[Z]$	array matrix

Greek Symbols

$\alpha_{m\mu}$	peak radiation angle of (m, μ) mode
β	argument of circumferential array factor = $(m - \omega\eta)$
β_x	argument of axial array factor = $(a_{m\mu} - c\eta_x)\ L/\lambda$
$\gamma_{m\mu}$	wall incidence angle of (m, μ) mode wave normal
Δ, δ	increments or errors
η	circumferential array delay rate (secs/radian)
η_x	axial array delay rate (secs/unit distance)
θ	angular duct coordinate
λ	wavelength
λ_m	circumferential wave length of n-th mode
μ	radial mode index
$\xi_{m\mu}$	cutoff ratio of (m, μ) mode
$\Pi_{m\mu}$	acoustic power flux of (m, μ) mode
ρ	fluid density
φ	phase angle
Ω	fan angular velocity
Ω_m	angular velocity of mth circumferential mode
ω	circular frequency

Indices

M, m, j, k	mode designation indices
n	microphone index

Symbols

*	complex conjugate
[ ]	vector or matrix
|| ||	norm of vector or matrix